

Control of Crystalline Particle Properties by Spray Drying

A thesis presented for the degree of
Doctor of Philosophy
in the Faculty of Science
of the University of Strathclyde

by

Rebecca Amy Halliwell

Strathclyde Institute of Pharmacy and Biomedical Sciences

March, 2017

Declaration of Authors Rights

This thesis is the result of the author's original research. It has been composed by the author and has not been previously submitted for examination which has led to the award of a degree.

The copyright of this thesis belongs to the author under the terms of the United Kingdom Copyright Acts as qualified by University of Strathclyde Regulation 3.50. Due acknowledgement must always be made of the use of any material contained in, or derived from, this thesis.

Signed:

Date:

Acknowledgements

Firstly, I would like to thank my supervisor Professor Alastair Florence for giving me the opportunity to work with him, his research group and the wider community that makes up the Centre for Innovative Manufacturing in Continuous Manufacturing and Crystallisation (CMAC) within the University of Strathclyde. I would like to thank EPSRC and the Doctoral Training Centre in Continuous Manufacturing and Crystallisation for funding this work.

Special thanks go to members of the Florence research group, in particular Dr Cameron Brown, Dr Humera Siddique, Mr Vishal Raval and Mr Fraser Mabbott for their constant assistance, support and kindness throughout my research. I would also like to thank Dr Rajni Bhardwaj, Dr Naomi Briggs, Dr Jaclyn Dunn, Dr Pól MacFhionnghaile and Dr Murray Robertson.

I would particularly like to thank my family and friends for their constant love and support, without such I could not have achieved this thesis.

Finally, I would like to dedicate this thesis to the memory of my beloved mother who taught me the most important lessons in life; to love deeply, to work hard and to be honest.

Abstract

Although spray drying has been common place in the pharmaceutical industry for decades, the integration of the technique into continuous manufacturing can offer an extensive array of particle engineering applications. Continuous manufacturing aims to deliver consistent and sustainable drug products of a better and higher quality. Spray drying is a continuous processing technique typically adopted for amorphous solid production. However, the unique conditions of the technique can also be adapted and applied to crystallisation enabling particle property engineering. The semi-continuous lab-scale Büchi B-290 Mini spray dryer is widely available and has been previously studied extensively for particle engineering and as a development platform for applications including pulmonary drug delivery, sustained release formulations and amorphous solid dispersions.

The focus of this work is to engineer and enhance particle properties through the use of the Büchi spray dryer. Particle formation has been investigated, with specific focus in terms of polymorph formation in carbamazepine, to develop a predictive model for crystallisability and for co-spray drying of metformin hydrochloride with mannitol and lactose. Particle formation has been described in terms of theoretical drying kinetics and combined with off line characterisation to determine size and form of product. The metastable polymorph, form IV, of carbamazepine was made reproducibly by spray drying with the combination of rapid evaporation and product isolation shown to be crucial to prevention of solution mediated transformation. The application of non-invasive Raman spectroscopy was also utilised to assess product form. A crystallisability predictive model based on a Random Forest method was successfully produced through combining molecular descriptors with published and experimental outcomes. The model provided up to 79 % accuracy in predicting whether an amorphous or crystalline product would be expected from rapid drying. This shows considerable utility in streamlining process development. Finally, co-spray drying in the

Büchi system using a three-fluid nozzle was used to produce multicomponent composite particles comprising of two crystallite phases. The effect of process configuration and material properties on the resultant particles was assessed using particle sizing, SEM, XRPD and Raman mapping. The results were compared on the basis of theoretical drying kinetics to assess the ability to predict the resultant particle morphology. Four multicomponent composite particles were produced by co-spray drying from metformin hydrochloride (MF), mannitol and lactose. MF-mannitol composites produced three-phase physical mixtures with both components present on the particle surfaces. The particle surface compositions were contradictory to the expected particle outcomes from the drying parameters. MF-lactose composite particle also produce three-phase physical mixtures with a relatively equal distribution of components present on particle surface. This is consistent with the expected particle from the drying parameters. The different particle outcomes suggest that co-spray drying of miscible multicomponent feeds using the three-fluid nozzle is highly dependent on the drying parameters for each component due to equal mixing of the feed at atomisation of droplets.

Contents

Declaration of Authors Rights	i
Acknowledgements	ii
Abstract	iii
List of Figures	viii
List of Tables	xii
Chapter 1. Introduction	1
1. Introduction	2
1.1. Drying	3
1.1.1. Spray Drying	4
1.1.1.1. Process Stages	5
1.1.1.2. Drying Principles	9
1.1.1.3. Spray Dryer Configurations	13
1.1.1.4. Spray Drying Process Parameters	15
1.1.1.4.1. Aspirator Rate	16
1.1.1.4.2. Inlet Temperature	17
1.1.1.4.3. Outlet Temperature	17
1.1.1.4.4. Spray Gas Flow Rate	18
1.1.1.4.5. Feed Pump Rate	18
1.1.1.4.6. Other Parameters	19
1.2. Crystallisation	19
1.2.1. Continuous Crystallisation	26
1.3. Particle Types	27
1.3.1. Critical Quality Attributes	27
1.3.1.1. Particle Size and Size Distribution	28
1.3.1.2. Particle Morphology	29
1.3.1.3. Solid-State Form	30
1.3.2. Particle Attribute Measurements	33
1.4. Spray Drying Applications	34
1.4.1. Particle Optimisation	34
1.4.2. Multicomponent Systems	37
1.5. Motivation for research	42
Chapter 2. Aims and Objectives	44
2. Aims and Objectives	45

2.1.	Aims	45
2.2.	Objectives	45
Chapter 3. Materials and Methods		47
3.	Materials and Methods.....	48
3.1.	Materials	48
3.2.	Methods.....	48
3.2.1.	X-Ray Powder Diffraction (XRPD).....	48
3.2.2.	Spectroscopy	49
3.2.2.1.	Raman	49
3.2.2.2.	Raman Microscopy	49
3.2.3.	Imaging	50
3.2.3.1.	Scanning Electron Microscopy (SEM)	50
3.2.4.	Particle Sizing	50
3.2.5.	Thermal Analysis	50
3.2.6.	Data Presentation	51
Chapter 4. Polymorph Control and Isolation via Spray Drying		52
4.	Polymorph Control and Isolation via Spray Drying	53
4.1.	Introduction.....	53
4.1.1.	Carbamazepine.....	54
4.1.2.	Spray Drying.....	55
4.2.	Experimental	56
4.2.1.	Spray Drying Method.....	56
4.2.2.	Carbamazepine Characterisations	56
4.3.	Results and Discussion	57
4.3.1.	CBZ IV.....	57
4.3.2.	CBZ IV Solution Mediated Transformation	64
4.4.	Summary	77
Chapter 5. Prediction of Crystallisability in Spray Drying using Random Forest		78
5.	Prediction of Crystallisability in Spray Drying using Random Forest.....	79
5.1.	Introduction.....	79
5.1.1.	Spray Drying Crystallisation Propensity Models.....	79
5.1.2.	Random Forest	80
5.1.3.	Random Forest Models for Crystallisation	81
5.2.	Experimental	81

5.2.1.	Spray Drying Method.....	81
5.2.2.	Crystallisation Characterisation	85
5.2.3.	Random Forest	85
5.3.	Results and Discussion	86
5.3.1.	Van Eerdenbrugh Model.....	86
5.3.2.	Van Eerdenbrugh Model with Spray Dryer Compounds	89
5.3.3.	Spray Dried Model.....	93
5.3.4.	Spray Dryer Model Supplemented with Known Amorphous Compounds	96
5.3.5.	Models Tested with BCS Compounds	99
5.4.	Summary	105
Chapter 6. Co-Spray Drying for Multicomponent Particles using the Three-Fluid Nozzle		106
6.	Co-Spray Drying for Multicomponent Particles using the Three-Fluid Nozzle	107
6.1.	Introduction.....	107
6.1.1.	Co-Processing of Pharmaceuticals.....	108
6.1.2.	Co-Processing by Spray Drying.....	109
6.1.3.	Metformin Hydrochloride, Mannitol and Lactose	110
6.2.	Experimental	112
6.2.1.	Compound Selection	112
6.2.2.	Spray Drying Method.....	112
6.2.3.	Three-fluid Nozzle	113
6.2.4.	Composite Particle Characterisation	114
6.3.	Results and Discussion	115
6.3.1.	Multicomponent Composite Particles.....	115
6.3.1.1.	MF – Mannitol Co-Spray Dried Composites	115
6.3.1.2.	MF – Lactose Composites.....	129
6.4.	Summary	143
Chapter 7. Conclusion and Future Work		144
References.....		150

List of Figures

Figure 1.1. Schematic of spray drying process: (1) Delivery of feed to nozzle, (2) Atomisation of feed by nozzle, (3) Heating of drying gas, (4) Drying process of atomised droplets, (5) Collection of solid particles, (6) Separation of solid particles from drying gas and (7) Separation of fines (Büchi Labortechnik AG).....	4
Figure 1.2. The drying rate trend through the progression of key drying stages of spray drying.....	10
Figure 1.3. Schematic illustration showing expected particle structures formed under conditions of high and low Peclet numbers.....	12
Figure 1.4. Schematic of spray dryer modes: Co-current, Counter-current and Combined...	13
Figure 1.5. Closed mode operation of Büchi B-290 and B-295 Inert loop. (1) feed, (2) product, (3) exhaust gas, (4) solvent, (5) preheat exchanger, (6) condensation and (7) cooling unit (Büchi Labortechnik AG 1997 - 2002).....	15
Figure 1.6. Schematic of solubility curve in relation to concentration versus temperature detailing regions of undersaturation, metastable zone width (MSZW) and supersaturation.	22
Figure 1.7. Free energy diagram for nucleation (Erdemir et al. 2009).	23
Figure 4.1. Molecular structure of Carbamazepine.....	54
Figure 4.2. Calculated XRPD patterns for CBZ I, II, III, IV and V compared with the experimental data for spray dried methanol CBZ solution.	57
Figure 4.3. Pawley fit of the data from the spray dried CBZ sample. Observed profile (o), calculated profile (-) and difference plot (Yobs-Ycal) of the Pawley fit in the range of 6-34° 2θ (Pawley $\chi^2 = 1.790$).	58
Figure 4.4. Raman spectra of spray dried CBZ samples produced under different spray dryer process conditions in comparison to CBZ IV offline reference.....	60
Figure 4.5. Morphological image of spray dried CBZ IV by SEM at 5 kV.....	61

Figure 4.6. Particle size and size distribution measurements, based on the CE diameter, of CBZ IV.	62
Figure 4.7. DSC profiles of three CBZ forms.	63
Figure 4.8. XRPD analysis of CBZ IV 30, 60 and 90 days after formation.	64
Figure 4.9. Droplet diameter and CBZ supersaturation as a function of drying time.	72
Figure 4.10. XRPD patterns of single crystal references of CBZ III and IV in comparison to measured supersaturations samples at 2.79 and 5.58 in rapidly cooled methanolic CBZ solutions.	74
Figure 4.11. XRPD patterns of scaled up hot plate analysis for CBZ comparing hot plate CBZ sample to single crystal reference patterns of CBZ I and IV.	75
Figure 5.1. RF workflow used to create and develop the predictive crystallisability model.	85
Figure 5.2. Mean error plots for Van Eerdenbrugh based RF models showing the predictive accuracy of each model with increasing training set sizes and different classification directions.	88
Figure 5.3. XRPD patterns of the 11 crystalline compounds produced by the spray dryer. ...	90
Figure 5.4. XRPD patterns of 6 amorphous compounds produced by the spray dryer.	91
Figure 5.5. Mean error plot for spray dryer model trend showing predictive accuracy of models with increasing training set size.	94
Figure 5.6. PCA scores plot of compound diversity of all model training and test set compounds against 6119 pharmaceutical compounds from DrugBank (The Metabolics Innovation Centre).	95
Figure 5.7. PCA scores plot with 17 training set supplemented with 7 further amorphous compounds based on literature reports against 6119 pharmaceutical compounds from DrugBank (The Metabolics Innovation Centre).	98
Figure 5.8. PCA scores plot of BCS I and IV compounds against 6119 pharmaceutical compounds from DrugBank (The Metabolics Innovation Centre).	104

Figure 6.1 Schematic of two-fluid nozzle (left) and three-fluid nozzle (right) showing passage of fluid streams with proposed droplet structures (Kašpar et al. 2013).	113
Figure 6.2. Expected particle structures for configurations 1 (where mannitol dominates the surface and MF present but in lower concentration) and 2 (equal quantities of MF and mannitol) based on theoretical drying calculations.....	117
Figure 6.3. Starting material reference XRPD patterns for MF and mannitol compared with the XRPD patterns from spray dried composite particles of configurations 1 and 2.....	118
Figure 6.4. Multi-phase Pawley fit of the data for co-spray dried configuration 1. Calculated profile (o) (MF I, β -mannitol I and α -mannitol I), and difference plot (Yobs - Ycal).....	119
Figure 6.5. Multi-phase Pawley fit of the data for co-spray dried configuration 2. Calculated profile (o) (MF I, β -mannitol I and α -mannitol I), and difference plot (Yobs - Ycal).....	120
Figure 6.6. DSC profiles of MF and mannitol references and configurations 1 and 2.	122
Figure 6.7. SEM images: (a) SEM of configuration 1, (b) SEM of configuration 2, (c) X-ray map of chlorine distribution of configuration 1 and (d) X-ray map of chlorine distribution of configuration 2 gained from EDX analysis.....	124
Figure 6.8. Reference Raman spectra for MF and mannitol highlighting differential peak regions; 500 – 600 cm^{-1} for MF (red) and 800 – 900 cm^{-1} for mannitol (green).....	126
Figure 6.9. Surface composition identification by Raman mapping of a particle produced using configuration 1 showing MF in red and mannitol in green. The peak regions at 700 – 800 and 800 – 900 cm^{-1} were used to indicate the presence of MF and mannitol, respectively.	127
Figure 6.10. Surface composition identification by Raman mapping of a particle produced using configuration 2 showing MF in red and mannitol in green. The peak regions at 700 – 800 and 800 – 900 cm^{-1} were used to indicate the presence of MF and mannitol, respectively.	128
Figure 6.11. Particle size and size distribution measurements for configurations 1 and 2. .	129

Figure 6.12. Expected particle structures for configuration 3 (lactose dominates surface) and 4 (MF dominates surface) based on theoretical drying calculations.	131
Figure 6.13. Starting material reference XRPD patterns for MF and lactose compared with the XRPD patterns from spray dried composite particles of configurations 3 and 4.	132
Figure 6.14. Multi-phase Pawley fit of the data of co-spray dried configuration 3. Calculated profile (o) (MF I, α -monohydrate I and anhydrous I) and difference plot ($Y_{obs} - Y_{cal}$). ...	133
Figure 6.15. Multi-phase Pawley fit of the data of co-spray dried configuration 4. Calculated profile (o) (MF I, α -monohydrate I and anhydrous I) and difference plot ($Y_{obs} - Y_{cal}$). ..	134
Figure 6.16. DSC profiles of MF and lactose references and configurations 3 and 4.	136
Figure 6.17. SEM images: (a) SEM of configuration 3, (b) SEM of configuration 4, (c) X-ray map of chlorine distribution of configuration 3 and (d) X-ray map of chlorine distribution of configuration 4 gained from EDX analysis.	138
Figure 6.18. Reference Raman spectra for MF and lactose highlighting differential peak regions; 500 – 600 cm^{-1} for MF (green), 250 – 500 cm^{-1} (red) for lactose.	139
Figure 6.19. Surface composition identification by Raman mapping of a particle produced using configuration 3 showing MF in green and lactose in red. The peak regions at 500 – 600 and 250 – 500 cm^{-1} were used to indicate the presence of MF and lactose, respectively. ...	140
Figure 6.20. Surface composition identification by Raman mapping of a particle produced using configuration 4 showing MF in green and lactose in red. The peak regions at 500 – 600 and 250 – 500 cm^{-1} were used to indicate the presence of MF and lactose, respectively. ...	140
Figure 6.21. Particle size and size distribution measurements for configurations 3 and 4 ..	142

List of Tables

Table 1.1. Reported spray drying applications and designed particle types.	5
Table 1.2. Atomisation device classification (Walzel 2011).	7
Table 1.3. Process parameters of the lab-scale Büchi B-290 Mini Spray Dryer (Büchi Labortechnik AG , Cal and Sollohub 2010b).	16
Table 1.4. Other material parameters relevant for spray drying.	19
Table 1.5. Definition of relevant particle types for spray drying.	27
Table 1.6. Different analytical techniques used to measure particle attributes.	33
Table 4.1. Summary of spray dryer parameter conditions.	56
Table 4.2. Summary of operating conditions for the spray drying of CBZ, which was monitored by on-line Raman spectrometry.	59
Table 4.3. Definition and values of terms of equations 4.1 – 4.11 including diffusion coefficient, evaporation rate and Peclet number calculation values.	69
Table 5.1. Summary of spray dryer parameter conditions kept constant for crystallisability investigations.	82
Table 5.2. Reported solubility values of crystallisability prediction compounds.	83
Table 5.3. Compound classification of crystallisability from (Van Eerdenbrugh et al. 2010).	87
Table 5.4. Spray drying predictive comparisons with observed experimental results and predicted outcomes based on the different models produced in 5.2.1.	92
Table 5.5. Molecular structures of compounds reported in the literature to form amorphous forms.	97
Table 5.6. 32 selected compounds classified as BCS I and IV from literature reports.	101
Table 5.7. Predictive results for BCS I and IV compounds using the spray dryer plus amorphous RF model.	102
Table 6.1. Molecular structures of MF, mannitol and lactose.	110

Table 6.2. Summary of co-spray drying parameter conditions.....	113
Table 6.3. Summary of co-spray drying configurations of the fluid streams of the three-fluid nozzle for different two-component spray dried systems.	114
Table 6.4. Theoretical drying kinetics for MF and mannitol calculated from equations 1.2, 1.3, 1.4 and 1.14 (Vehring 2008).....	116
Table 6.5. Phase identifications of configurations 1 and 2 by CSD refcodes showing the refined lattice parameters obtained from each of the fits.....	121
Table 6.6. Theoretical drying kinetics for MF and lactose calculated from equations 1.2, 1.3, 1.4 and 1.14 (Vehring 2008).	130
Table 6.7. Phase identifications of configurations 3 and 4 by CSD refcodes showing the refined lattice parameters obtained from each of the fits.....	135

Chapter 1. Introduction

1. Introduction

Spray drying is a technique that has been used extensively for the production of particles for a wide range of different applications across the food industry, in agrochemical manufacture and in the manufacture of pharmaceuticals (Nandiyanto and Okuyama 2011a). It is an inherently continuous process which is widely used across small-scale laboratory development applications (Nijdam and Langrish 2005, Hay et al. 2017) through to industrial scale manufacture of large volume products (Jin and Chen 2009). In addition to removal of moisture or solvent from the process stream, spray drying has been extensively studied for particle engineering (Vehring 2008). It has been shown to be suitable for producing a wide range of particle attributes of amorphous and crystalline solids (Chow et al. 2007, Chiou and Langrish 2008), composite mixtures of excipient and active ingredient (Gharsallaoui et al. 2007, Gonnissen et al. 2008c) as well as homogenous formulated particles with active dispersed in suitable excipients (Paudel et al. 2013, Singh and Van den Mooter 2016). The ability to generate consistent, small micronised material has led to particular interest in the application of the process to the formation of particles for inhalation, where aerodynamic properties are crucial for performance (Chow et al. 2007) and the potential for new therapeutic strategies (Marshall et al. 2016). However the combination of solidification and drying in a single step has wider benefits for the direct formation of crystalline particles in the range of 3-20 μm and lends itself to utilisation within continuous manufacturing approaches. Traditional crystallisation typically would produce larger particles, followed by filtration, washing, drying and subsequent milling steps to achieve similar particle dimensions. This thesis aims to investigate the capability of spray drying to contend with and offer an alternative approach to the traditional crystallisation methodologies through the exploration of crystal prediction and particle engineering. These approaches can present spray drying as a highly useful technique for polymorph screening, crystallisability prediction

and co-processing for the design of formulated particles that can improve the efficiency of crystallisation, drug manufacture and promote the case for continuous manufacturing.

1.1. Drying

Drying is an integral processing step in the manufacture of pharmaceutical compounds that offers a route for particle and formulation engineering and process development (Byrn et al. 2015). The fundamental process of drying is the evaporation of a volatile material from a second material to gain a solid product (Perry and Green 2008). The integration of continuous drying methods will aim to achieve efficient drying for a wide variety of applications in a practical processing time frame (Byrn et al. 2015). There are many examples of drying techniques used in the pharmaceutical industry such as fluid-bed dryer, freeze drying, vacuum dryers and spray dryers. This thesis will focus on the application of lab-scale spray drying for different approaches to particle engineering.

1.1.1. Spray Drying

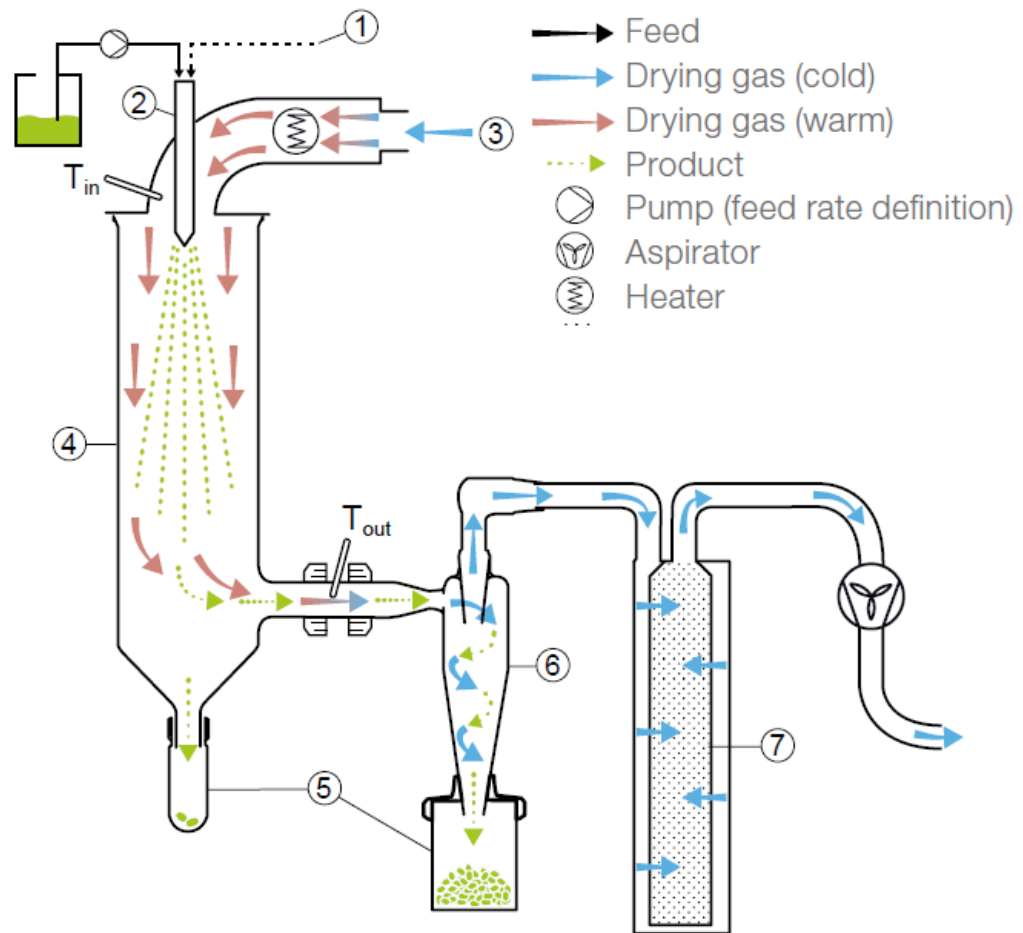


Figure 1.1. Schematic of spray drying process: (1) Delivery of feed to nozzle, (2) Atomisation of feed by nozzle, (3) Heating of drying gas, (4) Drying process of atomised droplets, (5) Collection of solid particles, (6) Separation of solid particles from drying gas and (7) Separation of fines (Büchi Labortechnik AG).

The process of spray drying, presented in Figure 1.1, is defined as the ‘transformation of feed from a fluid state into a dried particulate form by spraying the feed into a gaseous drying medium’ (Cal and Sollohub 2010a). Spray drying is often used for pharmaceutical manufacture as it is an adaptable technology that can produce a high purity product with the process parameters enabling extensive control over particle attributes (Nandiyanto and Okuyama 2011b). To achieve a successfully dried product, the spray dryer operates in three

consecutive stages; atomisation, droplet-to-particle conversion or solidification and particle collection. Each stage has a significant effect on the drying efficiency of the process and the characteristics of the final product. The particle formation process by spray drying is governed by the drying kinetics and rates (Vehring et al. 2007). It is worth noting that spray drying is generally characterised by very rapid drying kinetics compared with other pharmaceutical drying processes. For example, total drying times in a lab-scale spray dryer are typically less than 1-2 s. Spray drying offers a wide variety of particle types that can be produced for a number of different applications, presented in Table 1.1.

Table 1.1. Reported spray drying applications and designed particle types.

Spray Drying Applications	Particle Types
Pulmonary Drug Delivery (Chow et al. 2007, Marshall et al. 2016)	Nanoparticles (Alfagih et al. 2015, Mokale et al. 2016)
Sustained Release (Karanje et al. 2013)	Microparticles (Naikwade et al. 2009)
Particle Encapsulation (Anandharamakrishnan and Ishwarya 2015b)	Co-crystal (Alhalaweh and Velaga 2010, Patil et al. 2014)
Particle Engineering (Vehring 2008)	Composite (Kadota et al. 2015)
Co-Processing (Gohel and Jogani 2005, Shur et al. 2008)	Solid Dispersions (Singh and Van den Mooter 2016)
Biological Stabilisation (Walters et al. 2014)	Co-Amorphous (Dengale et al. 2016)

1.1.1.1. Process Stages

The first stage of spray drying is the process of atomisation; defined as ‘bringing fluid or solid substances into a state of minute division’ (Anandharamakrishnan and Ishwarya 2015a). Fundamentally this distributes the input liquid mass over a large number of small droplets with a very large surface area across which drying can occur. This is achieved in

different ways dependent on the type and scale of dryer used; such as piezo actuators for nanoscale drying and rotary atomisers for industrial dryers (Písecký 2005). Atomisation is thus an important stage of the process as droplet qualities such as, size distribution, surface tension, composition and viscosity determine the final particle size and particle attributes (Nandiyanto and Okuyama 2011a, Anandharamakrishnan and Ishwarya 2015a). With the lab-scale Büchi B-290 Mini Dryer, for the liquid feed to undergo atomisation it must be in the form of a solution, suspension or emulsion that can be pumped and homogenised and free from impurities (Büchi Labortechnik 2007). There are a variety of different atomisers and nozzles that deliver different characteristic atomisation performance for different particle specifications detailed in Table 1.2, including rotary atomisers and pressure nozzles such as ultrasonic and pneumatic (Cal and Sollohub 2010a). A two-fluid nozzle works by exposing the liquid fluid to a high velocity gaseous fluid causing the break-up of the liquid thus atomising and creating droplets (Anandharamakrishnan and Ishwarya 2015a). The creation of droplets by atomisation follows into the next stage of the process, droplet drying.

Table 1.2. Atomisation device classification (Walzel 2011).

Atomiser Type	Approach to Droplet Formation
Rotary atomiser	Centrifugal Energy <ul style="list-style-type: none">- High speed-rotating wheel to disperse bulk into droplets
Pressure nozzle	Pressure energy <ul style="list-style-type: none">- Causes bulk fluid rotation and uses liquid potential energy under pressure into kinetic energy and so the liquid leaves nozzle as droplets
Two-fluid nozzle	Kinetic energy <ul style="list-style-type: none">- Combines liquid and pressured gas streams to force stream through atomiser
Ultrasonic atomiser	Ultrasonic energy <ul style="list-style-type: none">- Liquid placed on rapidly vibrating surface to become unstable and form droplets

The most important and complex stage of the spray drying process is that of droplet drying. This stage enables the atomised droplets to be converted to dried particulates within a drying chamber. This stage is the most complex as it encompasses different drying modes and dryer parameters that will determine drying efficiency and thus the success of the process.

The basic aim of the drying stage is to convert solution droplets to a dried particulate by solvent evaporation. The atomised droplets are sprayed into a drying chamber and dispersed in a heated drying gas to drive evaporation (Büchi Labortechnik 2007). The drying gas is circulated through the dryer by an aspirator motor and heated to a defined temperature by a heater. The heated drying gas enters the chamber with the droplets and will cause evaporation of the solvent from the droplets. The remaining dried particulates will then be

transported in the drying gas through the drying chamber to the final stage of the process. Given the significance of this step in dictating key particle attributes further consideration of key principles follows in the sections below.

The final stage and completion of the spray dryer process is the collection of the dried particulate mass which is achieved by separation of the particulates from the drying gas stream. The recovery of particulates is split into two types of separation, primary and secondary, that are dependent on particulate size. In primary separation, larger particulates that form the majority of product will separate from the drying gas at the base of the drying chamber (Figure 1.1) (Anandharamakrishnan and Ishwarya 2015a). For smaller particulates or 'fines' a cyclone is used as a secondary separation device to recover small particulates (Büchi Labortechnik 2007). The cyclone uses inertial and centrifugal forces to cause the drying gas to separate from the particulates by travelling in a downward outer vortex and meeting an inner vortex. This meeting is caused by the geometry of the cyclone which ensures that the drying gas enters a larger barrel and moves downward narrowing to a 'cone'. At this point particulates will fall through the cone into a collection vessel and the drying gas will continue in the inner vortex and be exhaled out of the dryer (Anandharamakrishnan and Ishwarya 2015a). Particle size is critical to the efficiency of particle recovery as particles of $<2 \mu\text{m}$ will remain in the drying gas and these can be recovered in a bag filter that is located at the exit point of the cyclone (Maury et al. 2005). Furthermore, the crucial process parameters that dictate the drying kinetics can have a detrimental effect on particle recovery by semi-dried droplets sticking onto the walls of the cyclone. Different cyclone geometries can overcome the recovery of small particles as smaller cyclones have been found to increase particle recovery by a higher level of separation and fine particle recovery (Bogelein and Lee 2010). The point of particulate collection is the endpoint of the drying process.

1.1.1.2. Drying Principles

To design and operate a robust spray drying process a detailed understanding of the different drying stages, rates and kinetics that govern the behaviour of the process is required. Drying can be split into two stages; spray-air contact and evaporation of moisture (Anandharamakrishnan and Ishwarya 2015b). The spray-air contact stage involves the meeting of the atomised droplets with the heated inlet gas. This leads to the initiation of evaporation. As the droplets are first mixed with the heated drying gas, the thermal energy from the gas is used for the evaporation of surface moisture of the droplets causing a rapid drying rate and reduction of gas temperature. At the same time the moisture from the droplets begins to saturate the drying gas until the equilibrium evaporation temperature is reached, also known as the wet-bulb temperature (T_{wb}). This process occur very rapidly and is estimated from (Vehring 2008) the solvent boiling point (T_b) and the gas outlet temperature (T_G):

$$T_{wb} = 137 \left(\frac{T_b}{373.15} \right)^{0.68} \log(T_G) - 45 \quad \text{Eqn. 1.1}$$

The next, most dynamic and significant stage within the drying process is that of evaporation of moisture enabling particle formation; this is the core task of spray drying and relies on heat and mass transfer rates influenced by temperature, vapour pressure and liquid diffusivity (Chen and Mujumdar 2009). This stage can be further split into a constant rate period and a falling rate period (Anandharamakrishnan and Ishwarya 2015b) as shown in Figure 1.2.

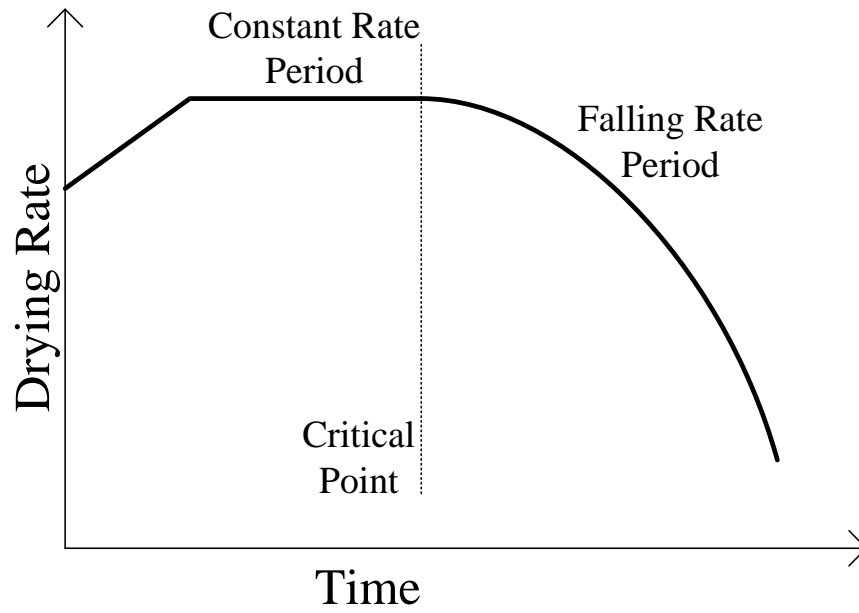


Figure 1.2. The drying rate trend through the progression of key drying stages of spray drying.

The constant rate period is defined by the evaporation rates and temperature changes of the droplets that determine the drying efficiency and dictate particle properties including morphology and density (Vehring 2008). At this point the droplet surface is saturated and is recorded at the wet-bulb temperature; the minimum temperature that will initiate evaporation in equilibrium with the gas and will remain constant through simultaneous heat and mass transfer rate (Chen and Mujumdar 2009, Huang 2011). From this point, evaporation of liquid from a droplet will reduce the droplet size (Chen and Mujumdar 2009). Simultaneously, the dissolved solute present in the liquid droplet will diffuse through the droplet. This is described by the diffusion coefficient, D (m^2/s) (Wilke and Chang 1955, Coulson and Richardson 1996) and the evaporation rate κ (m^2/s) (Vehring 2008):

$$D = \frac{1.173 \times 10^{-16} \varphi^{0.5} M^{0.5} T}{\mu V^{0.6}} \quad \text{Eqn. 1.2}$$

$$\kappa = 8D \frac{\rho_g}{\rho_l} (Y_S(T_e) - Y_\infty) \quad \text{Eqn. 1.3}$$

The diffusion coefficient and evaporation rates involve specific measurements of the solutes, solvents and drying gas used, such as solvent association factor (ϕ), solvent molecular weight (M), solvent viscosity (μ), droplet temperature (T), solute molar volume (V), drying gas density (ρ_g), droplet liquid density (ρ_l), and mass fraction of solvent at droplet surface ($Y_S(T_e)$).

Furthermore the dimensionless Peclet number, Pe , that describes the ratio of surface evaporation to solute diffusion has been shown to explain different particle densities (Vehring et al. 2007, Vehring 2008).

$$Pe = \frac{\kappa}{8D} \quad \text{Eqn. 1.4}$$

Where the drying process has a $Pe < 1$ then the diffusion of the solute is faster than the evaporation rate of the solvent meaning the solute can diffuse to the core of the droplet and create a particle of even composition. If the drying process has a $Pe \gg 1$ then the diffusion of the solute is slower than the evaporation of the solvent resulting in enrichment at the surface and shell formation of the solute, typically creating a hollow particle, refer to Figure 1.3.

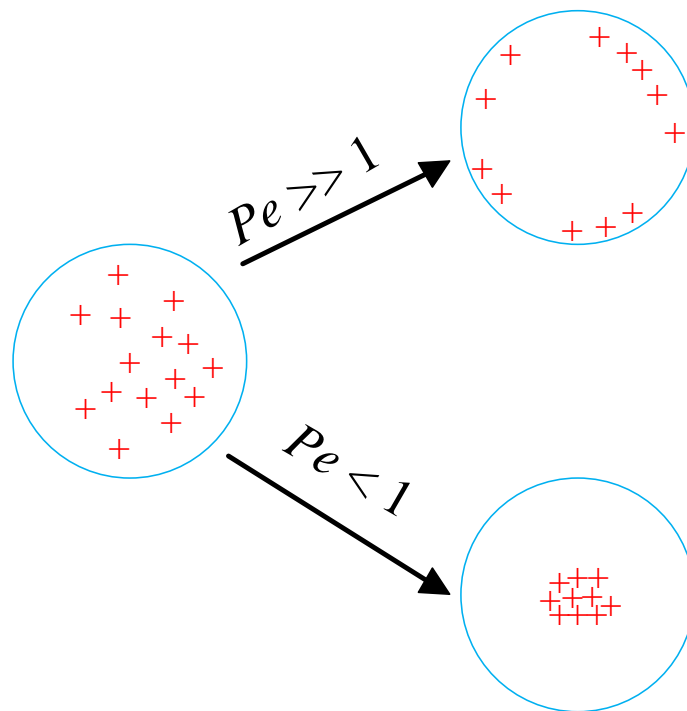


Figure 1.3. Schematic illustration showing expected particle structures formed under conditions of high and low Peclet numbers.

At the point where the droplet moisture is no longer in equilibrium with the drying air, the droplet has passed the critical moisture point and drying enters the falling rate period (Huang 2011). The mass transfer rate slows due to the formation and stabilisation of a crust at the surface (Litster 2016) and the droplet / particle temperature increases above the wet-bulb temperature to meet the outlet gas temperature normally just above the boiling point temperature of the solvent (Chen and Mujumdar 2009). This typically occurs near the end of the drying chamber with the drying gas near or at the outlet temperature; the coolest stage for the drying gas in the drying process. This controls the maximum droplet temperature as it can never go above the outlet temperature. As all remaining moisture or solvent evaporates and is removed from the solidifying droplet, particle formation is now complete with the last of the droplet liquid evaporated due to the increase in temperature.

The change in droplet temperature is key to the drying and solidification of particles during the process. The equilibration of the initial droplet to the wet-bulb temperature enables a constant rate of heat and mass transfer and once crust formation has occurred, the mass transfer rate decreases and the final drying rate is controlled by the heat transfer to the droplet resulting in the solidification of a particle. The behaviours of the different droplet components and the drying temperature and rates are defined as the heat / mass transfer principle of evaporative drying.

1.1.1.3. Spray Dryer Configurations

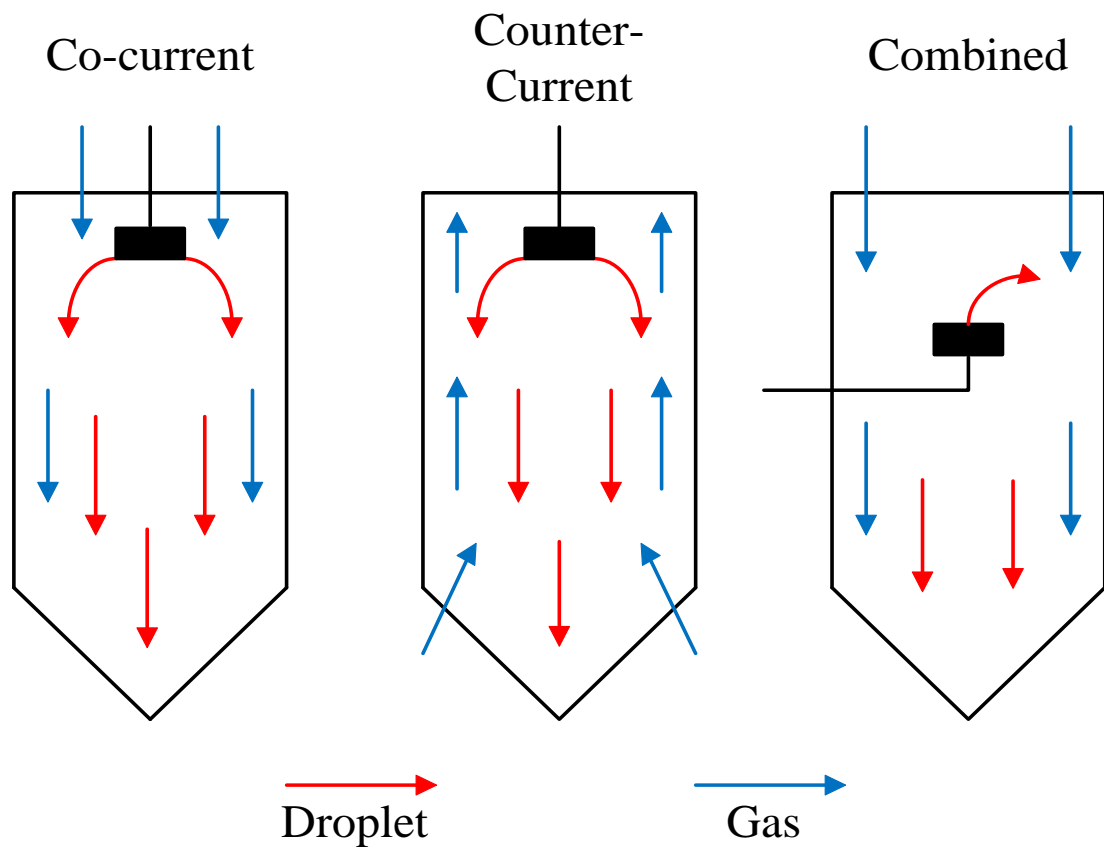


Figure 1.4. Schematic of spray dryer modes: Co-current, Counter-current and Combined.

There are several different processing modes and process parameters that can have a significant influence on the drying process. The first crucial decision that must be taken for drying efficiency is the drying chamber configuration. The dryer can exist in three different configurations that will change the manner in which the droplets and the drying gas will come into contact; these modes are called co-current, counter-current and combined mode, refer to Figure 1.4 (Büchi Labortechnik 2007). Co-current drying chambers work by introducing the droplets and drying gas in the same descending direction to the chamber; this ensures the droplets will meet the drying gas at its highest temperature and cause immediate evaporation (Cal and Sollohub 2010b). In co-current mode the droplets fall through the chamber in various air streams of the spray gas (Cal and Sollohub 2010a). This is the basis of the Büchi Mini-Dryer, shown in Figure 1.5. Counter-current drying chambers work by introducing the atomised droplets at the same point of the chamber and drying gas in opposite ends of the chamber. This results in the liquid droplets falling into the rising hot drying gas limiting the application of counter-current drying to thermally sensitive materials (Gharsallaoui et al. 2007). The final mode merges the principles of the two previous configurations, called combined mode, and introduces the droplets from the base of the chamber. Each mode provides a set of drying conditions that will be more appropriate for products that differ in thermal stability (Büchi Labortechnik 2007).

For the Büchi B-290 Mini Spray dryer, the dryer is configured with a co-current chamber design and can be operated in a further open or closed loop mode (Büchi Labortechnik 2007). These modes are designed so that the drying gas can either be exhaled from the dryer (open mode) or kept contained within the process (closed mode). The type of mode used is dependent on the solvent used; aqueous solvents can be operated in open mode while organic solvents must be operated in closed mode. Typically for open mode, aqueous solvents are used and the drying gas pulled in by the aspirator is air which will be exhaled at the end of the process containing the evaporated solvent. As organic vapours can be hazardous, it is

preferred to operate under closed mode with nitrogen acting as both the spray and drying gas. The gas is circulated through the dryer and into the coupled Büchi B-295 Inert Loop that will condense the solvent from the gas and collect the solvent separately.

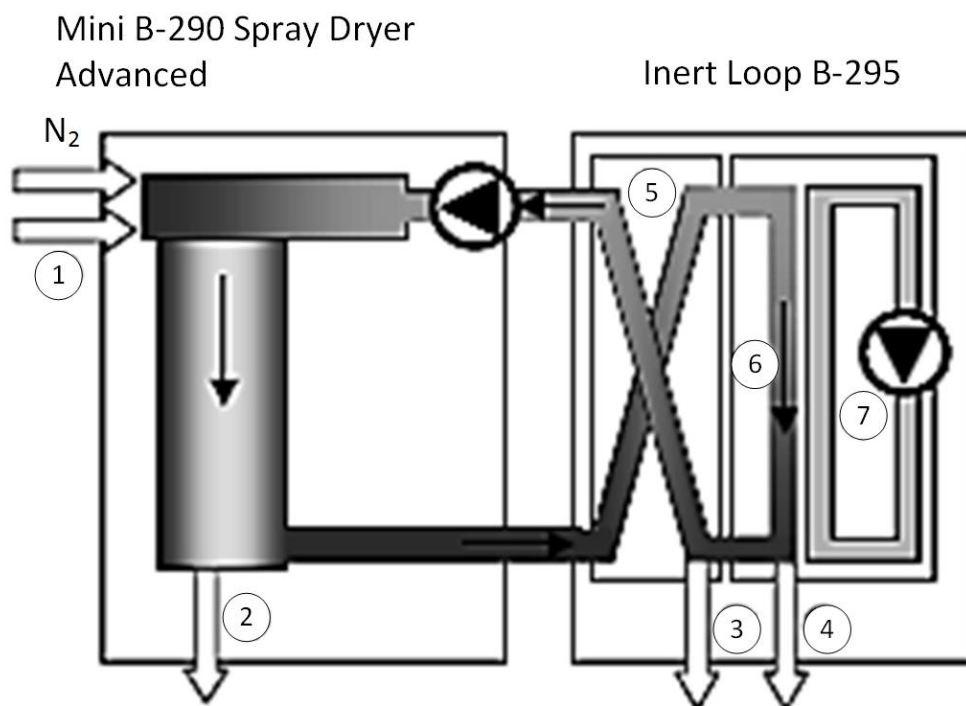


Figure 1.5. Closed mode operation of Büchi B-290 and B-295 Inert loop. (1) feed, (2) product, (3) exhaust gas, (4) solvent, (5) preheat exchanger, (6) condensation and (7) cooling unit (Büchi Labortechnik AG 1997 - 2002).

The different dryer modes and configurations will have a direct effect on the behaviour of the droplets within the chamber and thus the particulates that are produced.

1.1.1.4. Spray Drying Process Parameters

Spray drying can be a successful technique for a variety of different drying applications due to the range of control accessible from the different process parameters that can influence the process performance. It is clearly important to understand the role and effect that each

parameter has and how the combination of these parameters can be manipulated to produce the highest quality of product. For the lab-scale Büchi B-290 Mini spray dryer, there are key process parameters (Table 1.3) that are crucial to the success of the technique and can directly affect particle properties including size, moisture content and yield (Büchi Labortechnik 2007).

Table 1.3. Process parameters of the lab-scale Büchi B-290 Mini Spray Dryer (Büchi Labortechnik AG , Cal and Sollohub 2010b).

Process Parameters	Range	Units	Particle Property Examples Affected by Parameter
Aspirator Rate	0 – 100	%	Moisture Content (Ståhl et al. 2002)
Inlet Temperature	0 – 220	°C	Morphology (Walzel 2011) Hygroscopicity (Santhalakshmy et al. 2015)
Outlet Temperature	0 - 220	°C	Surface structure (Maas et al. 2011)
Spray Gas Flow Rate	200 - 800	L / h	Particle size (Kemp et al. 2015)
Feed Pump Rate	0 – 100	%	Particle size distribution (Anish et al. 2014)

1.1.1.4.1. Aspirator Rate

The aspirator rate is the first parameter that must be defined. An aspirator motor pulls the drying gas through the dryer at a controlled rate creating under-pressure in the dryer (Büchi Labortechnik AG 1997 - 2002). The setting of the aspirator rate will determine the volume of drying gas circulating in the dryer per unit of time and residence time of the drying mass.

The volume of drying gas will directly determine the evaporation capacity within the drying chamber and thus drying performance. Dependent on the particle properties sought, a change in aspirator rate can influence the moisture content of the particles (Ståhl et al. 2002).

1.1.1.4.2. Inlet Temperature

The inlet temperature is one of the most important parameters describing the drying process as it can have a direct influence over the drying kinetics and therefore dictates key particulate attributes of the final product. The inlet temperature is the temperature that the drying gas will be heated to on entry to the drying chamber and thus the temperature at the first point of contact with the droplets (Litster 2016) triggering evaporation. For the Büchi B-290 Mini spray dryer the drying gas is pulled by the aspirator into the drying chamber through an electric heater that will heat the drying gas to the temperature set by the operator (Büchi Labortechnik 2007). Due to the influence of temperature on the drying kinetics, the inlet temperature is an intrinsic parameter that can affect several physicochemical properties, such as morphology (Walzel 2011) and hygroscopicity (Santhalakshmy et al. 2015).

1.1.1.4.3. Outlet Temperature

To achieve the most appropriate drying environment for the droplets through the temperature gradient across the drying chamber, it is important to understand the influence of the outlet temperature. This temperature is taken from the exit point as droplets leave the chamber and enter the cyclone dispersed in the drying gas. To ensure that the solvent can be fully evaporated from the droplets it is essential that the outlet temperature is close enough or higher than the boiling point of the solvent (Litster 2016). For the Büchi B-290 Mini spray dryer this parameter is unique from the other important parameters as it cannot be set directly by the instrument. To gain control over the outlet temperature understanding of the relationship between three other parameters is required; inlet temperature, aspirator rate and

feed rate (Büchi Labortechnik 2007). As the outlet is a derivative of the inlet temperature, increasing the inlet will increase the outlet (Cal and Sollohub 2010a). By decreasing the aspirator rate, the volume of spray gas decreases thus causes the decrease in the gradient of the gas temperature and therefore the decrease in outlet temperature. If the feed pump rate is decreased it will increase the outlet temperature as the required enthalpy per unit of solvent will decrease. The outlet temperature has been found to influence the surface structure and therefore the interaction forces between particles, highlighting the importance for outlet temperature understanding (Maas et al. 2011).

1.1.1.4.4. Spray Gas Flow Rate

The spray gas is an integral part of the atomisation stage of the spray drying process as it acts as the driving force behind droplet creation. The spray gas is delivered to the atomiser under high pressure which on impact to the droplets is what will propel the droplets to the nozzle and spray the atomised droplets into the drying chamber (Büchi Labortechnik 2007). In closed mode for the Büchi B-290 Mini spray dryer the spray gas acts also as the drying gas and this is commonly nitrogen; the spray gas is circulated through the Büchi B-295 Inert Loop and is pulled through the heater by the aspirator motor. The flow rate of the spray gas sets the volume of drying gas per unit time available to dry the droplets (Cal and Sollohub 2010a) and the speed in which the gas travels through the atomiser can influence the droplet size and in turn effect the particle size (Kemp et al. 2015).

1.1.1.4.5. Feed Pump Rate

The feed pump rate is the final parameter to be determined for the process but must be taken into consideration in conjunction with the other parameters. The liquid is transported to the nozzle by a peristaltic pump and can have a direct effect on the drying efficiency of the process (Büchi Labortechnik 2007). A higher feed rate will supply a higher mass of drying

feed to the chamber per unit time directly affecting the temperature gradient between the inlet and outlet temperature and as such influencing the drying kinetics. Similarly to the spray gas rate, the feed flow rate can directly affect the particle size distribution due to the ratio of feed to drying gas per unit time and the effect this ratio has on droplet size and kinetics (Anish et al. 2014).

1.1.1.4.6. Other Parameters

To fully understand and successfully operate the spray dryer there are other process parameters that can dictate and influence the drying kinetics and as such affect the particle properties. These parameters also require understanding and control and are presented in Table 1.4 below.

Table 1.4. Other material parameters relevant for spray drying.

Other Parameters	Particle Property Example Affected by Parameter
Feed Composition	Surface composition (Porowska et al. 2016)
Feed Concentration	Particle size (Elversson et al. 2003)
Solvent Selection	Porosity (Ni Ogain et al. 2012)

1.2. Crystallisation

Crystallisation is a manufacturing process fundamental to a wide range of chemical industries for the separation and purification of intermediates and final products (Shekunov and York 2000). With regards to the pharmaceutical industry, crystallisation is intrinsically crucial to the manufacture of active pharmaceutical ingredients (APIs) and can dictate the ease of manufacture and performance of APIs through its dominant influence over

recrystallised particle properties (Chen et al. 2011). For the production of APIs certain particle attributes such as crystal structure, habit, purity, size and yield are vitally important to control and possible variations can have a serious impact on downstream processing, pharmaceutical efficiency and safety of the final product (Shekunov and York 2000, Chow et al. 2008, Tung 2013).

Crystallisation from solution involves the process of solid crystal formation and relies on interactions between the different components that exist within a system (Davey and Garside 2000). The different phases that make up a system are the solute, solvent and solution and it is the state of each of these phases with respect to each other that will determine the progress and outcome of the crystallisation process. At the point in which the chemical potentials of the solid (μ_{solid}) and the solute in solution (μ_{solution}) are equal, a solution can be described as in equilibrium and is described as saturated ($\Delta\mu = 0$).

$$\Delta\mu = \mu_{\text{solution}} - \mu_{\text{solid}} \quad \text{Eqn. 1.5}$$

When a solution exists with an excess chemical potential of solvent, the solution is undersaturated. In this state, the addition of further solid will lead to dissolution. Inversely, when a solution exists with an excess chemical potential of the solute, the solution is supersaturated; this is the only solution state in which crystallisation can occur and the extent of supersaturation provides the thermodynamic driving force for crystallisation (Schwartz and Myerson 2002). To enable the expression of supersaturation, first the chemical potential is defined in terms of the standard potential (μ_0) and standard activity (α) shown in Eqn. 1.6.

$$\mu = \mu_0 + RT \ln \alpha \quad \text{Eqn. 1.6}$$

Allowing α to represent the standard activity of the solution phase and where R = gas constant and T = absolute temperature, the fundamental supersaturation (S) can be expressed through the revision of Eqn. 1.5 as the ratio of α to the standard activity of the crystalline phase (a^*) shown in Eqn. 1.7.

$$\frac{\Delta\mu}{RT} = \ln\left(\frac{\alpha}{a^*}\right) = \ln S \quad \text{Eqn. 1.7}$$

where $\Delta\mu$ = chemical potential difference. Supersaturation is typically expressed in terms of concentration:

$$\ln S = \ln \frac{c}{c^*} \quad \text{Eqn. 1.8}$$

where c = actual solute concentration and c^* = equilibrium solute concentration (at constant temperature and pressure). Furthermore, to simplify with respect to relative supersaturation, σ , supersaturation is defined as follows.

$$S = \sigma + 1 \quad \text{Eqn. 1.9}$$

To distinguish between different saturation levels, the solubility is expressed as the point at which the solute and solvent are at equilibrium at a given temperature and pressure (Davey and Garside 2000). This will create a solubility curve that shows the regions of undersaturated and supersaturated, presented schematically in Figure 1.6.

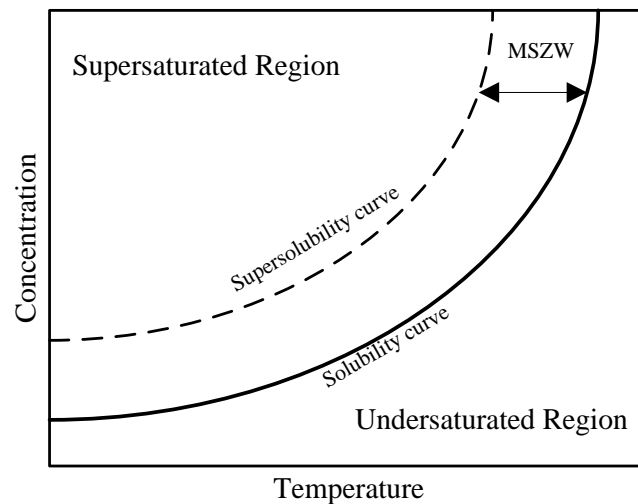


Figure 1.6. Schematic of solubility curve in relation to concentration versus temperature detailing regions of undersaturation, metastable zone width (MSZW) and supersaturation.

The metastable zone width (MSZW) is the region above the solubility curve but below the supersolubility curve in which spontaneous crystallisation is unlikely (Mullin 2001). At a point where the solution composition lies within the metastable zone, whilst supersaturated, only growth will be observed. As supersaturation is increased it passes the supersolubility curve into the supersaturated (labile) region, the first stage of crystallisation, namely nucleation can occur enabling the creation of a new solid phase (Myerson and Ginde 2002). This new solid phase has been formed through the change of solute phase; transforming from its dissolved state in solution to a new solid phase in order to reduce the excess chemical potential. The process of nucleation in solution involves solute molecules associating together to form a cluster, which once successive collisions and additions have occurred, reach a critical size, r_{crit} , and forms a stable crystal nuclei (Erdemir et al. 2009). The exact size of crystal nuclei is not directly measurable, however may contain tens to hundreds of molecules packed together with relatively weak intermolecular forces (Mullin 2001). Above the critical nucleus size the total free energy difference (ΔG) for the crystal nuclei, comprising the sum of free energy required to create a surface (ΔG_s) and the volume free

energy (ΔG_v) means it is more favourable for the nucleus to grow (Eqn 1.10) (Davey and Garside 2000).

$$\Delta G = \Delta G_v + \Delta G_s \quad \text{Eqn. 1.10}$$

Therefore, to stabilise a crystal nuclei the cluster must reach a size in which the free energy of the volume will outweigh the free energy of the surface of the cluster; the cluster will then have reached critical size (ΔG_{crit}) and thus stabilise and allow growth to occur. This process is described by classical nucleation theory (CNT) which was developed by Gibbs in the 19th century (Erdemir et al. 2009).

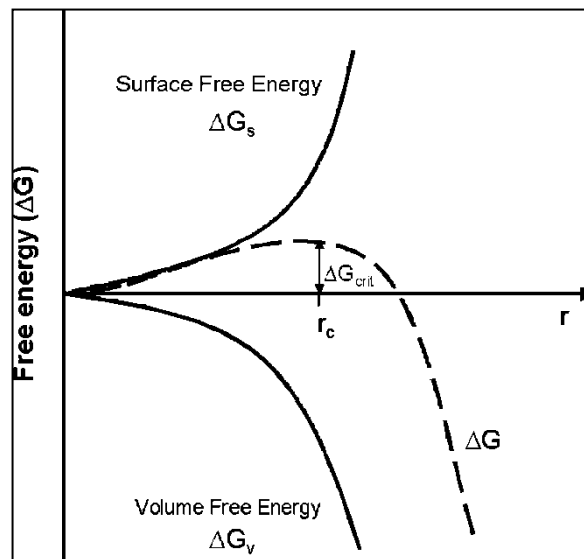


Figure 1.7. Free energy diagram for nucleation (Erdemir et al. 2009).

The critical size for nucleation will be influenced by the supersaturation level; at high supersaturations the free energy (ΔG) and cluster size is lower which in turn will lead to a faster rate of nucleation (Davey and Garside 2000, Myerson and Ginde 2002). Nucleation is a complex process however and the rate of nucleation can also be affected by stirring (Sypek

et al. 2012), volume (Kadam et al. 2011) or the presence of particles or impurities (Mullin 2001).

In a solution, nucleation can occur spontaneously or by artificial induction and these are classified as primary or secondary nucleation (Mullin 2001). Primary nucleation is defined as the occurrence of a nucleation process where no crystalline material is present in the system prior to the nucleation event (Mullin 2001). Primary nucleation can be further sub-divided depending on the purity of the system. Homogeneous nucleation is the formation of solid molecules from a homogeneous liquid phase. However, it is generally accepted that in most practical circumstances almost all crystallisation takes place in the presence of trace impurities or foreign particles suspended in the solution (Mullin 2001). Therefore, in primary nucleation it is more common in the vast majority of practical situations for heterogeneous nucleation to be the dominant process. Heterogeneous nucleation will occur in the presence of solid impurities that provide an adsorption surface for solute molecules reducing the free energy barrier required for the formation of critical nuclei (Davey and Garside 2000).

The second main classification of nucleation is termed secondary nucleation (Mullin 2001). This type of nucleation occurs in a system, where crystals are already present that induce further nucleation of new crystals. This is commonly achieved by deliberate seeding; through the inoculation of a supersaturated solution with small particles of the desired product crystals to be grown from the solution (Mullin 2001). Secondary nucleation is also a relatively complex process with several mechanisms having been reported in different systems; initial breeding, needle breeding, polycrystalline breeding and collision breeding (Mullin 2001, Myerson and Ginde 2002). Agitation of the crystals within the crystalliser and collisions between crystals, the vessel walls and impellers have been shown to contribute to the overall rate of secondary nucleation in supersaturated solutions. Seeding is regularly used in industrial crystallisation to govern the product size and particle size distribution that will

be gained from the crystallisation without reliance on primary nucleation (ter Horst et al. 2015).

The establishment of a stable critical nucleus enables the progression from nucleation to crystal growth. In this phase, stable nuclei exist in a supersaturated solution and attract solute molecules to the nucleus surface (Davey and Garside 2000). Mass transfer of solute from the bulk to the surface is followed by adsorption and integration of these growth units into the lattice of the crystal faces. This process is the basis of the crystal growth model with the principle based on the growth units binding in a sequential manner under the influence of supersaturation (Mullin 2001). Crystal growth (G) can be expressed in its simplest form by the rate of length (L) increase (Eqn. 1.11).

$$G = \frac{dL}{dt} \quad \text{Eqn. 1.11}$$

Growth kinetics can be expressed in terms of supersaturations through fundamental rates of nucleation (B) (Eqn. 1.12) and growth (Eqn. 1.13).

$$B = k_b \Delta c^b \quad \text{Eqn. 1.12}$$

$$G = k_g \Delta c^g \quad \text{Eqn. 1.13}$$

Where k_b is the nucleation rate constant, b is nucleation order, k_g is the growth rate constant and g is the order of growth.

The rate of growth unit binding creating crystal faces and growth layers will depend on the strength of surface and growth unit interaction (Davey and Garside 2000). The size of crystal faces are dictated by the rate and direction of growth due to the underlying lattice structure

and molecular recognition processes. As a consequence of the anisotropic nature of organic crystal lattices, crystals can exhibit different habits with variation of the specific faces expressed on the surface of the crystal (Mullin 2001). Molecular crystals can show a wide range of morphologies from plates, prisms through to elongated needles (Mullin 2001). Morphology can be affected by the rate of growth, solvent or impurity adsorption at specific faces impeding integration of solute growth units.

1.2.1. Continuous Crystallisation

The traditional and most widely used and accepted method for pharmaceutical manufacturing through crystallisation is by the batch method; large quantities of raw material processed over long periods of time to produce solids typically by stirred tank reactors. However, this method can have detrimental and serious complications during manufacture as process variability will have direct effects on the product outcomes of further downstream processing steps (Chen et al. 2011). To overcome these issues, the alternative continuous manufacturing methods could be adopted. Continuous manufacturing applies an integrated and systematic approach to manufacturing with end-to-end process monitoring, control and modelling (Badman and Trout 2015). Continuous aims to provide consistent and sustainable manufacturing methods that deliver uniform and reproducible conditions to create products under a higher degree of control (Badman and Trout 2015). This should in turn enable better, more quality products to be made. Some of the challenges for adoption of continuous processing include increased use of modelling, standardisation of equipment for flow processing, the development of toolboxes for different processing stages, exploitation of PAT for real time control and real time release testing (Baxendale et al. 2015). In addition, there is a need for the development of skills in the future workforce to develop and operate these new manufacturing technologies including advanced control strategies.

1.3. Particle Types

Within the pharmaceutical application of spray drying there are many different particle types that can be used and produced. The particle types that will be relevant to this project have been clearly defined in Table 1.5.

Table 1.5. Definition of relevant particle types for spray drying.

Particle Type	Definition
API	An active pharmaceutical ingredient is the compound in which gives the pharmaceutical response that the drug product aims to achieve
Excipient	A molecule that is combined with the API to create a formulation that can be aide the drug processing and delivery
Co-crystal	A molecular complex that consists of 2 or more different molecules
Co-former	A molecule that combined with an API can form a co-crystal
Composite	A single particle consisting of different components
Amorphous	A particle with a disordered molecular structure
Crystalline	A particle with ordered molecular structure
Molecular Dispersion	A particle that consists of a API dispersed within a co-former

1.3.1. Critical Quality Attributes

Quality by design (QbD) is an approach to enhance the quality of pharmaceutical products through the application of scientific understanding (Yu 2008). For an API to be developed into a formulation and medicinal product it is important to fully understand the relevant critical quality attributes (CQA). By developing a knowledge of the dependence of CQAs on critical material attributes (CMA), relating to the physical properties of the component materials, and critical process parameters (CPP), defining the processing history of the

materials, CQAs can be delivered more consistently. The CMAs enable an acceptable range of material properties to be specified for raw materials or intermediates that when processed under conditions that lie with an acceptable range of the CPPs will assure CQAs are achieved (Rathore 2009, Yu et al. 2014). CQAs for an API may include particle size and distribution, morphology, polymorphic form, purity and yield (U.S. Food and Drug Administration 2009, Yu et al. 2014).

1.3.1.1. Particle Size and Size Distribution

A fundamental CQA for manufacturing is the size and size distribution of particles. This attribute is highly important as it can determine the API's ability to be manufactured into formulations and products and furthermore, it can have a significant effect on the performance of the API (Price 1997). Particle size is typically measured as the geometric diameter of a particle but depending on the nature of the particle and method of measurement particle size values may be represented in a number of ways (Vehring 2008). As it is impractical to monitor individual particle sizes, the most common measure used is the particle size distribution of the crystalline product (Mullin 2001). This test enables a measure of the degree of fineness and coarseness of the population of particles in the product size distribution. Particle size measurement can be carried out by a number of techniques (Section 1.3.2). Typically, a narrow size distribution would be the ideal result, comprising a product with a uniform, narrow range of particle sizes. This uniformity is important for the pharmaceutical industry for a variety of reasons; uniform particle size improve manufacturing quality and accuracy as well as a uniform performance (Mullin 2001). Particle size distribution can affect filtration performance (Chang et al. 2008), mixing and segregation (Gray and Chugunov 2006) and dose uniformity (Rohrs et al. 2006).

1.3.1.2. Particle Morphology

Particle morphology is an important attribute that can influence bulk performance of an API that in turn will have a significant effect on downstream processing and formulation efficiency. Morphology can be expressed through variations in shape, structure and surface properties (Vehring 2008). Under standard solution crystallisation methods, typical crystal morphologies include needle, prism and cubic. The resulting morphologies are dependent on the preferential growth rates of the crystal faces (Mullin 2001). Crystal morphology can be calculated using the Bravais-Friedel-Donnay-Harker (BFDH) method by assuming the binding energy of the crystal lattice governs the intermolecular forces of the crystal faces. The different crystal morphologies can vary considerably due to the interaction of the intermolecular forces of the faces with solvent, growth rate dispersion and supersaturation so this is a complex problem to control. Spray drying however, will be expected to produce a different range of particle morphologies and shapes compared with standard solution crystallisation methods due to the specific crystallisation kinetics arising from rapid drying and the localised nature of particle formation within a droplet impacting mass transfer. Due to the creation of spherical droplets, the typical particle structure will tend to be spherical in shape. Particle formation occurs through heat and mass transfer processes govern the rates at which dissolved solute will diffuse through a droplet relative to the rate of evaporation of solvent from the droplet surface. The balance of these parameters can lead to the formation of either a shell of solid on the droplet surface (Figure 1.3) or where solute diffusion exceeds the rate of solvent evaporation a solid core may be expected to form. This can be represented by a Peclet number, Pe (Eqn. 1.4). For conditions that create low Peclet number ($Pe \leq 1$), typical particle structures include solid cores or evenly distributed crystallites throughout the dried solid that show a density close to true density of the solute (Vehring 2008). For high Peclet number conditions ($Pe \geq 1$) a wider range of particles morphologies may occur depending on the surface properties of the droplet shell (Vehring 2008). For $Pe < 20$, the concentration of crystallite at the surface in relation to the average solid concentration can be

estimated to determine the level of surface enrichment (E), Eqn. 1.14 (Vehring 2008) where (c_s) is the surface concentration and (c_m) is the average concentration.

$$E = \frac{c_s}{c_m} = 1 + \frac{P_e}{5} + \frac{P_e^2}{100} - \frac{P_e^3}{4000} \quad \text{Eqn. 1.14}$$

If the shell solidifies quickly, a rigid hollow particle will form; if the shell is too slow to solidify then a particle structure with dimpling is likely to occur (Vehring 2008). These principles have been applied to a wide range of particle engineering strategies for spray dried particles. For example, spray drying of budesonide to produce a PulmoSphere, a particle that is hollow and porous, to improve lung delivery by passive dry powder inhalers (DPI) (Duddu et al. 2002), improving delivery of poorly water soluble particles by amorphous solid dispersions (Singh and Van den Mooter 2016) and dissolution enhancement of carbamazepine, indomethacin, piroxicam and nifedipine (Martins et al. 2012a).

1.3.1.3. Solid-State Form

Polymorphs are distinct crystalline structures that have identical chemical composition (Brittain 1999, Sarma et al. 2011). Polymorphism can occur during the process of crystal nucleation where differing lattice arrangements of the same original API are produced. Polymorphism can be affected by different solvents (Khoshkhoo and Anwar 1993, Gu et al. 2001), supersaturation, agitation or shear (Sypek et al. 2012) or by impurities (Poornachary et al. 2008). Significant effort is often applied to early preclinical development to evaluate the extent of polymorphism that a given molecule may display and the conditions under which they can be formed. This is carried out by screening a wide range of conditions and characterising the resultant crystal form (Florence 2009).

Different polymorphs display distinct properties due to the differences in packing and lattice energy. These include melting point, hygroscopicity, compressibility, surface energy and solubility (Brittain 2009). For example, the different polymorphs of L-glutamic acid, α and β , have different solubilities in different aqueous solvent mixtures (Mo et al. 2011). Under rapid crystallisation conditions with elevated supersaturation, metastable polymorphs can often be produced. However the lowest free energy at ambient T and P displays the lowest solubility and is therefore commonly selected for development as it presents the lowest risk to uncontrolled transformations to alternative crystal structures (Mullin 2001). However exposure to elevated temperature, contact with liquid or wetting and drying cycles or mechanical forces can induce polymorphic transformations. These transformations in some cases are interconvertible by a transition of solubilities of the stable and metastable forms; these are described as enantiotropic (Mullin 2001). For polymorphic systems in which the solubilities do not contain a transition point, they are described as monotropic. It is therefore important to define the thermodynamic relationship between any polymorphs that are identified from initial screening.

Solubility is important as variation can impact the oral bioavailability of the API and impact on the efficacy or safety of the product to the patient. If an undesired polymorph of high solubility is crystallised and formulated into a drug product this could lead to an overdose of the API in the patient and could have a fatal result (Brittain 2009). Alternatively, if a low solubility is produced the product may be rendered inactive, the classic example being Ritonavir (Bauer et al. 2001). It is for this reason that pharmaceutical companies try to regulate and control the production and consequence of polymorphism to ensure that it is only the desired polymorphs with specific properties are formulated into drug products. Methods to produce polymorphic forms in a controlled and consistent manner are therefore of considerable interest to enable control over material performance.

However, different compounds may produce more than one polymorphic form with only one form classified as thermodynamically stable at a given temperature. This polymorph will have the lowest Gibbs free energy and therefore have the lowest solubility in any solvent (Sarma et al. 2011). All further remaining polymorphs are less stable and classified as metastable or unstable depending on the ease with which they transform to the most stable form. One of the main challenges that the pharmaceutical industry faces in controlling quality is uncontrolled polymorph transitions of metastable polymorphs into more stable forms (Sarma et al. 2011). This can happen at various different stages within the manufacturing process so it is for this reason that the most stable polymorph is favoured for drug formulations. As the solubility and many other properties of the various polymorphs can vary, the transformation of different polymorphic forms can change the properties of the drug formulation which could result in a product that will not deliver the desired attributes in which the pharmaceutical industry intended. It is for this reason that many compounds undergo polymorphic screening to determine the number and properties of the different polymorphs that result from the crystallisation of the original compound.

In addition to polymorphic forms, APIs can form a range of other crystalline, multicomponent forms. These include salts, solvates and co-crystals. Whilst crystal structure prediction tools are developing (Price 2014, Wicker and Cooper 2015) it is still not possible to routinely predict which crystal structures can be produced from a given API and screening is relied upon to identify potential candidates. Consideration for possible development will depend on the physical properties and stability displayed by each form. Solvates can be used as the final form for formulation or used as a route to produce further new forms through desolvation (Sarma et al. 2011).

In addition to crystalline solids, molecular APIs can adopt non-crystalline or amorphous structures. These solids lack long range crystalline order and are less thermodynamically

stable than crystalline forms. As a consequence they display favourable attributes such as enhanced solubility (Yu 2001, Murdande et al. 2010, Babu and Nangia 2011) but can show a strong tendency to recrystallize. As a consequence there is considerable interest in formulation approaches to stabilise amorphous forms including molecular dispersions or co-amorphous forms (He and Ho 2015, Dengale et al. 2016). For example, spray drying of indomethacin with silica to create a solid dispersion improved dissolution properties (Takeuchi et al. 2005).

1.3.2. Particle Attribute Measurements

The control of CQAs by the understanding of CPPs and CMAs rely on measurement and characterisation of the particle properties. Accurate particle descriptions are crucial to the design and development of manufacturing processes ensuring that the best quality formulation and drug product can be achieved. Measurements can be conducted by offline and online techniques with the relevant techniques used in this thesis detailed in Table 1.6.

Table 1.6. Different analytical techniques used to measure particle attributes.

Particle Attribute	Method of Analysis
Particle Size	Optical microscopy, scanning electron microscopy (SEM)
Particle Size Distribution (PSD)	Optical microscopy, SEM
Particle Morphology	Optical microscopy, SEM, Raman mapping
Solid-State	X-ray powder diffraction (XRPD), differential scanning calorimetry (DSC), Raman spectroscopy

1.4. Spray Drying Applications

The pharmaceutical industry is continually driven by the target of developing and improving medicinal products that perform to the highest possible quality. This can be achieved through engineering current technologies to optimise the quality of products. The European Medicines Agency defined this objective by saying *“the goal of manufacturing process development for the drug substance is to establish a commercial manufacturing process capable of consistently producing drug substance of the intended quality”* (European Medicines Agency 2011). Therefore, engineering of critical quality attributes of a given API is an important opportunity for research as it can gain a large reward for industry.

Spray drying offers a flexible and controllable process to explore and engineer different particle properties and structures to target better, more efficient medicines. Current published literature of spray drying research covers a wide range of applications and some areas that show clear opportunities to deliver better medicines are highlighted below.

1.4.1. Particle Optimisation

Spray drying technique has been extensively researched to optimise a wide variety of pharmaceutically relevant compounds for a variety of different applications. This can be achieved through in-depth investigations and manipulation of the process parameters to target specific particle properties such as solubility and oral bioavailability.

Of the various process parameters accessible drying temperature is a key factor that can influence different particle attributes of a compound. Predominantly the drying temperature can determine the physical form of a compound and as such has a direct effect on crystal form, structure and polymorphism. Buckton and co-workers (Buckton et al. 2002) investigated the effect of feed temperature on the crystallisation and physical form of lactose.

As the most common application of spray drying is to produce amorphous particles, the feed temperature was varied for four temperatures to investigate if a higher degree of crystallinity can be found for α -lactose monohydrate. Buckton and co-workers found that changing feed temperature will have an effect on the drying time and thus will directly affect the crystallisation behaviour of α -lactose monohydrate.

However, crystallisation behaviour during spray drying is complex and must include consideration of the other environmental factors influenced by the process parameters. Prinn and co-workers (Prinn et al. 2002) investigated the influence of several different parameters on powder characteristics of bovine serum albumin. The selected parameters measured were solution feed rate, atomising nitrogen flow rate, drying air rate and drying air temperature. This study found that the combination of these parameters can affect particle size, outlet temperature and yield characteristics and that a model can be created to allow a degree of control over the resulting powder in terms of these attributes.

Likewise, Bianco and co-workers (Bianco et al. 2012) looked to investigate the influence of different process configurations and solution characteristics on the solid state manner of sulfathiazole and sulfathiazole sodium. This compound and its salt were selected due to their large number of known physical states, such as polymorphs and hydrates, and were targeted through the different drying modes of the spray dryer and solvent systems for the two compounds. This study emphasised the point that the different modes, parameters and initial particle system characteristics will affect different environmental conditions, such as humidity and pressure, and thus affect the drying ability and kinetics during spray drying. Bianco and co-workers proposed that spray drying can act as an alternative method for crystallisation and suggest that it may be most viable in crystallisation of highly polymorphic compounds.

Investigations into the use of spray drying as a method to overcome certain obstacles faced by the pharmaceutical industry has shown the potential of the technique. The development of new and adapted drug formulations can be tested using spray drying to achieve a better performance of the current drug formulations and mitigate the need for drug discovery. Yi and co-workers (Yi et al. 2008) looked to create a new solid self-microemulsifying formulation by spray drying and thus improve the oral bioavailability of a poorly water-soluble drug, nimodipine. The study compared the new solid formulation to the pre-existing liquid formulation and found that both particle and bulk properties correlated with the performance of the initial liquid formulations in terms of dissolution and absorption enhancement. Yi and co-workers therefore underlined the ability of the spray dryer to act as a method to provide new drug formulations.

Not only does the spray dryer provide a method of investigating API particle properties and formulations; it can be used to study excipients and carrier particles crucial to formulations and secondary processing. Sloth and co-workers (Sloth et al. 2009) targeted commonly used excipient and carrier particles to gain understanding and investigate the influence of the drying process through spray drying. The authors reported that as the drying process within the spray dryer is highly complex and significantly influenced by the unique environmental conditions, gaining accurate data for drying kinetics are likely to be unachievable; this resulted in the authors studying a purpose built droplet dryer (Jørgensen and Engineering 2005) in which the droplets are created at the entrance of a drying tower at which they are mixed with a heated gas and fall down the tower. Sloth and co-workers found that the inclusion of different compounds can either increase or have no effect on the droplet temperature based on the chemical structures of the compound. This increase will have a subsequent effect on the drying rate and thus can influence particle properties such as particle morphology that can be important in the success of excipients and carrier particle function in formulations.

A large focus within the literature for inhaled drug delivery is the effect of spray drying on excipients. Sarrate *et al.*, 2015 (Sarrate et al. 2015) chose to study the influence of the pneumatic two fluid nozzle in the spray dryer on the morphology, particle size and distribution and the compressibility. The excipients were classified as soluble, partially soluble and practically insoluble in water with spray dryer settings made specific for each. The overall results for the excipients found that the flowability and compressibility of the bulk is greatly influenced by the changes at particle level and the attributes targeted are the most crucial.

1.4.2. Multicomponent Systems

Spray drying has been extensively studied as an approach to co-process multiple components to create a wide variety of formulated particles. Multicomponent particles can exist in a physical mixture as composites or in a chemical mixture with the production of co-crystals. These particles can be used to reduce formulation processing steps, improve CQAs of actives and overcome delivery issues.

Many studies have used spray drying to improve the performance of poorly soluble compounds by targeting particle engineering. Boraey *et al.*, 2013 (Boraey et al. 2013) investigated spray drying budesonide in combination with leucine in a mixed solvent system of water and ethanol with the hope to improve the dispersibility of budesonide. Budesonide has a reported aqueous solubility of $28 \mu\text{g ml}^{-1}$ at 298 K (24.85 °C) and if spray dried from pure ethanol will cause highly cohesive particles. Leucine was used as an enhancer for dispersibility and process engineered to enable leucine to precipitate first and form a solid shell surface from the droplet containing the budesonide solution. Boraey and co-workers found that budesonide was partly encapsulated by leucine with dispersibility improved and particles meeting standard requirements for inhalation delivery.

As well as co-processing an active compound with excipients, spray drying can also spray dry an active with another active compound to form a composite. Tajber and co-workers (Tajber et al. 2009) aimed to spray dry budesonide with another inhalation API, formoterol fumarate, to investigate the influence of the process parameters on dried particle characteristics. The spray dryer parameters that were varied were the inlet temperature, spray dryer airflow rate, pump rate, aspirator setting and feed concentration to influence the physicochemical, micromeritic and aerodynamic properties of the composite particles. The result of this study found that air flow and feed concentration were the most influential of the five parameters varied and the composite particle demonstrated an improved aerodynamic performance through a 2.6-fold respirable fraction increase and better dose uniformity.

Research conducted by Coucke and co-workers aimed to improve the bioadhesive nasal delivery of a maize starch with a polymer by spray drying (Coucke et al. 2009b). The study focussed on the co-processing of the two compounds and to investigate if, done by spray drying, the formulation will improve in efficiency and the process can be achieved in a simple step. A feature that can indicate the performance of the formulation is the particle size and if it is in the uniform range which is required for nasal delivery. However, the investigations found that the spray drying technique even though it is a single step process, did not add value to the bioavailability of the formulation.

Current research into spray drying for pulmonary drug delivery spans a range of effective strategies. Labiris and co-workers (Labiris and Dolovich 2003) detailed the different devices, nebulizers, pressurised metered dose inhalers (pMDIs) and dry powder inhalers (DPIs) that can deliver drug products to the lungs and discussed how changing the formulation can provide an improved therapeutic result. DPIs are of specific interest for pulmonary drug delivery as they can reduce patient handling errors found for pMDIs as they rely on self-

respiration and not co-ordination. In relation to spray drying, it detailed the new formulation of a large hollow porous particle names Pulmospheres™ (Labiris and Dolovich 2003) that are compatible with pMDIs and DPIs. These new particles have been found to have low particle densities and better dispersibility whilst still meeting the aerodynamic property requirements for inhalable products. This is achieved by the large geometric size and low particle density combined with the porous structure of a particle which performs the same as a particle with a small geometric diameter. Pulmospheres™ can be produced through spray drying of an oil-in-water emulsion through the delay of shrinkage and pores formation by the oil that is serving as a ‘blowing agent’. It is proposed that Pulmospheres™ can improve the bioavailability of drugs.

Some research has also been conducted to investigate the capability of spray drying to engineer nanoporous microparticles (NPMPs). Nolan and co-workers (Nolan et al. 2009) targeted NPMPs of budesonide through spray drying in combination with ammonium carbonate in a mixed solvent system of ethanol and water. The particle attributes that were targeted in this study were the particle size, density, surface area and also *in vitro* deposition was measured to determine aerodynamic performance. The results from these characterisations were compared to the standard solid particles of budesonide to highlight the potential of this method. It was found that NPMPs of budesonide exhibited a better aerodynamic performance than the standard solid particles and that these particles have the potential to improve the oral inhalation drug delivery of budesonide.

Spray drying can be used to improve the formulation characteristics of crystalline particles so as to eliminate subsequent downstream processing steps. The aim is to improve control over powder production and streamline the overall manufacturing process. One approach that has been studied is the co-processing of an API with excipients to create a powder that can provide better compressibility; this would allow granulation for example to be avoided.

There have been many papers published by the Gonnissen, Remon and Vervaet groups into the use of a spray dryer to produce composite powders that are directly compressible.

Gonnissen and co-workers co-processed an API with excipients to produce directly compressible powders from a continuous spray drying technique (Gonnissen et al. 2007). Spray drying was used to co-process acetaminophen with different carbohydrate excipients to improve the compactability, flowability and hygroscopicity of the resultant powders. A pilot plant Mobile MinorTM spray dryer was used to co-process binary and ternary mixtures to improve the properties without changing the chemical characteristics. PXRD, thermal and SEM analysis was used to assess the powders along with hardness, bulk density and compaction analysis to characterise the product. Powder containing acetaminophen co-processed with erythritol, maltodextrin and mannitol as binary mixtures were successful at improving the compactability of the powder and other physical properties. However, powders of these compounds as ternary mixtures showed that there was area for improvement in the properties of the powders.

In progression from this work, Gonnissen and co-workers published work into the area of co-processing by spray drying that was previously researched in the last paper by the same group (Gonnissen et al. 2008b). From the research into co-processing acetaminophen with excipients, this study has progressed to investigating the ability to improve the compactability of formulations containing acetaminophen, ibuprofen and cimetidine through co-spray drying with excipients. Feed suspension was optimised for the spray dryer using a design of experiments (DoE) approach which enabled the maximum concentration of the drug to be co-processed with the excipients. Furthermore, this approach was also used to investigate the scale-up parameters of acetaminophen and ibuprofen. Two different types of spray dryers were used depending on the type of compounds that were investigated; a Mobile MinorTM spray dryer for micronized API and SD 28 spray dryer for course grade

APIs. It was found that continuous co-spray drying was successful in co-processing the APIs with selected excipients to produce directly compressible powders that once tableted found improvement in tablet strength and friability. Thus the spray drying technique of co-processing was found to eliminate some traditional formulation steps such as milling or blending by successfully producing these directly compressible drug powders in a single continuous technique.

Furthermore, Gonnissen and co-workers (Gonnissen et al. 2008a) investigated the possibility of avoiding traditional formulations steps commonly used in batch manufacturing methods. By optimisation of the drug concentration present in the feed suspension enhancements of the powder physical properties of the APIs were achieved. Increased feed suspension concentration improved the flowability and disintegration time of the powder due to co-processing of APIs with specifically selected excipients. For the investigation into process parameters it was concluded that the atomisation pressure of the process for the feed suspension has no effect on the yield outcome and physical properties of the resultant powder.

For research into composite powder production, other approaches used the spray dryer to investigate the co-processing of different compounds for multicomponent crystals. Alhalaweh and co-workers (Alhalaweh and Velaga 2010) focussed on co-crystallisation using a spray dryer. As spray drying uses solvent evaporation to produce dry powders, this environment was explored to investigate if the mixture of two feed streams resulted in a mixture of phases or in pure co-crystal formation. It was found that new co-crystals were successfully formed by the spray drying technique and that the technique is appropriate for preparation and scale-up of co-crystallised pharmaceutical compounds. Successful scale-up technologies for co-crystals is an important target for the pharmaceutical industry to

overcome issues found for co-crystallisation by standard crystallisation approaches (Blagden et al. 2014).

Furthermore, co-processing of APIs and excipients with polymers has been investigated. Spray drying lactose in the presence of polyethylene glycol 4000 (PEG) was used to improve the crystallinity of lactose (Chidavaenzi et al. 2001b). Lactose/PEG samples were spray dried using a Büchi 190 mini spray dryer and further analysis of the samples was carried out using a thermal activity monitor to assess the crystallinity as well as PXRD and thermogravimetric analysis. This paper found that the presence of PEG in a mixture with lactose caused the lactose to crystallise instead of producing an amorphous material as is found when it is spray dried alone.

1.5. Motivation for research

Considering the principles of drying and particle solidification and the capability of the lab-scale spray drying technique for particle investigation and engineering, this research will focus on the application of spray drying to the development of particle understanding and design for pharmaceutically relevant compounds. Firstly, the focus of spray drying will be directed to the control and production of a metastable polymorphic form of carbamazepine. This work looks to understand the formation of the polymorph by spray drying and how the technique can overcome the issues reported by literature of the inability to produce this form in a robust and reproducible manner. Secondly, spray drying has been presented as an approach for crystallisability prediction of pharmaceutically relevant compounds. The use of a machine learning tool, random forest, has been adopted for the modelling and crystallisability prediction by spray drying. Finally, the influence of spray drying process configuration was explored through the application of co-processing. In particular, the

adoption of a three-fluid nozzle was examined for the influence of feed configuration during the co-processing of multiple components.

Chapter 2. Aims and Objectives

2. Aims and Objectives

2.1. Aims

The overall aim for the research presented in this thesis was to explore and utilise the spray drying technique to manipulate and engineer different particle systems achieving an enhancement of understanding of particles properties. The fundamental drying principles and the relationship of process parameters and material properties were crucial to the understanding, engineering capabilities and applications of this technique. Three research areas are presented, each highlighting the capability of the technique to provide a different approach for crystallisation.

2.2. Objectives

The overall objective for the research presented in this thesis was to investigate the different crystallisation capabilities of spray drying by testing the influence of the drying principles and process parameters on the material properties and critical quality attributes.

- I. Utilise spray dryer to produce a metastable polymorph of carbamazepine
 - i. Identify polymorphic form and characterise material
 - ii. Rationalise polymorphic result by spray drying and provide evidence to support argument
- II. Develop a crystallisability prediction model for spray drying
 - i. Create crystallisability prediction model from published literature data
 - ii. Create crystallisability prediction model from spray drying experimental data
 - iii. Indicate the capability and need for an extensive crystallisability prediction model for spray drying

- III. Explore the capability of the spray dryer three-fluid nozzle to produce a composite particle by co-processing
 - i. Identify and characterise composite material
 - ii. Analyse the influence of process configuration and conditions on the material properties of composite particles

Chapter 3. Materials and Methods

3. Materials and Methods

3.1. Materials

Carbamazepine (CBZ) was purchased from Molekula (form III, CAS 298-46-4) and methanol (HPLC grade, $\geq 99.5\%$) was sourced from Sigma-Aldrich. For the crystallisability prediction screening, aspirin ($\geq 99.0\%$, CAS 50-78-2), D-(-)-fructose ($\geq 99.0\%$, CAS 57-48-7), D-(+)-galactose ($\geq 98\%$, CAS 59-23-4), D-(+)-glucose monohydrate ($\geq 99.5\%$, CAS 14431-43-7), glycine ($\geq 99\%$, CAS 56-40-6), D-(+)-maltose monohydrate ($\geq 99\%$, CAS 6363-53-7), D-mannitol ($\geq 98\%$, CAS 69-65-8), L-ascorbic acid ($\geq 99\%$, CAS 50-81-7), L-asparagine monohydrate ($\geq 99\%$, CAS 5794-13-8), L-aspartic acid ($\geq 99\%$, CAS 56-84-8), L-glutamic acid ($\geq 98.5\%$, CAS 56-86-0), α -lactose monohydrate ($\geq 99\%$, CAS 64044-51-5), paracetamol (CAS 103-90-2), sucrose ($\geq 99.5\%$, CAS 57-50-1), valine (99+ %, CAS 72-18-4), urea (CAS 57-13-6) were purchased from Sigma Aldrich. Metformin hydrochloride (CAS 1115-70-4) was sourced from Molekula. Deionised water was sourced on site using a Millipore *Milli-Q* water systems with 0.22 μm filters.

3.2. Methods

3.2.1. X-Ray Powder Diffraction (XRPD)

All spray dried powders were analysed using XRPD. Samples for form identification were analysed using transmission foil XRPD data collected on a Bruker AXS D8-Advance transmission diffractometer equipped with θ/θ geometry, primary monochromated radiation ($\text{Cu K}\alpha_1$, $\lambda = 1.54056 \text{ \AA}$), a Vantec 1D position sensitive detector and an automated sample stage (Florence et al. 2003). Samples were mounted on a 28 position sample plate supported on a polyimide (Kapton, 7.5 μm thickness) film. Data were collected from each sample in the range $4\text{--}35^\circ 2\theta$ with a $0.015^\circ 2\theta$ step size and 1 s/step count time. Samples were oscillated 0.5 mm in the x-y plane at a speed of 0.3 mm/s throughout data collection.

Resultant forms were identified by standard procedures including pattern matching and Pawley refinement (Pawley 1981) using the Topas software package. Crystallisability prediction samples were collected on a Bruker D2 phaser benchtop diffractometer equipped with θ - θ geometry, primary monochromated radiation (Cu $K\alpha_1$, $\lambda = 1.54056 \text{ \AA}$ line focussed), operating voltage of 30 kV and current of 10 mA, a LynxEye1D detector and an automated 6 sample auto changer carousel. Samples were mounted on a stainless steel sample holder or Si single crystal sample ring. Data were collected from each sample in the range of $4\text{-}35^\circ 2\theta$ with a $0.01^\circ 2\theta$ step size and a 1 s/step count time.

3.2.2. Spectroscopy

3.2.2.1. Raman

Raman spectra were collected from samples using offline measurements and from the spray dryer using a Kaiser RXN1 Raman spectrometer equipped with PhAT probe. The PhAT probe uses a 400 mW class 3 laser with a wavelength of 785 nm and a spot size of 6 mm, and enables non-invasive measurement of Raman spectra from solids (Allan et al. 2013). For the offline measurements, a glass vial containing sample was analysed. The number of accumulations was 5 and the exposure time was 30 seconds. For the online measurements, the PhAT probe was positioned at the collection vessel of the high performance cyclone to measure the final dried product emerging from the process every few minutes.

3.2.2.2. Raman Microscopy

Raman spectra and mapping of composite and reference samples were collected using the Horiba Scientific Raman XplorA microscope equipped with a 532 nm, 20-25 mW class 3B laser, CCD detector and an Olympus microscope BX41/51. Samples were mounted onto a glass microscope slide. Data were collected for each sample using an acquisition time of 5

seconds, with the x50 objective, grating 1800 gr/mm, 100 % filter, slit of 10 and 50 μm and hole of 200 and 300 μm , with a step size of $<2 \mu\text{m}$ using the LabSpec6 Spectroscopy Suite.

3.2.3.Imaging

3.2.3.1. Scanning Electron Microscopy (SEM)

The morphology and particle size of spray dried samples were imaged using a Hitachi SU6600 Analytical VP FEG-SEM. Samples were imaged by two modes, secondary electron (SE) along-with elemental analysis by energy-dispersive X-ray spectroscopy (EDX) for composite particles. Samples were mounted, gold plated and analysed at 5 and 15 kV.

3.2.4.Particle Sizing

Particle size and particle size distributions of the spray dried samples were analysed using a Malvern Morphologi G3 instrument. This technique integrates compressed air dispersion with automated microscopy to image and collect size and shape data for the sample particle population. The three-dimensional particles are imaged in two-dimensions. The diameter of a circle is then calculated with equal area to the projected area of the particle known as the circle equivalent (CE) diameter (Malvern Instruments Ltd. 2015). Samples were introduced from a 5mm^3 spatula, dispersed and allowed particle settling onto a glass plate and analysed using 20x and 50x magnification CE diameter measurements were analysed against the volume distribution for samples with the D_v50 size measurements and the span particle size calculated by $(D_v90 - D_v10) / D_v50$.

3.2.5.Thermal Analysis

Simultaneous thermal analysis (STA) comprising differential scanning calorimetry (DSC) of samples was carried out in a Netzsch STA 449 C instrument. Samples were placed in a 10

μL Al crucible with a pierced lid to allow loss of water vapour. The samples were analysed using a heating rate of $263.15\text{ }^{\circ}\text{C}$ (10 K) /min from $20\text{ }^{\circ}\text{C}$ to $220\text{ }^{\circ}\text{C}$.

3.2.6.Data Presentation

All diffraction, spectroscopy, particle sizing and thermal analysis data were presented in graphical form using the OriginPro 9.0 and 2016 software.

Chapter 4. Polymorph Control and Isolation via Spray Drying

4. Polymorph Control and Isolation via Spray Drying

4.1. Introduction

APIs and formulated dosage forms are largely produced using traditional batch manufacturing methods. However there is increasing interest in exploiting the potential advantages of continuous processing that include improved consistency, process efficiency and reduced cost of goods in the manufacture of pharmaceuticals (European Medicines Agency 2011). Spray drying enables particle formation and isolation in a single continuous operation and so presents the opportunity to simplify multiple batch operations into a single step. The present study therefore investigates particle formation of the API carbamazepine (CBZ) in a spray dryer.

Many APIs exhibit multiple polymorphic forms that can display different physical attributes (Mullin 2001). This range of accessible properties can lead to variability during processing and ultimately in use through changes in stability, flow, shape, aerodynamic performance, solubility, dissolution or bioavailability (Hilfiker 2006). Consequently, there is a requirement to understand and control the polymorphic forms which are used in products. Capabilities for *ab initio* crystal structure prediction of polymorphs from molecular structure have developed considerably in recent years (Price 2014). However, they are not yet routinely applicable to gain the complexity of typical APIs. Therefore, extensive experimental investigations are still largely required to define the range of potential polymorphic structures, their relative thermodynamic experimental stabilities and the conditions under which they can be formed (Stahly 2007).

4.1.1. Carbamazepine

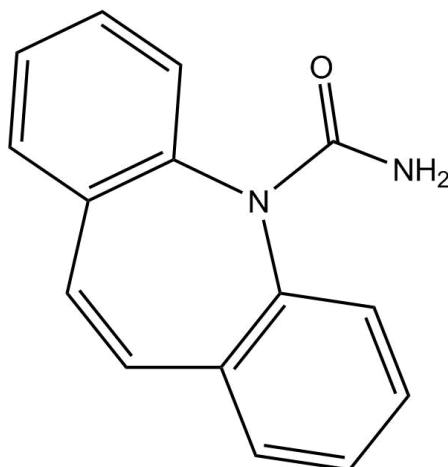


Figure 4.1. Molecular structure of Carbamazepine.

Carbamazepine (CBZ) is an API which is used in the treatment of epilepsy and trigeminal neuralgia as an anticonvulsant (Koester et al. 2004, Martins et al. 2012b). CBZ has a low water solubility (<200 µg/ml) (Koester et al. 2004) and falls within class II of the Biopharmaceutical Classification System (BCS) and can show dissolution limited absorption (Patterson et al. 2008). The solid state forms of CBZ have been widely studied and it has been reported in five different polymorphic forms, CBZ I, II, III and IV (Lang et al. 2002) and V (Arlin et al. 2011) in addition to a large number of solvated (Harris et al. 2005), co-crystalline forms (Florence et al. 2006) (Fleischman et al. 2003), salts (Childs et al. 2009) and nanocrystalline forms (Billinge et al. 2010). The thermodynamically stable form at room temperature is the monoclinic CBZ III (Getsoian et al. 2008).

Polymorphism of CBZ has been widely investigated using different screening approaches (Getsoian et al. 2008, McCabe 2010), theoretical analysis (Rustichelli et al. 2000) and crystal structure prediction (Florence et al. 2006). CBZ IV was first obtained by re-crystallisation from methanol solution in the presence of hydroxypropylcellulose (Lang et al. 2002) and was subsequently reported using polymer heteronucleation (Grzesiak et al. 2003). However,

subsequent attempts to obtain form IV from solution, including multiple solvent screens (Florence et al. 2006) and single solvent screens (Getsoian et al. 2008) did not produce any evidence of CBZ IV. This was explained due to the absence of polymer additives in these studies. Notably, Kipourous and co-workers (Kipourous et al. 2005, Kipourous et al. 2006) in a study of analytical techniques of polymorphic mixtures, stated that the CBZ IV used in that study was produced by spray drying from methanol. No further detail on the method was provided or mechanism proposed for the occurrence of CBZ IV.

4.1.2.Spray Drying

Spray drying is an important technique for pharmaceutical manufacturing and is generally used to isolate from a suspension through conversion of a liquid or solution stream into a solid powder through controlled, rapid evaporation of solvent or liquid by a heated drying gas (Cal and Sollohub 2010b). It is well known for the formation of amorphous solids in pharmaceuticals and food areas (Gharsallaoui et al. 2007) as well as being applied to a range of particle engineering applications (Vehring 2008, Woo and Bhandari 2013b). However, it has also been demonstrated for the production of crystalline particles such as spray drying of the API nifedipine (Martins et al. 2012a), excipient mannitol (Guimarães et al. 2015) and co-crystals of CBZ and nicotinamide (Patil et al. 2014).

The current work seeks to investigate the formation of form IV CBZ during spray drying and the potential of polymorph control (Vehring 2008). Here we report a robust and reproducible method for production of CBZ IV that does not require polymer additives. The application of in situ Raman monitoring is also demonstrated.

4.2. Experimental

4.2.1. Spray Drying Method

CBZ solutions were spray dried using a Büchi B-290 Mini Spray Dryer coupled with the Büchi Inert Loop B-295 (Büchi Labortechnik AG, Switzerland) and configured with a high performance cyclone. The dryer was operated in co-current closed mode with nitrogen as the drying gas. The starting composition of the solutions introduced into the dryer was 10.4 g/L CBZ in methanol at room temperature. The spray dryer parameters used to obtain a dry powder can be found in Table 4.1.

Table 4.1. Summary of spray dryer parameter conditions.

Spray dryer parameter	Value
Aspirator rate	100 %
Inlet temperature	120 °C
Outlet temperature	65 – 75 °C
Pump percentage	10 %
Spray gas pressure	7 bar
Spray gas rate	439 – 667 L/h (at standard temperature and pressure, STP)

4.2.2. Carbamazepine Characterisations

Once the CBZ solution was spray dried and the powder was collected the sample was characterised for polymorphic form using XRPD. To obtain the size and size distribution of the sample powder particles, the Malvern Morphologi G3 was used with the dry dispersion unit. For particle shape the SEM was used and for thermal behaviour DSC was used.

4.3. Results and Discussion

4.3.1. CBZ IV

The spray drying process conditions successfully produced a dry, crystalline CBZ sample. The sample was identified as CBZ IV by comparison of the experimental XRPD data with calculated XRPD reference patterns for forms I-V (Figure 4.2). The data comprised sharp diffraction peaks with no evidence of an elevated background scattering that might indicate amorphous content. This result was confirmed through analysis using a Pawley type fit in the program Topas (Figure 4.3).

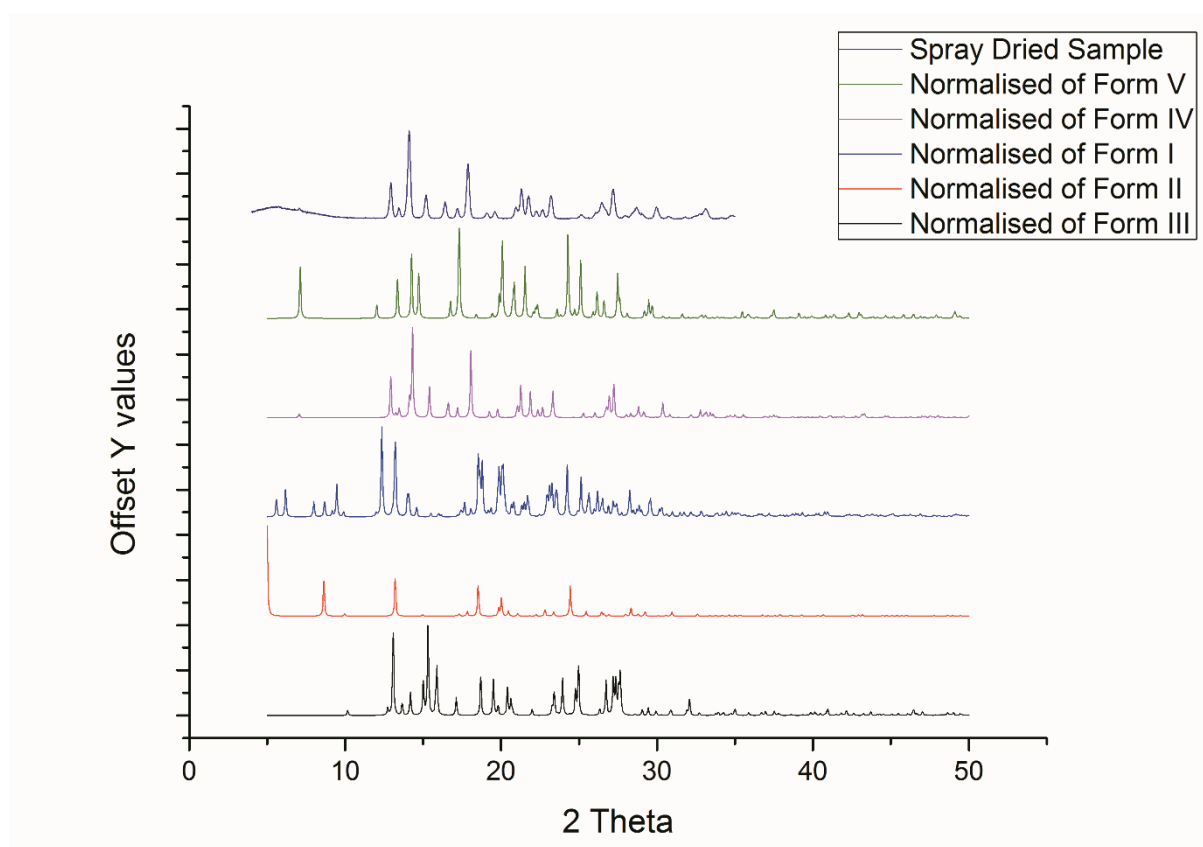


Figure 4.2. Calculated XRPD patterns for CBZ I, II, III, IV and V compared with the experimental data for spray dried methanol CBZ solution.

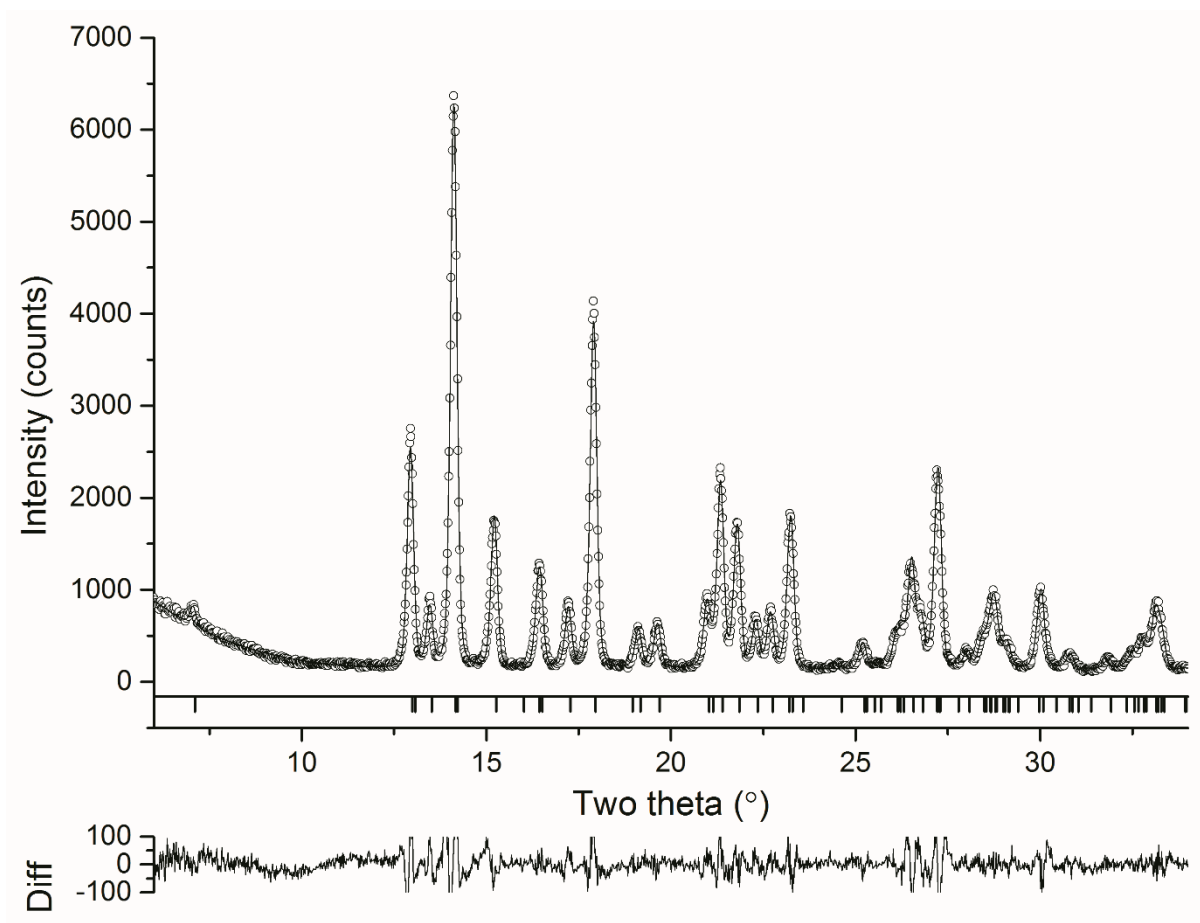


Figure 4.3. Pawley fit of the data from the spray dried CBZ sample. Observed profile (o), calculated profile (-) and difference plot ($Y_{obs}-Y_{cal}$) of the Pawley fit in the range of $6-34^\circ$ 2θ (Pawley $\chi^2 = 1.790$).

The Pawley type fit to the data from the spray dried sample was carried out in the Topas software package (Bruker AXS 1999-2014). The fit to the data was very good and the refined, room temperature lattice parameters obtained were $a = 26.432(2)\text{\AA}$, $b = 7.0360(6)\text{\AA}$, $c = 13.9044(16)\text{\AA}$ and $\beta = 109.570(7)^\circ$, space group $C2/c$ [*cf.* the reported values from the single crystal study $a = 26.609(4)$, $b = 6.927(1)$, $c = 13.957(2)$ and $\beta = 109.7(1)^\circ$, CSD REFCODE: CBMZPN12] (Lang et al. 2002). There was no evidence of any diffraction peaks from the sample that are not

accurately described by the structure of CBZ IV, which confirmed the phase purity of the spray dried sample (Kipouros et al. 2005, Kipouros et al. 2006).

To understand the process robustness of the spray dryer with respect to CBZ IV formation, three process parameters were varied, specifically: inlet temperature and feed pump rate (Conditions 1-3) and solvent (Condition 4; Table 4.2). Conditions were selected that may be expected to affect the rate of drying and initial nucleation conditions within the range required to obtain a dry powder.

Table 4.2. Summary of operating conditions for the spray drying of CBZ, which was monitored by on-line Raman spectrometry.

	Inlet temperature (°C)	Pump rate (%)	Solvent
Original spray drying parameters	120	10	Methanol
Condition 1	100	10	Methanol
Condition 2	120	5	Methanol
Condition 3	100	5	Methanol
Condition 4	120	10	Ethanol

Non-invasive in situ Raman spectroscopy was utilised to obtain real-time measurements during each of the experiments. To investigate the impact of the different parameters, a comparison of the resultant Raman spectra along with an offline reference of CBZ IV is shown in Figure 4.4.

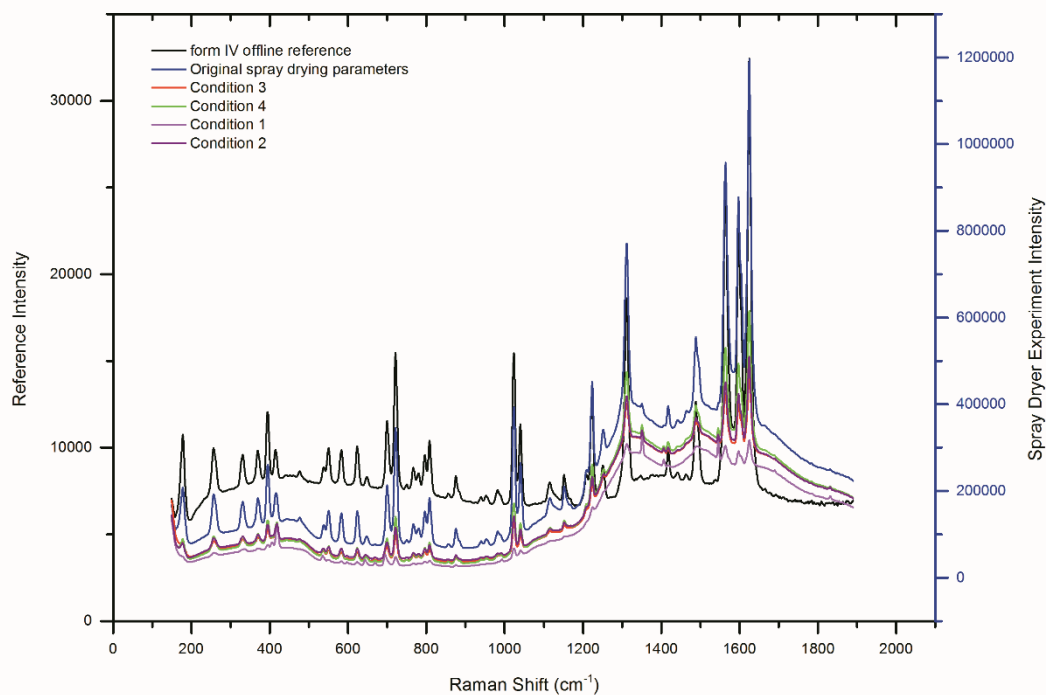


Figure 4.4. Raman spectra of spray dried CBZ samples produced under different spray dryer process conditions in comparison to CBZ IV offline reference.

The spectra collected from the spray dried samples produced from each Condition 1-4 (Table 4.2) showed some differences in baseline and signal-to-noise caused by process air pressure and rate; however the characteristic Raman bands showed a direct correspondence with the form IV Raman reference spectrum. No peaks from alternative CBZ forms were observed. The formation of CBZ IV by spray drying was highly reproducible and relatively insensitive to limited changes in the process conditions and a change of solvent from methanol to ethanol.

Samples of spray dried CBZ IV were characterised using SEM (Figure 4.5), particle sizing (Figure 4.6) and DSC (Figure 4.7). SEM showed particles with diameters in between $<1 - 5 \mu\text{m}$ consistent with expectation from the Büchi mini dryer (Büchi Labortechnik AG). The

particles were reasonably isometric and showed clearly defined facets with some evidence of agglomeration. In contrast, Lang and co-workers (Lang et al. 2002) reported the morphology of form IV crystals to be 'plate-like'.



Figure 4.5. Morphological image of spray dried CBZ IV by SEM at 5 kV.

The particle size and size distribution of spray dried material were measured using a Malvern Morphologi G3. CE diameter was determined against the volume distribution (Figure 4.6).

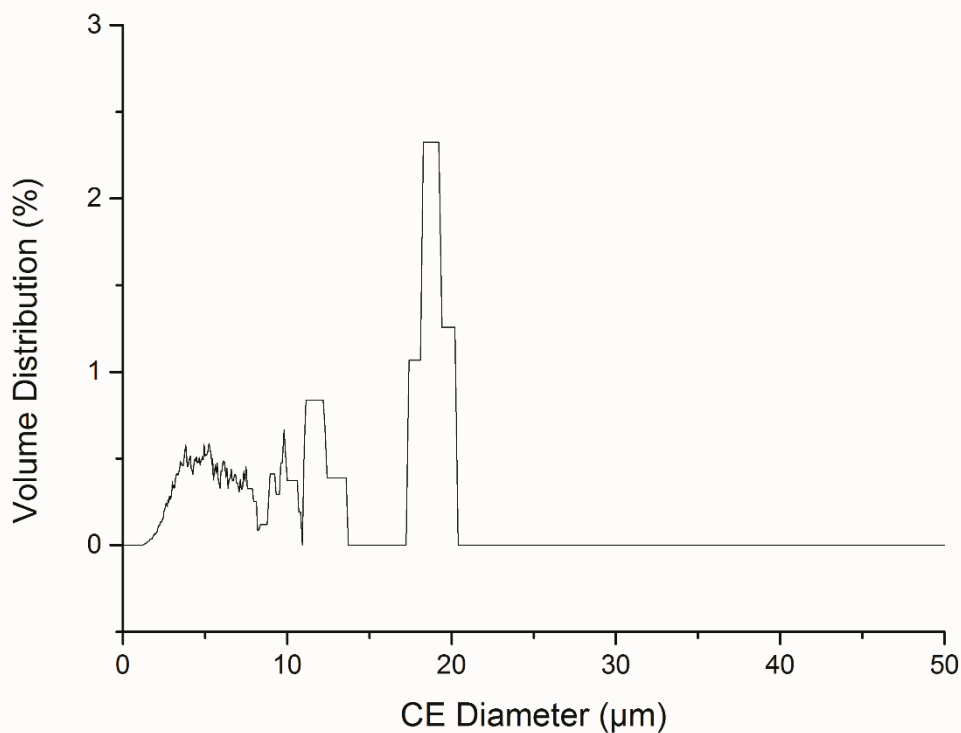


Figure 4.6. Particle size and size distribution measurements, based on the CE diameter, of CBZ IV.

The CE diameter illustrated a multi-modal distribution of particle sizes with a mean size of 5.5 μm with evidence of large aggregates, which is supported by the SEM images.

DSC analysis of the spray dried and previously obtained samples within the group (Briggs 2015) confirms the expected thermal behaviour of CBZ IV and showed good correspondence to the previously reported thermal analysis of anhydrous CBZ polymorphs (Grzesiak et al. 2003).

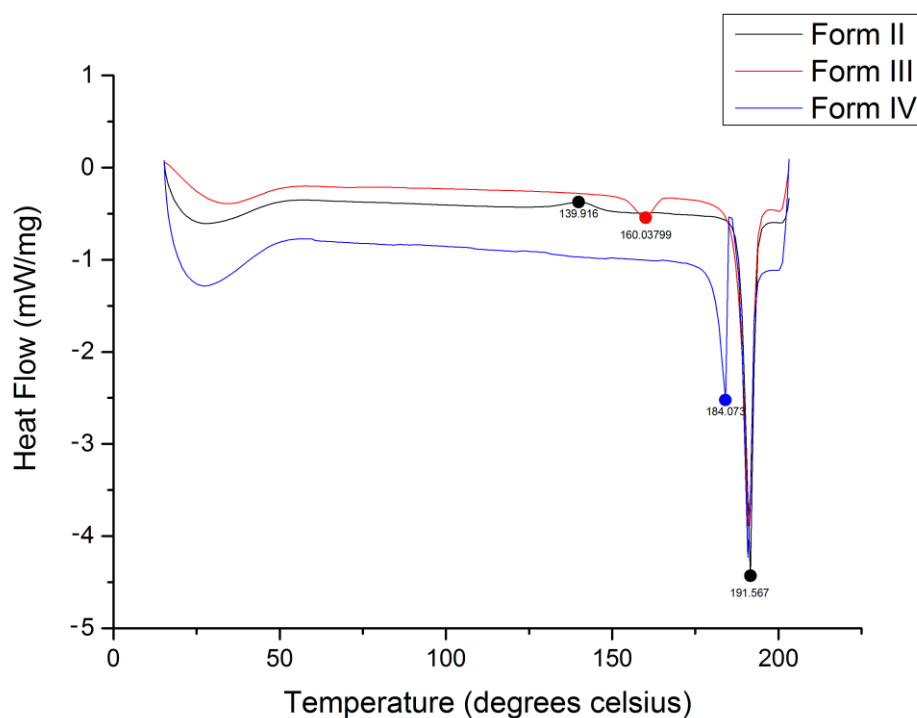


Figure 4.7. DSC profiles of three CBZ forms.

The melting profiles for the different forms of CBZ clearly show the temperature at which the forms will either undergo a solid-solid or a melt re-crystallisation transformation into a different form. For two of the forms there are distinct peaks that show the melting temperatures by decomposition; form III (red) at approximately 160 °C and form IV (blue) at approximately 184 °C. However, each of these forms shows a second peak in their profiles occurring at the exact same temperature. Furthermore, this peak at approximately 190 °C is the only melting temperature that occurs with the final form, form II (black) and this means that each of the three forms will melt and will undergo transformation to form II where all will melt at 190 °C. The melting behaviours observed for forms II, III and IV of CBZ are broadly consistent with the properties reported in literature, particularly Grzesiak and co-workers (Grzesiak et al. 2003) which reported the thermodynamically stable polymorph at room temperature to be CBZ III.

Further analysis using XRPD was carried out to determine CBZ IV particle stability over a three month time period under ambient conditions. Profiles for the different CBZ IV samples show clear consistency and uniformity suggesting form IV could remain stable in the solid state for up to a three month time period under ambient conditions.

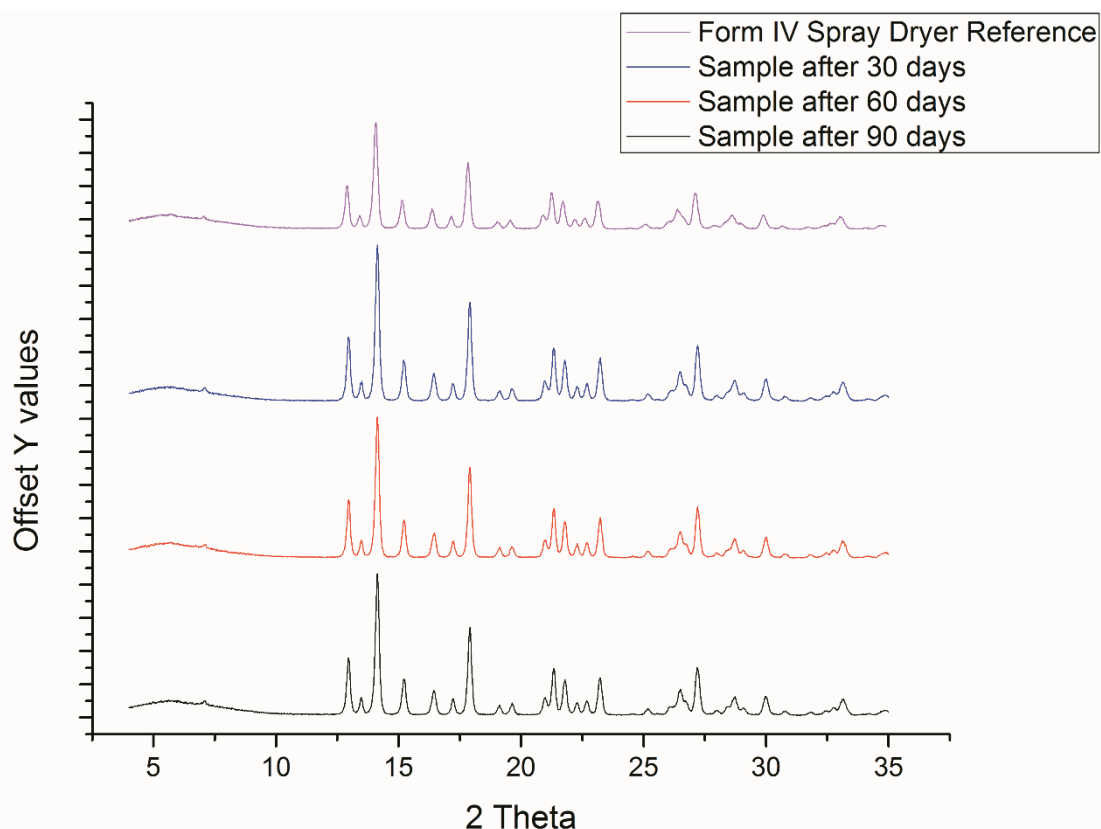


Figure 4.8. XRPD analysis of CBZ IV 30, 60 and 90 days after formation.

4.3.2. CBZ IV Solution Mediated Transformation

Whilst spray drying of methanol and ethanol CBZ solutions yields form IV, previous crystallisation studies that have included recrystallisation from methanol solution have not reproduced this metastable form (Lang et al. 2002, Grzesiak et al. 2003, Florence et al. 2006,

Getsoian et al. 2008). This is despite the inclusion of conditions conducive to rapid precipitation that may be expected to favour metastable forms.

The original report of CBZ IV (Grzesiak et al. 2003) produced the polymorph by slow evaporative recrystallisation from methanol solution in the presence of hydroxypropylcellulose at room temperature. Getsoian and co-workers (Getsoian et al. 2008) investigated CBZ polymorphs using a single solvent screen and observed CBZ I, II and III through temperature and supersaturation control. However, attempts to obtain reference samples of form IV by recrystallisation directly from solution were unsuccessful and a sample was ultimately obtained by de-solvation of a solvated form. It has been concluded by Florence and co-workers (Florence et al. 2006) that form IV requires polymers to act as templates and their absence prevents crystallisation of CBZ IV directly from solution. Electrospray crystallisation from methanol solution produced amorphous nanoparticles that transformed to CBZ III or I depending on post solidification annealing conditions (Wang et al. 2012). This suggested that under the conditions used during electro spraying, solidification occurs so rapidly that nucleation of crystals is predicted.

The reported inconsistency of solution crystallisation studies to reproduce CBZ IV is notable. This could indicate that form IV does not nucleate directly from solution and requires the presence of an additive that either templates CBZ IV or inhibits the nucleation of competing forms. However the occurrence of CBZ IV from spray drying of CBZ solution does not support this conclusion. The relative thermodynamic stabilities of CBZ I, II, III and IV have been reported as $III > I > IV > II$ based on thermal analysis (Grzesiak et al. 2003) with the reported thermodynamically stable polymorph at room temperature to be form III. Thus, under solution conditions where CBZ IV is nucleated, the metastable form would be expected to transform to the more stable polymorphs CBZ I or III via solution mediated

transformation (O'Mahony et al. 2012). It is therefore proposed in the spray dryer, that the combination of a high rate of supersaturation from rapid evaporation at elevated temperature may promote the formation of metastable CBZ IV and the rapid isolation of the metastable polymorph prohibits subsequent solution mediated transformation, enabling recovery of solid CBZ IV.

To support this hypothesis, the drying diffusion coefficient and rates that are crucial in the formation of CBZ IV by spray drying were calculated using a series of equations (Eqn. 4.1-4.11), with definition and values for each term given in Table 4.3. During droplet drying, the diffusivity of CBZ in methanol, $D_{CBZ/Me}$, would not only influence the morphology and structure of the final particles but influence the nucleation and growth rates during drying (Wang et al. 2012). Throughout the drying process it was assumed that the droplet liquid was at its wet bulb temperature, T_{wb} (Huang 2011). For drying in N_2 or air, the wet bulb temperature was estimated from (Vehring 2008):

$$T_{wb} = 137 \left(\frac{T_b}{373.15} \right)^{0.68} \log(T_G) - 45 \quad \text{Eqn. 4.1}$$

$D_{CBZ/Me}$ was calculated to be $1.101 \times 10^{-9} \text{ m}^2/\text{s}$ using the Wilke-Chang equation (Wilke and Chang 1955, Coulson and Richardson 1996). The physical properties (viscosity, density, etc.) of the droplet liquid were taken at T_{wb} :

$$D_{CBZ/Me} = \frac{1.173 \times 10^{-16} \varphi_{Me}^{0.5} M_{Me}^{0.5} T}{\mu V_{CBZ}^{0.6}} \quad \text{Eqn. 4.2}$$

To estimate the evaporation rate, κ , of methanol from the droplets during drying, Eqn. 4.3 (Vehring 2008) was used:

$$\kappa = 8D_{Me/N_2} \frac{\rho_g}{\rho_l} (Y_{S,Me}(T_e) - Y_{\infty,Me}) \quad \text{Eqn. 4.3}$$

To calculate $Y_{S,Me}(T_e)$ the equilibrium temperature, T_e , was approximated to the wet bulb temperature, T_{wb} , (Eqn. 4.1). The saturated vapour pressure at this temperature was calculated via the Antoine equation (Coulson et al. 1999) to be 0.060 bar. Furthermore, to estimate the mass fraction of methanol at the surface, $Y_{S,Me}(T_e)$, the mole fraction was firstly calculated using Dalton's law (Eqn. 4.4) before conversion to a mass fraction:

$$Y_{Me} = \frac{P_{Me}}{P_T} \quad \text{Eqn. 4.4}$$

Therefore, on calculation of Eqn. 4.3 the evaporation rate of methanol during drying was $1.024 \times 10^{-8} \text{ m}^2/\text{s}$.

The calculated diffusion coefficient of CBZ and the evaporation rate was expressed by the dimensionless Peclet number, Pe , that calculates the ratio of evaporation to molecular diffusion (Vehring et al. 2007). For CBZ the Pe number was calculated using Eqn. 4.5 (Vehring 2008):

$$Pe = \frac{\kappa}{8D_{CBZ/Me}} \quad \text{Eqn. 4.5}$$

To further investigate the possible structural outcome of the spray dried CBZ particles, the level of surface enrichment was approximated, using Eqn. 4.6 (Vehring 2008):

$$E_{CBZ} = 1 + \frac{P_e}{5} + \frac{P_e^2}{100} - \frac{P_e^3}{4000} \quad \text{Eqn. 4.6}$$

This equation indicated the concentration of CBZ at the surface relative to the average concentration of the particle, which would equate to 1.

To determine the process times for spray drying of CBZ, the total drying time was calculated using Eqn. 4.7 (Vehring 2008):

$$\tau_D = \frac{d_0^2}{\kappa} \quad \text{Eqn. 4.7}$$

Of the total drying time, a portion of time is required for the concentration to reach the point that crystallisation can occur, τ_{sat} . Firstly the initial supersaturation, S_0 , was determined as a ratio of the initial concentration to the saturated concentration of CBZ in methanol, using Eqn. 4.8 (Vehring 2008):

$$S_0 = \frac{C_0}{C_{sol}} \quad \text{Eqn. 4.8}$$

This value was used to calculate the time during drying after which crystallisation of CBZ can be possible using Eqn. 4.9 (Vehring 2008):

$$\tau_{sat} = \tau_D(1 - (S_0 E_{CBZ})^{2/3}) \quad \text{Eqn. 4.9}$$

It was also important to determine the time duration at which the process would need to reach to gain an amorphous form. Firstly the initial density of CBZ was determined using Eqn. 4.10 (Vehring 2008):

$$P_0 = \frac{C_0}{\rho_t} \quad \text{Eqn. 4.10}$$

Thus the time required to produce amorphous; by Eqn. 4.11 (Vehring 2008):

$$\tau_t = \tau_D (1 - (P_0 \cdot E_{CBZ})^{2/3}) \quad \text{Eqn. 4.11}$$

Table 4.3. Definition and values of terms of equations 4.1 – 4.11 including diffusion coefficient, evaporation rate and Peclet number calculation values.

Parameter	Value	Unit
Methanol boiling point, T_b	337.85	K
Gas outlet temperature, T_G	343.15	K
Wet bulb temperature, T_{wb}	279.66	K
Association factor, ϕ	1.9 (Wilke and Chang 1955)	
Molar volume, V_{CBZ}	0.155 (Kim and Boulder 2006)	m ³ /kmol
Solvent viscosity, μ	7.11x10 ⁻⁴ (Yaws)	N.s/m ²
Solvent molecular weight, M_{Me}	32.04	kg/kmol
Droplet temperature, T	279.66	K
Diffusion coefficient, $D_{CBZ/Me}$	1.101x10 ⁻⁹	m ² /s
Diffusion coefficient, D_{Me/N_2}	1.10x10 ⁻⁵	m ² /s

Drying gas density, ρ_g	1.251	kg/m ³
Droplet liquid density, ρ_l	803.8	kg/m ³
Mass fraction of solvent away from droplet surface, $Y_{\infty,Me}$	0	
Methanol saturated vapour pressure, P_{Me}	0.060 (Coulson et al. 1999)	bar
Drying chamber pressure, P_T	0.91	bar
Mole fraction methanol at droplet surface, Y_{Me}	0.066	
Mass fraction methanol at droplet surface, $Y_{S,Me}(T_e)$	0.075	
Evaporation rate, κ	1.024×10^{-8}	m ² /s
Peclet number, Pe	1.19	
Surface enrichment, E_{CBZ}	1.253	
Droplet diameter, d_o	25 (Büchi Labortechnik AG)	µm
Drying time, τ_D	0.061	s
Solute initial concentration, C_0	0.0104	g/ml _{Me}
Saturated concentration, C_{sol}	0.0460 (O'Mahony et al. 2013)	g/ml _{Me}
Initial supersaturation, S_0	0.226	
Time to crystallisation window, τ_{sat}	0.0347	s
Solute true density, ρ_t	1.296	g/ml
Initial density, P_0	0.008	
Time to amorphous concentration, τ_t	0.0582	s

As shown in Table 4.3 the Pe number calculated from Eqn. 4.5 was found to be 1.19. This value of approximately 1 suggested that CBZ diffused into the core of the droplet at almost the same rate that methanol was evaporating. Therefore, an approximately even distribution

of CBZ and a solid particle structure would be expected from the process. Furthermore, the surface enrichment of CBZ, E_{CBZ} , was found to be 1.254 which shows a low level of surface enrichment. Given this low value of surface enrichment and the errors associated with the approximations used in its calculation, it would not be unreasonable to assume that minimal surface enrichment may occur leading to a low likelihood of producing a hollow shell particle. This is backed up by SEM images in Figure 4.5 which show isometric and non-spherical shaped particles.

Based on the drying rate calculated above, Figure 4.9 shows the droplet diameter and CBZ supersaturation within the droplet throughout the constant rate drying period. The droplet size has been calculated based on the reduction in surface due to evaporation rate (Eqn. 4.12) and for supersaturation the concentration of CBZ has been calculated as a function of the droplet volume and enrichment factor (Eqn. 4.13).

$$d = \sqrt{d_o^2 - \kappa t} \quad \text{Eqn. 4.12}$$

$$S = \frac{\left(\frac{d_i^3 C_o}{d^3}\right)E}{C_{sat}} \quad \text{Eqn. 4.13}$$

Where d is the droplet size, d_o is the initial droplet size, κ is the evaporation rate, t is time, S is supersaturation, C_o is initial concentration and C_{sat} is saturated concentration. The constant rate period was found to be 0.061 s; this is realistic when compared to the approximated drying residence time of 1 – 1.5 s from Büchi (Büchi Labortechnik AG). Of this total drying period, the first 0.0347 s is concerned with the evaporation of methanol leading to an increase in CBZ concentration to a supersaturation of 1. After 0.0347 s crystallisation was feasible but may or may not of occurred depending on the nucleation kinetics. Furthermore, at 0.0582 s if crystallisation had not occurred, the concentration of

CBZ would be equal to the true density of solid CBZ. After this point an amorphous material would be expected. When comparing the time to reach the true density to the supersaturation curve in Figure 4.9, the maximum supersaturation before amorphous formation was found to be $S = 34.59$. As the XRPD patterns shown in Figure 4.3 do not provide any evidence of the presence of amorphous material it was assumed that CBZ crystallised before this time and supersaturation was reached. Therefore, it was concluded that the nucleation kinetics of CBZ are such that spontaneous nucleation would occur between supersaturations of 1 and 34.59.

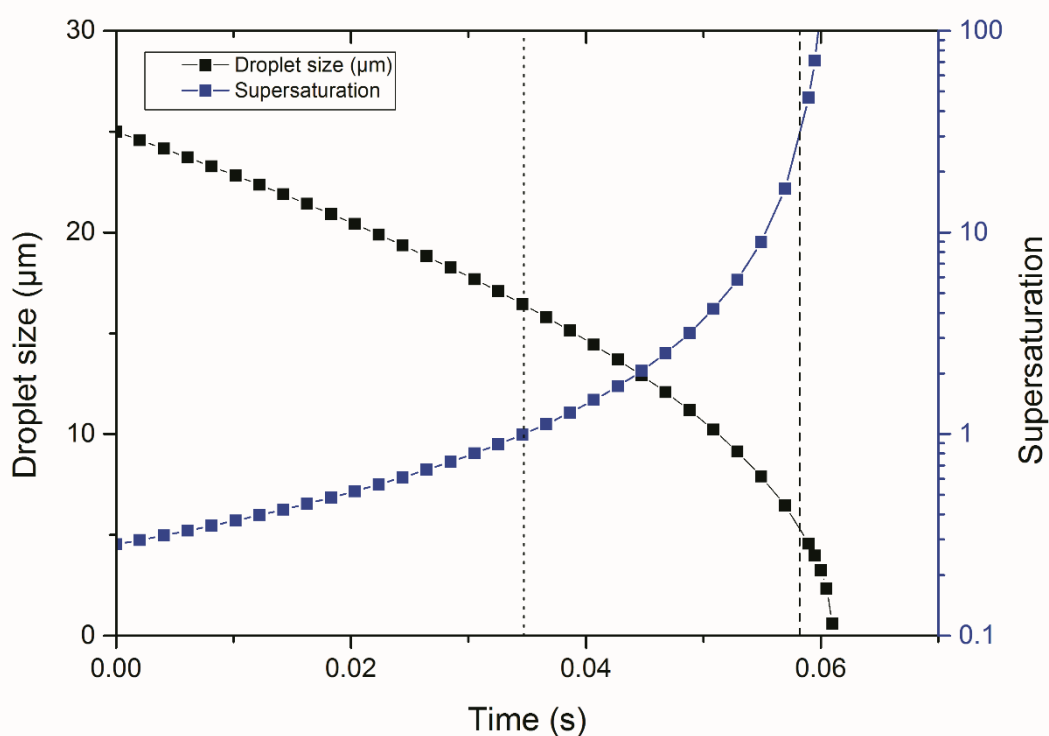


Figure 4.9. Droplet diameter and CBZ supersaturation as a function of drying time.

The final step in the formation of CBZ IV was the consideration of solution mediated transformation. O'Mahony and co-workers (O'Mahony et al. 2012) described the solution mediated transformation of CBZ I to III on the scale of minutes. Based on the previously calculated process times if CBZ IV nucleated at a supersaturation of 1, particles would only be in contact with solvent for a further 0.0263 s by which time all the solvent was removed

through drying. Therefore, in comparison to the times detailed (O'Mahony et al. 2012) solution mediated transformation to a more stable form may be unlikely.

To further investigate this, supersaturation, evaporation rate and particle isolation were studied independently out with the dryer. Firstly in terms of supersaturation, the high inlet temperature used in the spray dryer will lead to rapid evaporation of solvent from the surface of the droplets and a rapid rise in supersaturation until primary nucleation of CBZ occurs. Under high supersaturations metastable polymorphs are more likely (Getsoian et al. 2008). However, due to the multiple spray dryer conditions that contribute to supersaturation, such as feed concentration, drying temperature, drying rate, droplet diameter and number, experimental measurement of supersaturation in droplets during the process may be unfeasible. Supersaturation was studied using rapid cooling of methanol solutions from 55°C to -10°C of 5 mL in a multi-position crystallisation platform. Multiple samples were created with increasing supersaturations (SS) to identify a possible supersaturation increase by spray drying. Samples were monitored for the onset of crystallisation and crystalline samples quickly removed, dried and analysed to confirm polymorphic form using XRPD analysis (Figure 4.10).

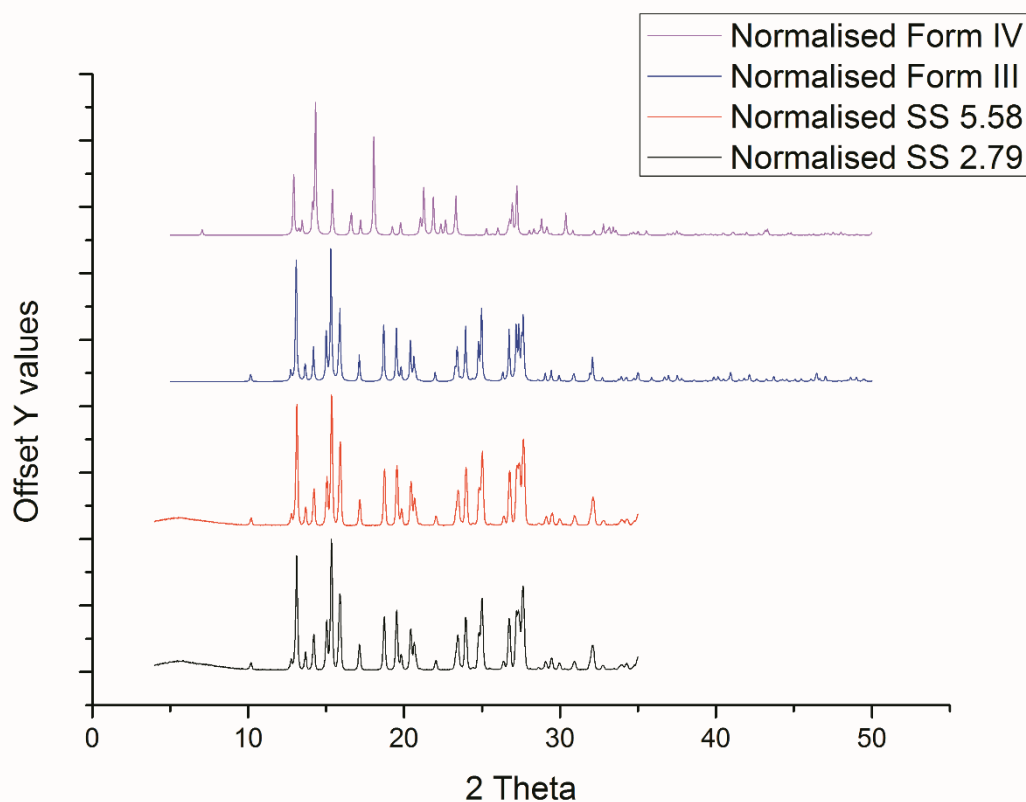


Figure 4.10. XRPD patterns of single crystal references of CBZ III and IV in comparison to measured supersaturations samples at 2.79 and 5.58 in rapidly cooled methanolic CBZ solutions.

All recrystallised CBZ samples were confirmed as the stable CBZ III form. Getsoian and co-workers (Getsoian et al. 2008) suggested that form II is more likely to be produced under high supersaturation however, Sypek and co-workers (Sypek et al. 2012) found that form III was produced when high supersaturations were exposed to magnetic stirring. These results reinforced the difficulty in obtaining CBZ IV from solution based crystallisation. This may also be due to rapid transformation of the initial nucleated form to the stable CBZ III. In order to more closely mimic the conditions within a spray dryer, CBZ methanol solutions were exposed to a combination of rapid evaporation and solution isolation environments by spraying solutions onto a heated glass pane. A single glass pane was heated to 120°C using a hot plate, with continuous spray of CBZ methanol solution introduced to the glass surface. A

suitable mass of powder was achieved in less than five minutes requiring small volumes of the sprayed solution and immediately analysed for XRPD (Figure 4.11).

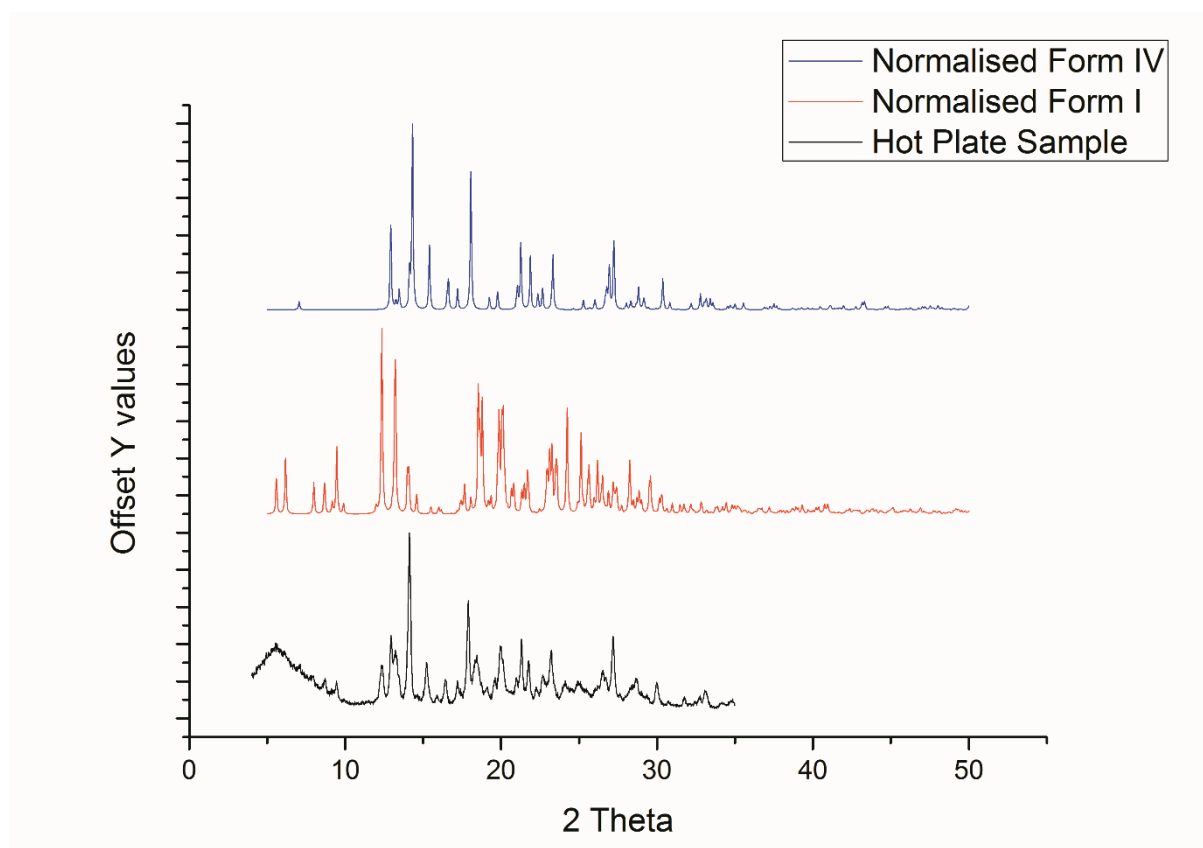


Figure 4.11. XRPD patterns of scaled up hot plate analysis for CBZ comparing hot plate CBZ sample to single crystal reference patterns of CBZ I and IV.

The sample produced using this rapid evaporation method comprised of a mixture of CBZ IV with a minor component of form I. This confirmed the formation of form IV by rapid drying of solution out with the spray dryer. The presence of a mixture of CBZ forms in the glass sprayed sample was suspected to be due to the lack of solid removal during continuous spraying. Hence, when the initial droplets strike the glass and evaporate the resulting form IV particles come into contact with further liquid droplets allowing the transformation to more stable forms. A thin layer of spray dried form IV particles were dispersed on a clean,

heated glass pane at 120 °C by continuous spraying of CBZ methanol solution for roughly five minutes. The particles that had been sprayed with methanol solution comprised a mixture of CBZ IV, III and I.

4.4. Summary

The aim of this work was to determine the particle formation mechanisms of CBZ by spray drying and how these may affect the solid-state form that can be produced. Spray drying of CBZ produced phase pure metastable form IV under reproducible conditions. CBZ IV was identified and confirmed by XRPD and Pawley fit analysis and particle attributes, such as size, morphology and thermal behaviour, were analysed by SEM, Malvern Morphologi G3 and DSC. Process monitoring was conducted by online non-invasive Raman spectroscopy and found spray drying of CBZ form IV to be a robust process.

Although CBZ IV formation by spray drying has been reported previously (Kipouros et al. 2005, Kipouros et al. 2006), this work aimed to determine the drying kinetics and critical process conditions that enable form IV to be successfully produced. The drying kinetics and combination of rapid drying and solid isolation in the spray dryer has shown that the technique is an effective means of producing metastable polymorphs. This highlights the utility of spray drying in the context of solid-state and polymorph screening experiments as an effective technique to form and isolate metastable forms that may not be readily obtained from solution crystallisation methods.

Chapter 5. Prediction of
Crystallisability in Spray Drying
using Random Forest

5. Prediction of Crystallisability in Spray Drying using Random Forest

5.1. Introduction

The propensity of APIs and inert compounds to crystallise is of fundamental importance as it will form the basis of decision making and consideration for drug formulation and delivery. The solid state will govern a wide variety of CQAs and bulk particle properties; solubility, dissolution rate and stability are some of the more significant attributes that must be fully understood during manufacture. Typically, APIs are manufactured in their crystalline state as it will provide particle stability due to its long-range ordered and rigid lattice structure of its unit cell (Mullin 2001, Rodriguez-Spong et al. 2004). Nonetheless, APIs can also exist in the amorphous state in which the unit cell can exist in a disordered manner lacking long-range order (Rodriguez-Spong et al. 2004). An amorphous API can provide advantages for drug formulations through a higher energy state changing the dissolution and solubility rates (Rodriguez-Spong et al. 2004). However, amorphous formulations do not deliver the level of stability needed for most products as exposure to certain conditions such as high humidity, can promote recrystallisation, for example by acting as a plasticiser and reducing the glass transition temperature, (T_g). The selection of either a crystalline or amorphous state is therefore a critical decision during manufacture and it therefore follows, that a prediction of crystallisability based on molecular structure would be of considerable utility, enabling rapid selection of conditions to achieve desirable outcomes.

5.1.1. Spray Drying Crystallisation Propensity Models

Spray drying is a technique that has been extensively used by the pharmaceutical and food industries to produce crystalline and amorphous solid forms (Gharsallaoui et al. 2007, Woo

and Bhandari 2013a). In addition, spray drying provides a method for particle engineering strategies to control key attributes (Vehring 2008) and for formulation design and optimisation (Chow et al. 2007, Singh and Van den Mooter 2016). However, to achieve the consistent and optimal application of the technique, fundamental understanding of the drying kinetics, particle behaviours and relationship between process parameters and particle attributes is required. Attempts to quantify the conditions and theoretical considerations of spray drying have been achieved through process modelling. Many aspects of the spray dryer have been modelled including fundamental drying kinetics (Mezhericher et al. 2010) and particle formation (Huang 2011, Patterson et al. 2014, Porowska et al. 2016). However, where crystallisation processes are also involved knowledge of nucleation and growth kinetics is also desirable. The acquisition of detailed experimental data can be time and material consuming, which may both be at a premium during early stage drug development. Hence, predictive tools that allow rapid selection of appropriate processes to achieve a particular outcome are of considerable interest.

5.1.2. Random Forest

Random forest (RF) is one of a large number of machine learning tools available for multivariate analysis of large data sets (Breiman 2001). Machine learning interprets data in order to make decisions or predictions. RF operates by constructing a series of decision trees that seek to partition a dataset by class using descriptor values. Each splitting point in a tree involves a partially-randomised choice of descriptor, thus creating a ‘forest’ of diverse trees. While any single decision tree is a poor model, considering the ensemble as a whole leads to a vastly increased performance. For a given dataset, the number of trees will influence the accuracy of a model up to the point at which the forest becomes saturated with similar trees. To gain the most accurate RF model, a large and diverse dataset is needed to allow a higher number of individual trees.

5.1.3. Random Forest Models for Crystallisation

RF has been applied to a wide variety of biological and chemical processes highly relevant for the pharmaceutical industry. RF has been used as a predictive tool for aqueous solubility of organic molecules (Palmer et al. 2007). RF has been applied for crystallisation in terms of crystallisability prediction of a large quantity of organic molecules (Bhardwaj et al. 2015, Wicker and Cooper 2015) and as a tool for targeted crystallisation of CBZ (Johnston et al. 2008). The prediction capability of RF models can advance and support the integration and monitoring of individual unit operations towards continuous manufacture (Byrn et al. 2015).

The current work sought to investigate if a crystallisability model can be produced using RF to predict the crystal form of a set of water soluble organic compound produced by spray drying. This model was based on the training set of 51 diverse compounds previously published as a crystallisability classification (Baird et al. 2010, Van Eerdenbrugh et al. 2010). The application of this model was compared to experimental results gained by spray drying.

5.2. Experimental

5.2.1. Spray Drying Method

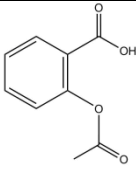
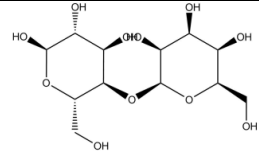
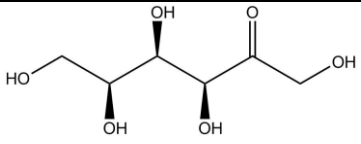
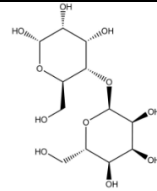
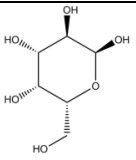
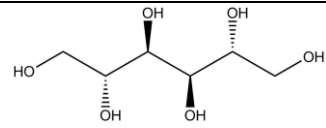
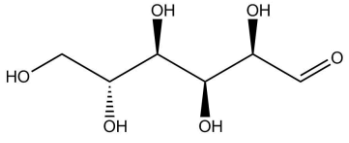
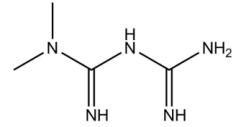
Crystallisability test solutions were spray dried using the Büchi B-290 Mini Spray Dryer (Büchi Labortechnik AG) coupled with the Perceptive Engineering PharmaMV automation. The dryer was operated in co-current closed mode with nitrogen as the drying gas. All test solutions were of an aqueous composition and saturated at room temperature. The spray dryer parameters used to test crystallisability at boiling point temperature are shown in Table 5.1.

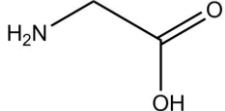
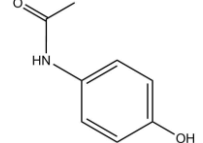
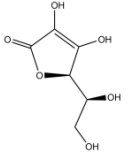
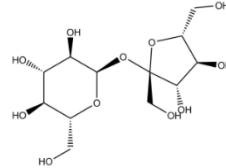
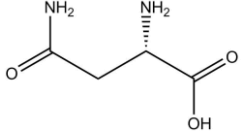
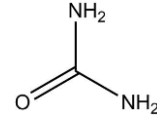
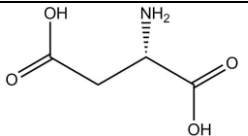
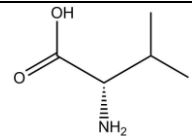
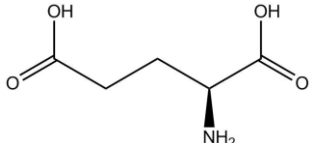
Table 5.1. Summary of spray dryer parameter conditions kept constant for crystallisability investigations.

Spray Dryer Parameter	Value
Aspirator rate	100 %
Inlet temperature	140 – 160 °C
Outlet temperature	100 °C
Pump percentage	10 %
Spray gas pressure	6 – 7 bar
Spray gas rate	10 SLM

Compound selection for the experimental crystallisability prediction was based on aqueous solubility and compound safety. To provide a degree of uniformity and comparison for the experiments, each compound was spray dried at its solubility limit at room temperature sourced from literature. The reported solubility and chemical structure for each compound can be found in Table 5.2.

Table 5.2. Reported solubility values of crystallisability prediction compounds.

Compound	Structure	Solubility	Compound	Structure	Solubility
Aspirin		0.3207 g / 100 g (Perlovich et al. 2004)	Lactose		20.5 g / 99 g (Siddique et al. 2015)
Fructose		1.8 g / 100 g (Sigma-Aldrich 2014a)	Maltose		85 g / 100 g (25°C) (Hanover and White 1993)
Galactose		18 g / 100 g (Sigma-Aldrich 2014b)	Mannitol		20.01 g / 100 g (Elversson and Millqvist-Fureby 2005)
Glucose		13.3 g / 100 g (Sigma)	Metformin HCl	 HCl	49 g / 100 g (Benmessaoud et al. 2016)

Glycine		22.4 g / 100 g (Ramasami 2002)	Paracetamol		1.278 g / 100 g (Granberg and Rasmuson 1999)
L-ascorbic acid		17.6 g / 100 g (Sigma-Aldrich 2014c)	Sucrose		203 g / 100 g (Nowak et al. 2009)
L-asparagine		2.785 g / 100 g (Lenka and Sarkar 2016)	Urea		48 g / 100 g (Sigma)
L-aspartic acid		1.1534 g / 200 g (Mischelevich and Apelblat 2008)	Valine		1.02 g / 100 g (Previously obtained within CMAC by Dr Anna Baczyńska)
L-glutamic acid		0.71 g / 100 g (Ono et al. 2004)			

5.2.2. Crystallisation Characterisation

Once each test solution was spray dried and the powder collected, the sample was characterised for crystallinity using XRPD.

5.2.3. Random Forest

The RF models and classifications were carried out and implemented using Pipeline Pilot (BIOVIA), using the CRAN-random forest package in the statistical computing environment 'R' (The R Foundation). This software gained the predictive results and performed model validation through the RF workflow (Figure 5.1).

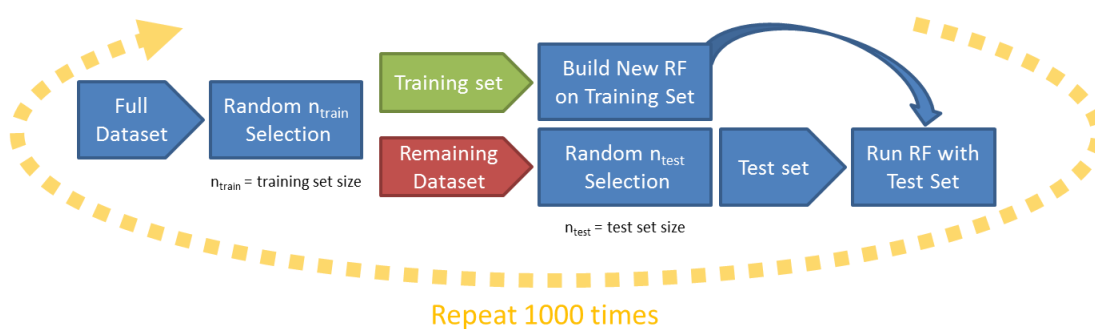


Figure 5.1. RF workflow used to create and develop the predictive crystallisability model.

Molecular descriptors (2D and 3D) for the datasets were calculated using MOE™ (Chemical Computing Group Inc. 2017). For each training set, 1000 RF models were built. For each repeat, the training set was randomly selected from the complete range of dataset compounds. A complementary test set was then chosen randomly from the remaining compounds. For each repeat the test set size was kept constant for all values of the training set in order to ensure a valid comparison of error rates across models.

At present, crystallisability from spray drying has been modelled using statistical and mathematical models with no reports of RF spray drying models. To investigate the practicality and success of RF for spray drying, published work by Van Eerdenbrugh and co-workers (Van Eerdenbrugh et al. 2010) was used as a template to create an RF model. Van Eerdenbrugh and co-workers published the crystallisation tendency classifications of 51 compounds in 3 different solvent systems by rapid solvent evaporation using spin coating. Crystallisation outcomes were classified into 3 separate classes dependent on experimental outcome; these compounds and classification results provided a diverse dataset and results suitable to create a RF model.

5.3. Results and Discussion

5.3.1. Van Eerdenbrugh Model

RF models were created from published experimental crystallisation data (Van Eerdenbrugh et al. 2010). All 51 compounds were spin coated from 3 different solvent systems; dichloromethane (DCM), ethanol (EtOH) and a 1:1 mix (DCM:EtOH) with their crystallisation tendency classified into 3 groups. Specifically: 1 (immediate semi-crystallisation occurrence); 2 (semi-crystallisation occurrence after 7 days) and 3 (predominantly amorphous after 7 days). The data selected to create the RF models was from the largest dataset of one solvent system; 34 compounds spin coated in DCM after compound exclusion due to degradation and / or sublimation. The RF classification results are presented in Table 5.3.

Table 5.3. Compound classification of crystallisability from (Van Eerdenbrugh et al. 2010).

Class 1	Class 2	Class 3
4-Biphenylmethanol	Clofoctal	Loratadine
4-Phenylphenol	Flubiprofen	Celecoxib
Anthranilic acid	4-Biphenylcarboxaldehyde	Clotrimazole
Benzamide	Bifonazole	Felodipine
Benzocaine	Carbamazepine	Indomethacin
Caffeine	Chlorpropamide	Itraconazole
Dibucaine	Fenofibrate	Ketoconazole
Flufenamic acid	Nilutamide	Ketoprofen
Lidocaine	Nimesulide	Miconazole
Phenacetin	Probucol	Pimozide
Tolbutamide	Tolazamide	Ritonavir
	Cinnarizine	

The crystallisability RF models created from the published results by Van Eerdenbrugh and co-workers (Van Eerdenbrugh et al. 2010), consisted of a training set of 34 diverse compounds spin coated from DCM, presented in Table 5.3. The model parameters used were the default settings of $n_{tree} = 500$ and $m_{try} = 12$; and the model was validated by reserving different numbers of the training set for testing and running the model to gain a predictive result from 1000 decision trees. To track the accuracy of the prediction, the mean error for each training set size was calculated.

To further evaluate the predictive capability of the RF models, the classification system for the training and test sets were manipulated to produce more accurate models. This was achieved through the reclassification of predictive class 2 results, either by instruction or by

guidance from the predictive result for each compound. This produced five different RF model trends of the crystallisability data published by Van Eerdenbrugh and co-workers. The mean error rates for each of the five model trends tested is shown in Figure 5.2.

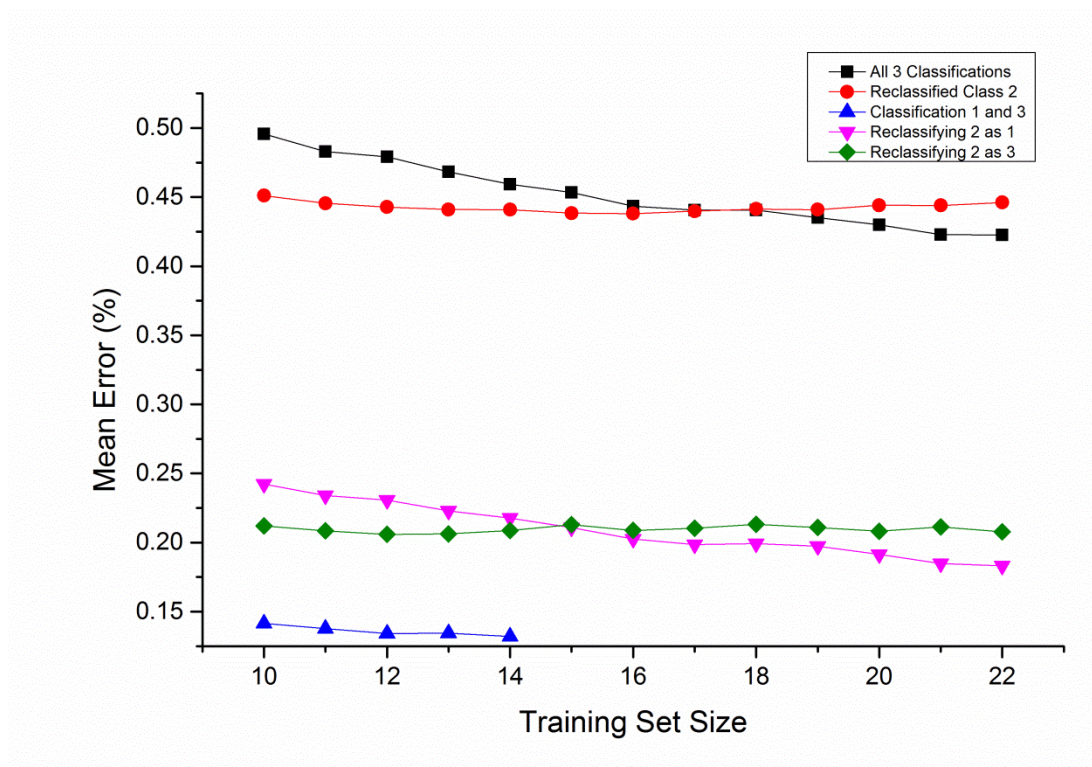


Figure 5.2. Mean error plots for Van Eerdenbrugh based RF models showing the predictive accuracy of each model with increasing training set sizes and different classification directions.

The five different mean error trends of the RF models showed a significant difference in the accuracy capability for crystallisability prediction. The original trend (black line in Figure 5.2) consisting of three classification results provided a relatively poor RF model trend with an accuracy of 57 %. This was significantly improved through the redistribution of allocated classifications relating to the class 2 results (i.e. those results deemed to be semi-crystalline after 7 days). The different model error trends clearly showed that instruction of reclassification of class 2 provided the most accurate of models. Specifically, the

reclassification of class 2 to class 1 and from class 2 to class 3 provided the most accurate predictive models of 82 and 79 % respectively. Furthermore, the exclusion of classification 2 altogether produced a model trend based only on molecules that form either class 1 (rapid crystallisation) or class 3 (stable amorphous). This produced a model trend with an excellent mean accuracy of 86.6 %. However, the exclusion of class 2 altogether significantly reduced the number of compounds available for the training and test sets and as such reduced the overall validity of the model. These resultant accuracies obtained for the RF models based on the Van Eerdenbrugh and co-workers data were higher than the previously reported RF crystallisability models (Johnston et al. 2008, Bhardwaj et al. 2015) thus showing the capability of RF as a predictive tool for recrystallisation from an amorphous state.

5.3.2. Van Eerdenbrugh Model with Spray Dryer Compounds

The successful construction of crystallisability predictive RF models highlighted the potential to incorporate predictive modelling into the design and integration of manufacturing process development workflows (Myerson et al. 2015). To support a continuous manufacturing workflow, modelling is required at all processing stages on a variety of different techniques and unit operations. As the RF crystallisability models were based on data collected by spin coating, the models were further tested using experimental data from spray drying to investigate the ability to translate the models based on recrystallisation from the amorphous state to recrystallisation from solution.

The crystallisability screen for spray drying successfully tested 17 different compounds, presented in Table 5.2, and measured the crystalline state using XRPD. Each compound was classified as either crystalline or amorphous by the emergence of sharp peaks within the observed diffraction patterns. Of the total of 17 tested compounds, 11 were found to be crystalline (Figure 5.3) and 6 amorphous (Figure 5.4).

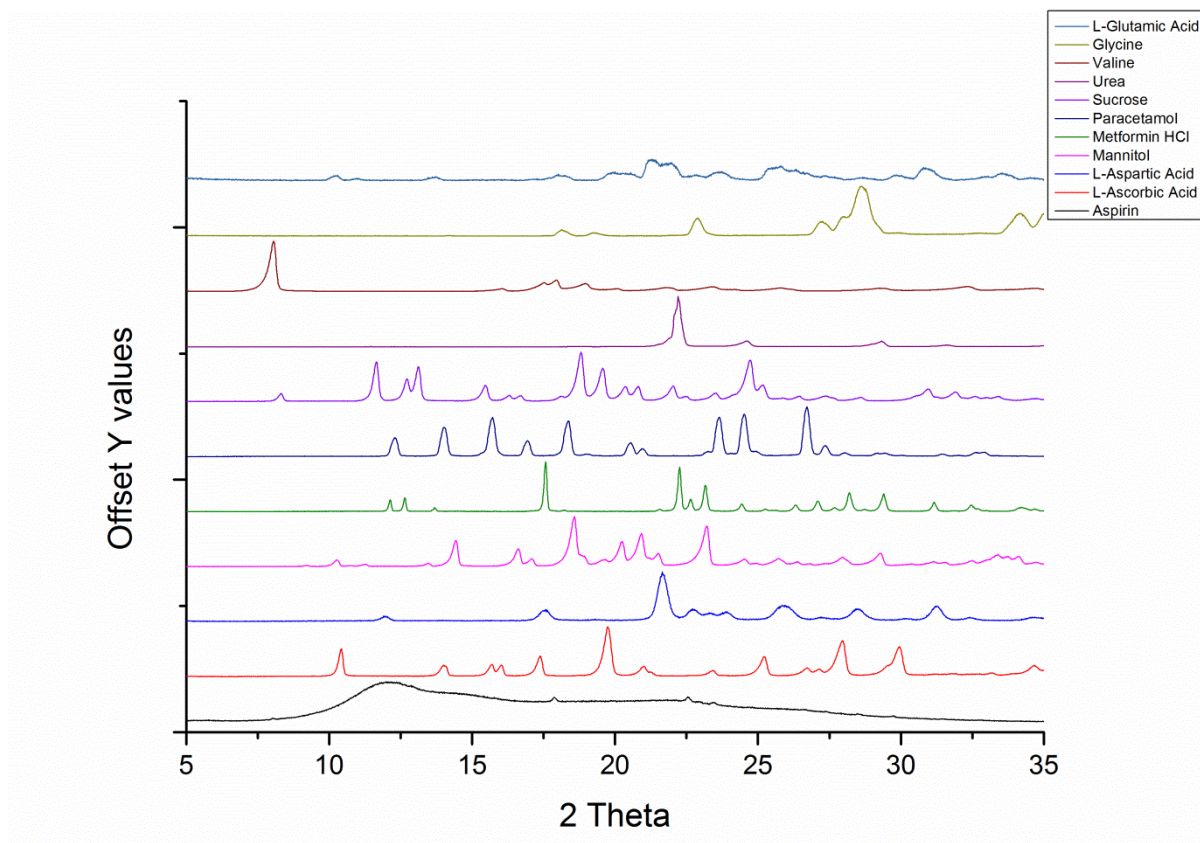


Figure 5.3. XRPD patterns of the 11 crystalline compounds produced by the spray dryer.

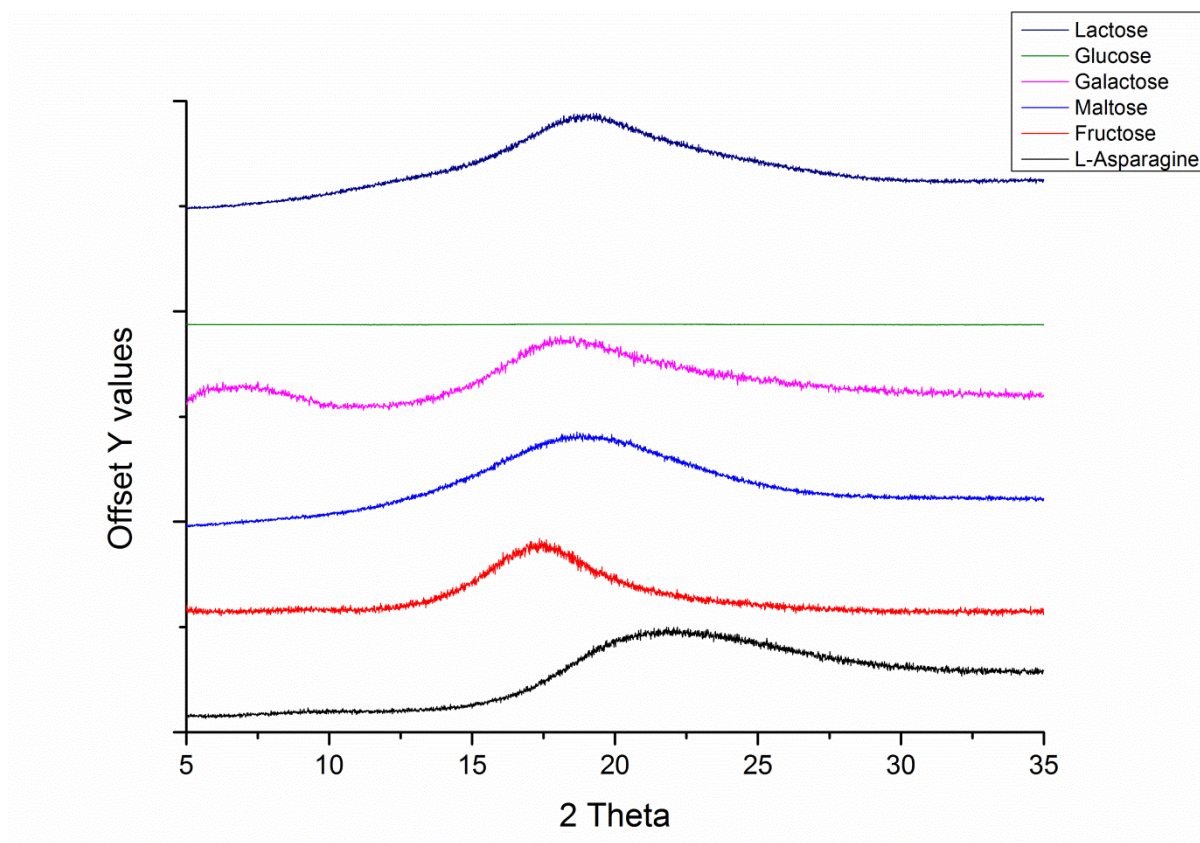


Figure 5.4. XRPD patterns of 6 amorphous compounds produced by the spray dryer.

To test the accuracy of the crystallisability predictive RF models, the 17 spray dried compounds were tested against the models developed in Section 5.3.1., with the predicted outcomes for each compound compared to observed experimental outcomes (shown in Table 5.4).

Table 5.4. Spray drying predictive comparisons with observed experimental results and predicted outcomes based on the different models produced in 5.2.1.

Compound	Experimental	Prediction		
		Re-classified 2 as 1 (64.7 %)	Re-classified 2 as 3 (70.5 %)	Only class 1 and 3 (64.7%)
Aspirin	<i>Crystalline</i>	Crystalline	Crystalline	Crystalline
Fructose	<i>Amorphous</i>	Crystalline	Crystalline	Crystalline
Galactose	<i>Amorphous</i>	Crystalline	Crystalline	Crystalline
Glucose	<i>Amorphous</i>	Crystalline	Crystalline	Crystalline
Glycine	<i>Crystalline</i>	Crystalline	Crystalline	Crystalline
L-ascorbic acid	<i>Crystalline</i>	Crystalline	Crystalline	Crystalline
L-asparagine	<i>Amorphous</i>	Crystalline	Crystalline	Crystalline
L-aspartic acid	<i>Crystalline</i>	Crystalline	Crystalline	Crystalline
L-glutamic acid	<i>Crystalline</i>	Crystalline	Crystalline	Crystalline
Lactose	<i>Amorphous</i>	Crystalline	Amorphous	Crystalline
Maltose	<i>Amorphous</i>	Crystalline	Amorphous	Crystalline
Mannitol	<i>Crystalline</i>	Crystalline	Crystalline	Crystalline
Metformin HCl	<i>Crystalline</i>	Crystalline	Crystalline	Crystalline
Paracetamol	<i>Crystalline</i>	Crystalline	Crystalline	Crystalline
Sucrose	<i>Crystalline</i>	Crystalline	Amorphous	Crystalline
Valine	<i>Crystalline</i>	Crystalline	Crystalline	Crystalline
Urea	<i>Crystalline</i>	Crystalline	Crystalline	Crystalline

Comparison of the RF crystallisability predictive models with the experimental results of 17 spray dried compounds, found a mean accuracy of 64.7, 70.5 and 64.7 % for the re-classification of results 2 to 1 and 2 to 3 and the exclusion of class 2 leaving only class 1 and

3 respectively. These accuracies concurred with the reported mean accuracy for the model published by Bhardwaj and co-workers based on slow crystallisation of sample solutions (Bhardwaj et al. 2015). An important consideration in the analysis of these models was the difference between the processes that were used for determinations of crystallisability; spin coating and spray drying. The two methods created and exposed the compounds to a different set of process conditions. Furthermore, the classifications for each process were significantly different; Van Eerdenbrugh and co-workers (Van Eerdenbrugh et al. 2010) included 3 classes with an intermediate class 2, whilst in these spray drying data, 2 classes were included, namely crystalline or amorphous. As the models were created with a class 2, this meant that testing with spray dryer compounds required some compounds to be reclassified. As spray drying classifications were based on a rapid crystallisation response measurement, it would be expected that most class 2 predictions from the literature models would be classed as the amorphous class 3 by spray drying.

5.3.3.Spray Dried Model

Whilst the RF model based on the published data from Van Eerdenbrugh and co-workers (Van Eerdenbrugh et al. 2010) attempted to predict the crystallisability of 17 compounds from spray drying, the difference in crystallisation methods was expected to have a significant effect on the ability of the model to predict accurately outcomes under substantially different conditions. Therefore, a model created from the known spray drying data collected from the 17 compounds tested in Table 5.4 may be more appropriate for spray drying crystallisability predictions.

Following the RF workflow (Figure 5.1) the training set size was varied over 5 – 11 compounds. Each individual model was tested at a tree number of 1000 variations. The mean predictive errors for each set of RF models are presented in Figure 5.5.

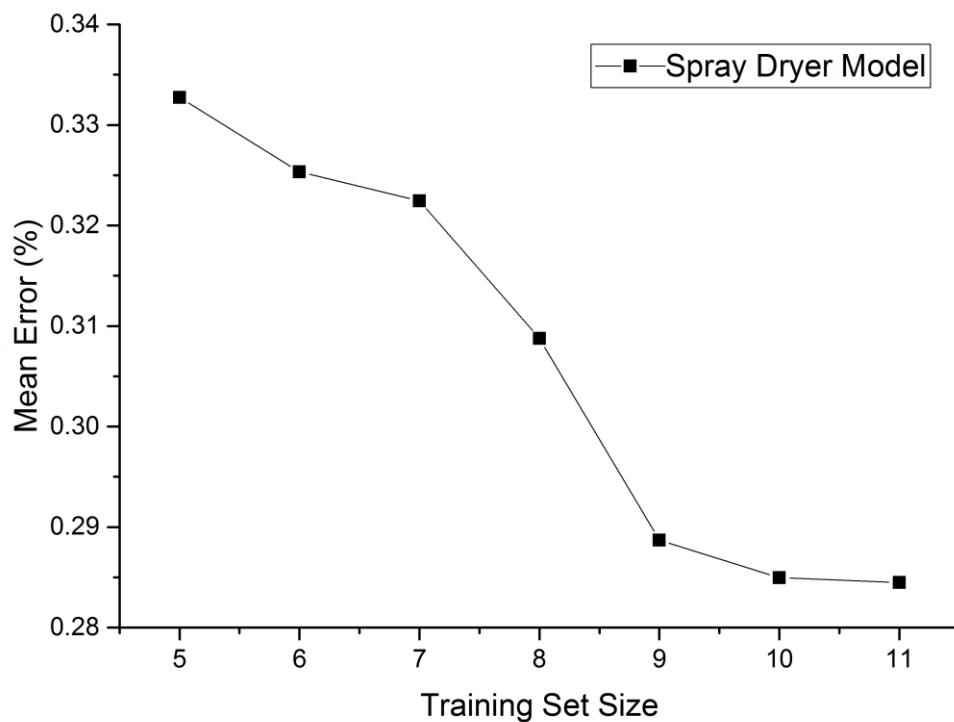


Figure 5.5. Mean error plot for spray dryer model trend showing predictive accuracy of models with increasing training set size.

The mean error trend for the spray dryer models was found to have a predictive accuracy of 71.55 %. This model trend showed an improvement for crystallisability prediction from spray drying to the Van Eerdenbrugh and co-workers based model from 64.7 and 70.5 % to 71.55 %, which highlighted the benefit of a technique specific model. Whilst this result was encouraging, there were several caveats that must be taken into account. Firstly, for RF to gain the best possible model, a large training and test set is required. The 17 spray dryer compounds were therefore, a very small dataset which restricts the number of random variations that could be tested during validation of the model. Furthermore, even though the 34 published literature compounds have not been experimentally tested the experimental results from the published spin coating experiments suggested that a 100 % crystalline result would not be likely to be the case. This result may also be due to the lack of compound

physical property diversity in the 17 training set compounds. Ideally, for a generally applicable model the RF based prediction would be developed using observed experimental outcomes from molecules that displayed a broad range of molecular size, flexibility, electronic properties and so on. To determine compound diversity for the training and test datasets and compare these to a large scale dataset of pharmaceutically relevant compounds a principal component analysis (PCA) was carried out, excluding descriptors of zero variance, and presented in Figure 5.6.

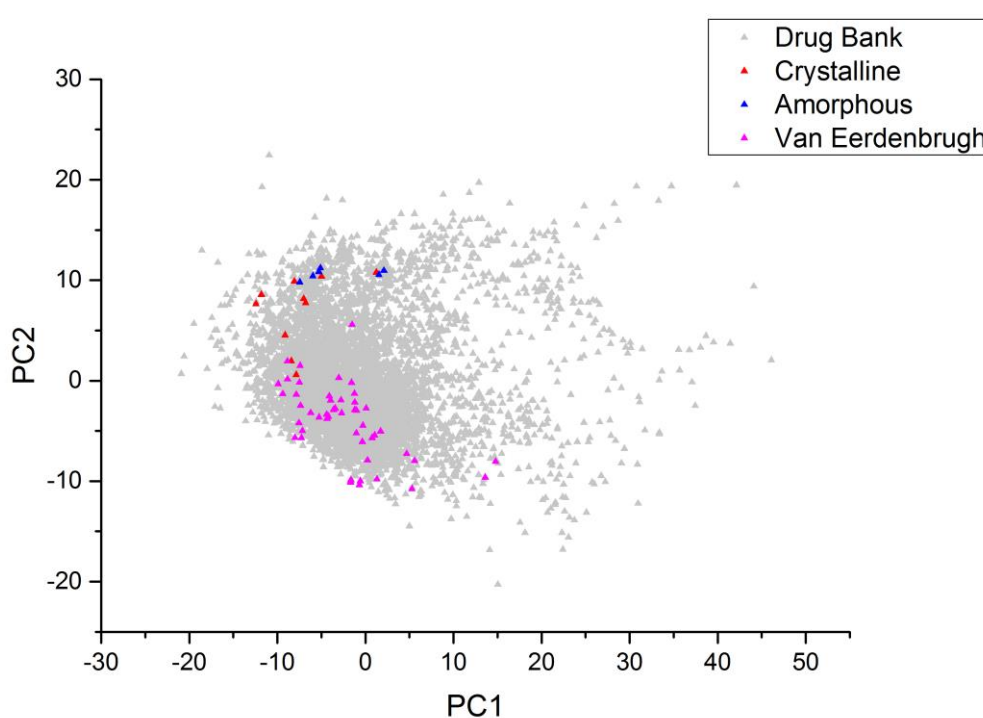


Figure 5.6. PCA scores plot of compound diversity of all model training and test set compounds against 6119 pharmaceutical compounds from DrugBank (The Metabolics Innovation Centre).

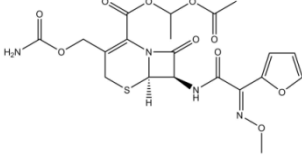
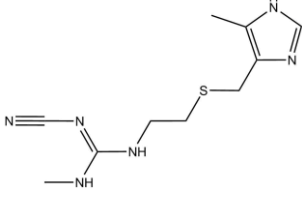
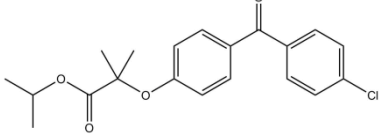
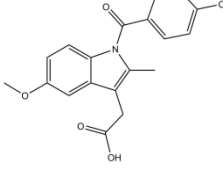
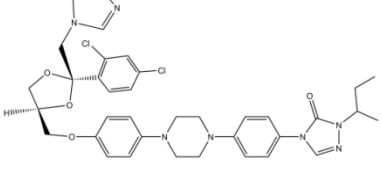
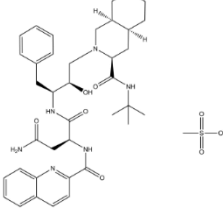
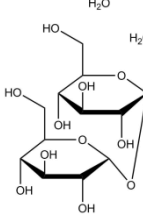
The PCA plot clearly illustrated the lack of diversity in the chemical space for the different compounds used to create and test the RF spray dryer models (red and blue points in Fig 5.6). PCA uses the calculated molecular descriptors of each compound to statistically

compare each compound through translation into a 2D plot. The 17 compound training set were split due to crystalline state; red are crystalline compounds and blue are amorphous. The 34 test set from published data are presented as pink markers and the grey markers are 6119 different pharmaceutically relevant compounds from DrugBank (The Metabolics Innovation Centre). As 5 out of the 6 amorphous compounds were sugars, the PCA clearly reflected this lack of chemical diversity, which suggested that spray dryer only derived RF models capable of predicting whether a compound is a sugar rather than if it will crystallise. Therefore these results, showed the need to build a more accurate and widely applicable RF model for spray drying, with a larger and more chemically diverse training set including the observed results from many more spray drying experiments.

5.3.4.Spray Dryer Model Supplemented with Known Amorphous Compounds

To overcome the lack of compound diversity of the spray dryer RF model, known amorphous compounds resulting from spray drying or rapid evaporative crystallisation were supplemented into the training set. It would be expected that an increase in amorphous compound diversity would result in a more accurate prediction capability due to the ability of the model to differentiate compounds further using molecular descriptors. The compound and structures supplemented into the spray dryer RF model can be found in Table 5.5.

Table 5.5. Molecular structures of compounds reported in the literature to form amorphous forms.

Compound	Structure
Cefuroxime Axetil	
Cimetidine	
Fenofibrate	
Indomethacin	
Itraconazole	
Saquinavir	
Trehalose	

The resulting RF model consisting of the 17 compounds spray dried and 7 known amorphous compounds produced a mean accuracy of 79 %. This was an improvement on the original spray dryer model, which highlighted the need to provide a highly diverse and large quantity training set to gain a significant accurate predictive model. The improvement in compound diversity is presented in the PCA plot in Figure 5.7.

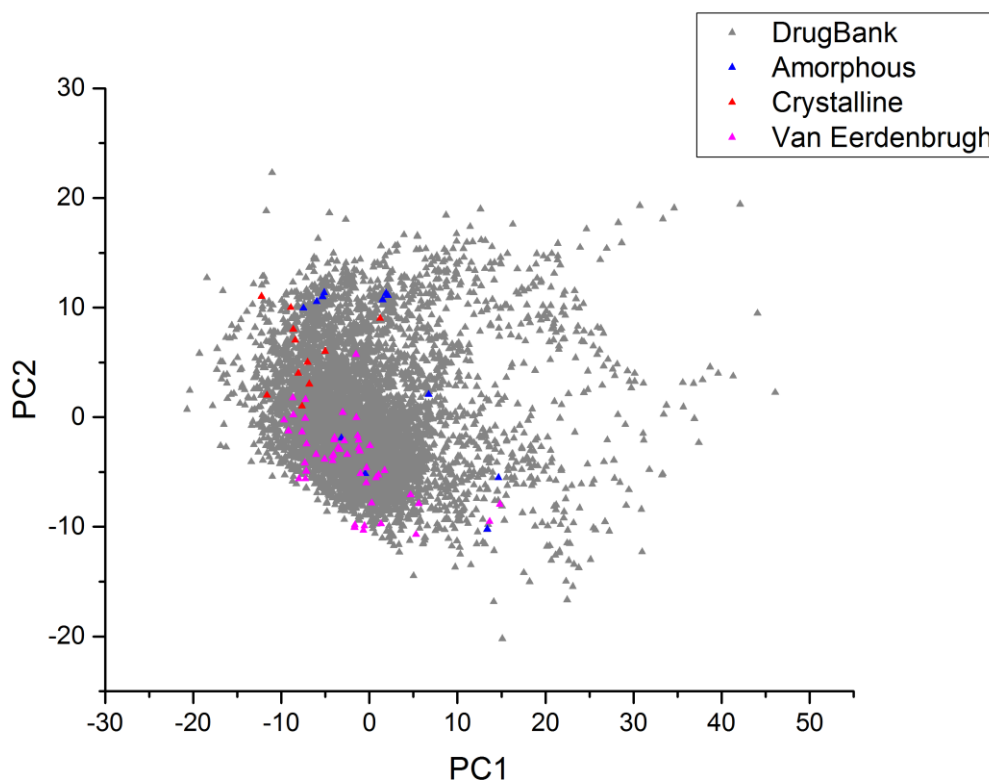


Figure 5.7. PCA scores plot with 17 training set supplemented with 7 further amorphous compounds based on literature reports against 6119 pharmaceutical compounds from DrugBank (The Metabolics Innovation Centre).

The 7 amorphous supplemented model compounds were incorporated into the blue class 3 markers of the PCA plot. The amorphous compounds overlap into the Van Eerdenbrugh published data range and showed a wider distribution versus the 6119 drug bank compounds, which confirmed a higher diversity and better representation of different compounds.

However, the training set for the model lacked the size and full diversity to represent the drug-like compounds that may be developed by pharmaceutical industry programmes.

5.3.5. Models Tested with BCS Compounds

The production of a RF model to predict crystallisability of pharmaceutically relevant compounds by spray drying offered a novel approach to integrate predictive modelling tools to support and inform continuous manufacturing development (Badman and Trout 2015). This may be of specific use for the determination of crystallisability of molecules based on molecular structure. The RF models generated from calculated molecular descriptors and a subset of known experimental results was further tested on compounds with different aqueous solubilities and permeabilities. This would allow the model to be used to assess whether there is any correlation between biopharmaceutical performance and crystallisability.

The Biopharmaceutical Classification System (BCS) is used to classify pharmaceutical compounds based on their aqueous solubility and permeability (Chavda et al. 2010). Compounds in BCS I have high solubility and high permeability whilst compounds in BCS IV have low solubility and low permeability (U.S. Food & Drug Administration). To overcome the issues surrounding BCS IV, a common approach is to develop methodologies to stabilise amorphous forms as formulated amorphous solid dispersions (ASDs) to enhance dissolution and bioavailability. Spray drying has been previously discussed (Section 1.4) as a technique capable for the production of a wide variety of particle structures including ASDs that aim to stabilise the amorphous form of a component by dissolving it in a polymer matrix enabling the delivery of poorly soluble compounds (Singh and Van den Mooter 2016). Spray drying can therefore be used to stabilise BCS IV compounds through ASD formation which may improve the performance of these compounds. Hence crystallisability predictive models

could act as a predictive screening for amorphous compounds that may inform their suitability for amorphous or ASD preparation by spray drying. Whilst BCS is a biopharmaceutical index and not one for crystallisability, it was interesting to explore whether any relationships existed between compound solubility, permeability and crystallisability. This could form the basis of a more rational approach to design physical properties through control of molecular structure. Specifically the crystallisability of a number of compounds with reported BCS classifications as I or IV was predicted using the spray dryer model with supplemented amorphous compounds described in Section 5.3.4. The tested compounds can be found in Table 5.6 with the predictive result presented in Table 5.7.

Table 5.6. 32 selected compounds classified as BCS I and IV from literature reports.

BCS I	BCS IV
Amiloride	Acetazolamide
Chloroquine	Amphotericin B
Cyclophosphamide	Cefuroxime
Diazepam	Chlorthalidone
Diltiazem	Chlorothiazide
Doxycycline	Cyclosporine
Fluconazole	Etravirine
Levonorgestrel	Famotidine
Metformin HCl	Furosemide
Metoprolol	Indinavir
Metronidazole	Itraconazole
Paracetamol	Nelfinavir
Phenobarbital	Ritonavir
Propranolol	Saquinavir
Pseudoephedrine Sulfate	Tobramycin
Theophylline	
Verapamil HCl	

Table 5.7. Predictive results for BCS I and IV compounds using the spray dryer plus amorphous RF model.

BCS I	SD + A	BCS IV	SD + A
Amiloride	<i>Amorphous</i>	Acetazolamide	<i>Amorphous</i>
Chloroquine	<i>Amorphous</i>	Amphotericin B	<i>Amorphous</i>
Cyclophosphamide	<i>Amorphous</i>	Cefuroxime	<i>Amorphous</i>
Diazepam	<i>Amorphous</i>	Chlorthalidone	<i>Amorphous</i>
Diltiazem	<i>Amorphous</i>	Chlorothiazide	<i>Amorphous</i>
Doxycycline	<i>Amorphous</i>	Cyclosporine	<i>Amorphous</i>
Fluconazole	<i>Amorphous</i>	Etravirine	<i>Amorphous</i>
Levonorgestrel	<i>Amorphous</i>	Famotidine	<i>Amorphous</i>
Metformin HCl	<i>Crystalline</i>	Furosemide	<i>Amorphous</i>
Metoprolol	<i>Amorphous</i>	Indinavir	<i>Amorphous</i>
Metronidazole	<i>Crystalline</i>	Itraconazole	<i>Amorphous</i>
Paracetamol	<i>Crystalline</i>	Nelfinavir	<i>Amorphous</i>
Phenobarbital	<i>Amorphous</i>	Ritonavir	<i>Amorphous</i>
Propranolol	<i>Amorphous</i>	Saquinavir	<i>Amorphous</i>
Pseudoephedrine Sulfate	<i>Crystalline</i>	Tobramycin	<i>Amorphous</i>
Theophylline	<i>Crystalline</i>		
Verapamil HCl	<i>Amorphous</i>		

The crystallisability predictive results for BCS I and IV from the spray drying RF models supplemented with amorphous compounds predominantly predicted a preference for amorphous form outcomes for the selected compounds. Amongst BCS class I compounds, the model predicted that small molecule salt forms were more likely to form crystalline solids with the exception of verapamil HCl. Salts are typically used to enhance solubility by

introducing ionised species into the lattice. These strong electrostatic intermolecular interactions would also be expected to favour the formation of ordered, highly directional crystalline packing arrangements. The larger verapamil molecule could be envisaged to kinetically hinder the ordering process compared with a smaller molecule such as metformin HCl during rapid crystallisation. Interestingly all BCS class IV have been predicted by the model to form an amorphous solid. This could suggest that all of the BCS IV compounds would be suitable for ASD formation by spray drying.

As the RF models were built on the calculated molecular descriptors for each compound, the predictive results for BCS I and IV may depend on specific or a combination of related descriptors. Of the 288 molecular descriptors used for these models (all of the MOE 2D and 3D descriptors minus zero variance entries), the descriptors with the highest importance seemed to favour molecular size and shape suggesting that larger molecules may tend towards an amorphous form by spray drying. The extension of the test set for BCS I and IV, with particular inclusion of small BCS IV compounds, would enable these descriptors to be isolated with further accuracy and experimental measurements for the crystallisability of the 32 BCS compound would allow validation of the models.

The molecular descriptors can also be used to examine the diversity of the BCS I and IV compounds. Using these descriptors, PCA analysis indicated their diversity thus giving some confidence in the reliability of the BCS crystallisability predictions. A PCA scores plot for the 32 BCS compounds against 6119 pharmaceutically relevant compounds is shown in Figure 5.8.

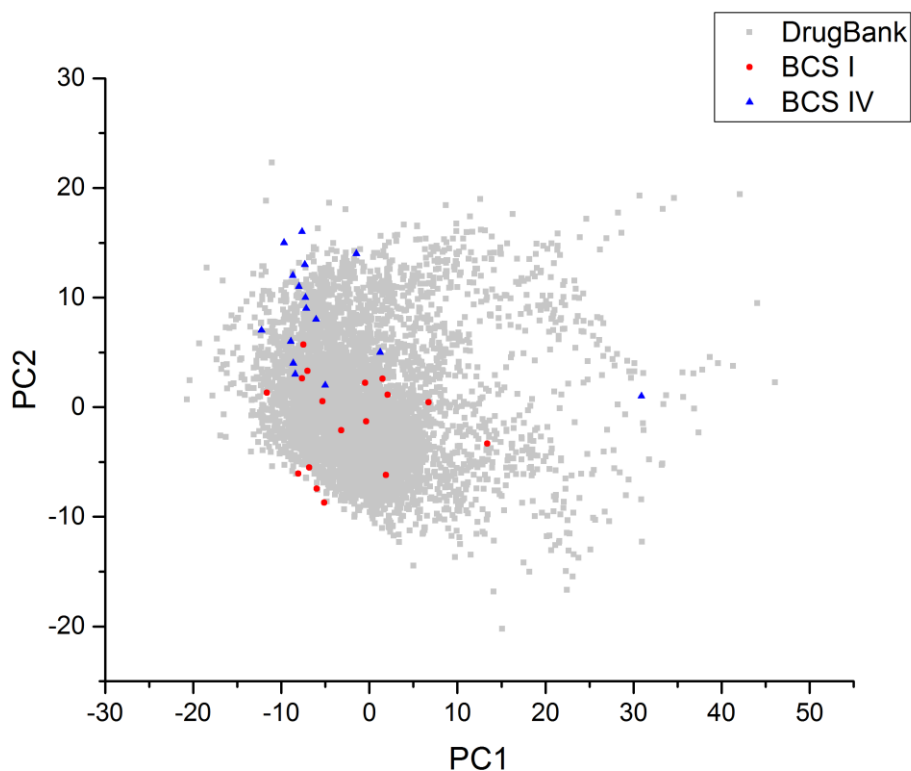


Figure 5.8. PCA scores plot of BCS I and IV compounds against 6119 pharmaceutical compounds from DrugBank (The Metabolics Innovation Centre).

The PCA of BCS class I and IV compounds showed a reasonably diverse spread of physicochemical properties of the tested compounds with two distinct clusters and minimal outliers. This indicated that PCA may be able to differentiate compounds based on BCS classification. Amongst the BCS I compounds, the crystalline compounds were dispersed within the cluster and do not enable crystallisability of BCS I to be defined. It would be expected that an expansion of the test set for BCS I and IV may provide further crystalline predictive results that could show cluster formation for amorphous and crystalline of BCS I compounds.

5.4. Summary

The aim of this work was to investigate whether a predictive model for the crystallisability of pharmaceutically relevant compounds can be developed using RF based on calculated molecular descriptors. This was first determined by creating a predictive model using previously published crystallisability data (Van Eerdenbrugh et al. 2010). Several RF models were produced through manipulation of the published classifications which produced very good mean predictive model accuracies of 79 – 86.6 %. These models were then analysed for spray drying crystallisability predictions delivering predictive accuracies of 64.7 – 70.5 %. In order to gain the most representative crystallisability prediction for spray drying, a spray drying model was then produced using the experimental data which returned a mean accuracy of 71.55 %. However, the small training and test sizes for the spray dryer model meant a limited compound diversity and therefore applicability of the model to other compounds would be limited at this stage. To overcome this, known amorphous compounds were supplemented into the spray dryer model and found a mean accuracy improvement to 79 %. Finally, an exploratory test of the spray dryer model with supplemented amorphous compounds to determine if compounds from BCS I and IV would be more or less likely to form amorphous solids was carried out. This showed a slightly higher tendency for the BCS I molecules tested to crystallise. The predictions for compounds to form amorphous solids may be an indicator of their suitability for ASD formation. The different crystallisability prediction RF models spray drying highlighted the capability for process modelling and that predictive screening of compounds can support the consideration for manufacturing.

Chapter 6. Co-Spray Drying for
Multicomponent Particles using the
Three-Fluid Nozzle

6. Co-Spray Drying for Multicomponent Particles using the Three-Fluid Nozzle

6.1. Introduction

Manufacturing processes for pharmaceutical products have predominantly consisted of separate unit operations performed under batch mode. However there is an increasingly strong focus on the adoption of continuous manufacturing approaches to achieve higher quality, greater consistency, less material and energy utilisation from smaller, more distributed plants. However, the pharmaceutical industry faces a considerable challenge in the adoption and integration of continuous manufacturing approaches and technologies across all processing stages in its supply chain (Badman and Trout 2015).

Integration of unit operations, in particular crystallisation and downstream stages, provides opportunities to implement alternative approaches to those traditionally used. One aspect that has been proposed is to utilise integrated continuous processes to achieve homogeneous processing of drug product components. Homogeneous, as opposed to heterogeneous, processing provides a method for component processing without significant segregation of materials irrespective of molecular nature and as such has been said to demonstrate ‘true continuous manufacture’ (Byrn et al. 2015). Spray drying is an excellent example of homogeneous continuous processing. Co-processing of APIs with functional excipients can occur via numerous mechanisms at different stages of the continuous manufacturing chain with direct monitoring and control of composition to ensure performance (Byrn et al. 2015). For example, addition of excipients during crystallisation or filtration could be used to overcome challenging physical properties such as low bulk density to ensure ease of downstream manufacture.

6.1.1. Co-Processing of Pharmaceuticals

Pharmaceutical oral solid dosage formulations largely consist of a single API blended and / or compacted in combination with multiple excipients and / or additives to deliver a drug product of high efficacy and consistent quality. Excipients and other inert compounds provide multi-functional roles within a formulation and are largely manufactured individually by batch processes. These can therefore be a potential source of product variation between batches or suppliers (Gohel and Jogani 2005, Badman and Trout 2015). Therefore the design of a formulation and drug product must consider the CQAs of the API and excipients to ensure product quality (European Medicines Agency 2011). CQAs are identified as the properties that are necessary to achieving a quality drug product and as such must be established to the standard set by the regulators (Yu 2008). However, manufacturing variation can result in a divergence of CQAs that can limit or even inhibit the success of many formulations. Co-processing can overcome these limitations by the creation of novel or engineered formulations that target specific CQAs in order to optimise product quality and reduce unit operations (Byrn et al. 2015). An important CQA that can be targeted under co-processing is the physical characteristics of an API and in particular physical structure (European Medicines Agency 2011). Investigations into crystal forms (Hancock et al. 2002) and polymorphism (Hilfiker et al. 2003, Getsoian et al. 2008) have shown the considerable effect these properties can have on other CQAs and the need for in-depth understanding to ensure high drug product quality. However, these investigations are based on single components and still may lead to issues in downstream processing. Co-processing of excipients is popular in the optimisation of excipient properties and functionality to improve downstream processing stages and product quality (Gohel and Jogani 2005). There are several co-processed excipients currently on the market that aim to improve formulations for direct compression by inclusion in the final dosage form to support the manufacture process, improve attributes and enhance overall effectiveness of the formulation. For example, Ludipress, consisting of α -lactose monohydrate, polyvinyl pyrrolidone and crospovidone,

increases disintegration time in comparison to α -lactose monohydrate and Cellactose, consisting of α -lactose monohydrate and cellulose, reduces moisture sorption compared to pure microcrystalline cellulose due to coating of cellulose fibres with lactose (Gohel and Jogani 2005). The combination of APIs with excipients, polymers and additives during crystallisation can produce a co-processed particle that will exhibit unique and optimised particle properties different from the original components (Li et al. 2017). For example, the inclusion of the additive PVP K30 to the crystallisation of metformin HCL improved the flowability and compressibility properties through a change of crystal morphology (Barot et al. 2012). Co-processed particles can provide an opportunity to overcome poor particle properties and performance.

6.1.2. Co-Processing by Spray Drying

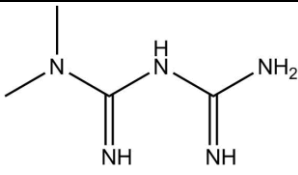
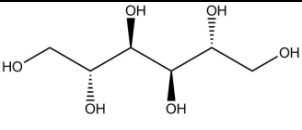
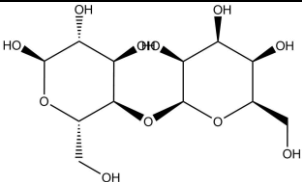
Spray drying is an adaptable technique that is appropriate for many different co-processing applications. The wide variety of feed compositions, parameters and process configurations enable flexibility in combining materials under controlled conditions to produce novel or optimised multicomponent particles and formulations with controlled and improved performance. The introduction to a spray dryer of a multicomponent feed can target a variety of different particle structures including coated particles (Vanhoorne et al. 2014), nanoparticles (Pilcer et al. 2013), composites (Kadota et al. 2015) and solid dispersions (Soulaïrol et al. 2015, Singh and Van den Mooter 2016). Also optimising the CQAs of an API by multicomponent co-processing has been demonstrated in order to modify solid form (Chidavaenzi et al. 2001a, Hulse et al. 2009, Baaklini et al. 2014), particle size (Coucke et al. 2009a) and particle surface characteristics (Shen et al. 2011) .

Typically, examples in the research literature of co-processing by spray drying (co-spray drying) have been conducted using a two fluid nozzle consisting of single feed comprising of

several components coupled with a gaseous feed. However, the Büchi Mini spray dryer platform can operate with a three-fluid nozzle; this nozzle operates two separate liquid feeds with a third gaseous feed. This nozzle offers further co-processing applications allowing immiscible solids and solvents to enter the dryer via separate feeds and be mixed at the point of atomisation (Legako and Dunford 2010). This has been used in the design of novel particles by microencapsulation (Jiang et al. 2013, Kondo et al. 2014, Sunderland et al. 2015) however, further examples are relatively limited in the literature and no examples of co-processing crystalline phases has been reported.

6.1.3. Metformin Hydrochloride, Mannitol and Lactose

Table 6.1. Molecular structures of MF, mannitol and lactose.

Metformin Hydrochloride	Mannitol	Lactose
 <p style="text-align: center;">HCl</p>		

Metformin hydrochloride (MF) is a biguanide, used in the treatment of diabetes type II as an anti-hyperglycemic agent (Setter et al. 2003, Barot et al. 2010). MF has a high water solubility ($> 300 \text{ mg/mL}^{-1}$ at 25°C) (Barot et al. 2010) but has low permeability thus falling into the Biopharmaceutical Classification System (BCS) class III (Cheng et al. 2004). MF has been spray dried in the presence of polyvinylpyrrolidone (PVP) to engineer particle properties to enhance compressibility (Barot et al. 2010) and has also been spray dried in the presence of ethyl cellulose to produce sustained release nanoparticles (Mokale et al. 2016). The solid-state forms of MF have been reported in two polymorphic forms; MF forms A and B (Childs et al. 2004). MF form A is the stable form of the two polymorphs, with the

metastable form B produced by evaporative crystallisation at elevated temperatures (Childs et al. 2004).

Mannitol is a hexahydric alcohol used highly frequently as an excipient, specifically as a diluent (Rowe et al. 2012). Mannitol has been a widely used model excipient in spray drying investigations including the effect of drying kinetics and profiles on the polymorphic form of mannitol (Lee et al. 2011), particle engineering studies of mannitol morphology through manipulation of spray dryer parameters (Maas et al. 2011) and understanding process parameters, such as droplet size, relate to surface properties, such as surface roughness (Littringer et al. 2013). Mannitol can exist as multiple polymorphs, β , α and δ and as a hemihydrate (Burger et al. 2000). β -mannitol is the stable form at ambient conditions. α -mannitol is produced from cooling crystallisation whilst δ , which is more difficult due to its metastable nature, can be produced by rapid cooling and filtration of hot saturated solutions (Burger et al. 2000). Spray drying of mannitol has found β and α -mannitol from pure solutions and δ -mannitol by co-spray drying with PVP (Vanhoorne et al. 2016).

Lactose is a disaccharide sugar and the most commonly used excipient in dry powder formulations for pulmonary delivery (Healy et al. 2014). Lactose has been extensively investigated using spray drying; co-spray drying with polymers using the two-fluid nozzle to investigate polymorphic form (Chidavaenzi et al. 2001a) and targeting vaccine stability through inclusion of lactose to produce spray dried vectors (LeClair et al. 2016). Lactose can exist in a number of distinct solid forms; α -lactose monohydrate, stable anhydrous, unstable anhydrous and β -lactose (Kirk et al. 2007). α -lactose monohydrate is the hydrated and stable form of the polymorphs with anhydrous forms produced by dehydration of α -lactose monohydrate and β -lactose produced at temperatures above 93.5 °C (Kirk et al. 2007).

The current work sought to investigate spray drying in a Büchi Mini spray dryer using a three-fluid nozzle configuration as an approach to produce multicomponent particles through co-spray drying. The influence of process stream configuration and drying kinetics was explored through composite particle production and structural characterisation using XRPD, DSC, Raman mapping and SEM coupled with EDX (3.2).

6.2. Experimental

6.2.1. Compound Selection

MF was selected as the model active compound along with β -mannitol and α -lactose monohydrate, which were selected specifically for this work due to the theoretical drying principles of each compound. The previous chapter screened mannitol and lactose for crystallisability by spray drying and found that a crystalline and amorphous form was produced respectively. As these were spray dried under the same process conditions, the drying and crystallisation kinetics for each compound must be different. For this reason these two compounds were selected, to enable an investigation on the effects of co-processing on the result particle form. The starting concentrations of solutions to the dryer were: MF at 24.5 g / 50 g, Mannitol at 10 g / 50 g and Lactose at 10.1 g / 50 g in water at room temperature.

6.2.2. Spray Drying Method

MF, mannitol and lactose solutions were spray dried using the Büchi B-290 Mini Spray Dryer coupled with the Büchi Inert Loop B-295 (Büchi Labortechnik AG). The dryer was operated in co-current closed mode with nitrogen as the drying gas. The spray dryer parameters used to obtain a composite particle for each combination are presented in Table 6.2.

Table 6.2. Summary of co-spray drying parameter conditions.

Parameter	MF and Mannitol	MF and Lactose
Aspirator rate	100 %	100 %
Inlet temperature	148 °C	180 °C
Pump rates inner	3-4 ml/minute	3-4 ml/minute
Spray gas pressure and rate	6 – 7 bar, 50 – 60 mmHg	6 – 7 bar, 50 – 60 mmHg

6.2.3. Three-fluid Nozzle

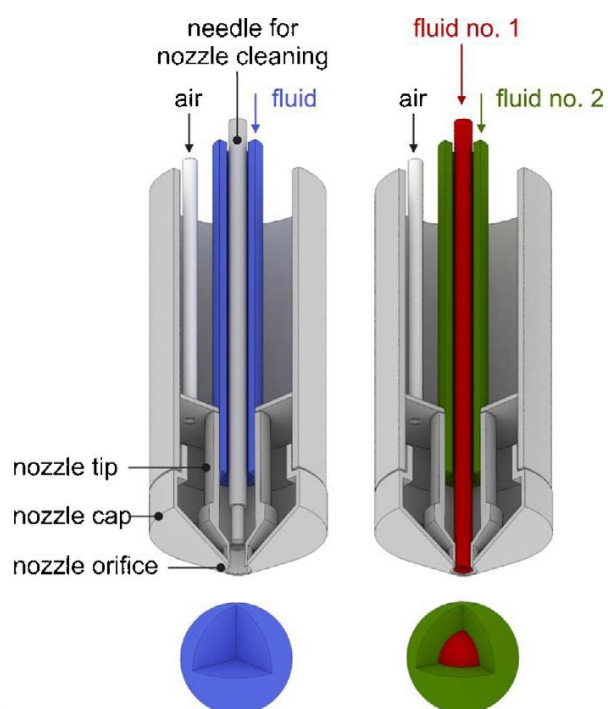


Figure 6.1 Schematic of two-fluid nozzle (left) and three-fluid nozzle (right) showing passage of fluid streams with proposed droplet structures (Kašpar et al. 2013).

The Büchi three-fluid nozzle operated on the introduction of 2 separate fluid streams that were delivered to the nozzle by separate peristaltic pumps. The Büchi B-290 Mini spray dryer unit had an internal peristaltic pump and a second external peristaltic pump was used to

deliver the second fluid stream. Both pumps were calibrated to volumetric flow rate (ml/minute) to ensure matching delivery of solutions to nozzle. The three-fluid nozzle brought the two fluid streams together along with the drying gas at the point where the fluid was atomised and sprayed into drying chamber. One feed was introduced to the side of the nozzle (outer); the second was introduced at the top of the nozzle (inner), instead of the drying gas for nozzle cleaning as found in the two-fluid nozzle. The different stream locations were expected to produce a different structural arrangement for the particles; the outer stream was expected to coat the inner stream, as seen in the proposed droplet in Figure 6.1. The different configurations for the co-spray drying experiments are presented in Table 6.3.

Table 6.3. Summary of co-spray drying configurations of the fluid streams of the three-fluid nozzle for different two-component spray dried systems.

Configuration	MF	Mannitol	Lactose
1	Inner	Outer	N/A
2	Outer	Inner	N/A
3	Inner	N/A	Outer
4	Outer	N/A	Inner

6.2.4. Composite Particle Characterisation

Once all four configurations of co-spray drying had been carried out each sample was characterised for particle structure using the SEM, images collected at 15 KV, SEM coupled with Energy-Dispersive X-ray spectroscopy (EDX) and Raman microscopy. Crystalline form was identified using XRPD, particle size and size distribution was measured using the Malvern Morphologi G3. Thermal transformations were analysed using DSC.

6.3. Results and Discussion

6.3.1. Multicomponent Composite Particles

The co-spray drying process coupled with the three-fluid nozzle successfully produced four different solid composite particles consisting of a different combination and configuration of MF, mannitol and lactose.

6.3.1.1. MF – Mannitol Co-Spray Dried Composites

MF and mannitol were successfully spray dried using the three-fluid nozzle and created two different samples of composite particles based on each nozzle feed configuration. The nozzle configuration consisted of an inner and outer feed delivery route that was proposed to promote the outer feed to coat or encapsulate the inner feed. The two composite particles produced consisted of the two different configurations; configuration 1 was MF as the inner feed and mannitol as the outer feed and configuration 2 was MF as the outer feed and mannitol as the inner feed.

The physical parameters relating to the drying kinetics that are representative of MF and mannitol particle formation by spray drying (based on conditions seen in Table 6.2) were determined in order to inform the expected particle outcome from co-spray drying of MF and mannitol with the three fluid nozzle. The theoretical diffusion coefficient and evaporation rate, the Peclet number and surface enrichment (Section 1.1.1) were calculated for MF and mannitol and can be found in Table 6.4.

Table 6.4. Theoretical drying kinetics for MF and mannitol calculated from equations 1.2, 1.3, 1.4 and 1.14 (Vehring 2008).

Drying Kinetics	MF	Mannitol
Diffusion Co-efficient, D (m ² /s)	7.605×10^{-10}	1.141×10^{-09}
Evaporation Rate, κ (m ² /s)	1.431×10^{-08}	1.431×10^{-08}
Peclet Number, Pe	2.35	1.57
Surface Enrichment, E	1.523	1.337

The theoretical drying kinetics for MF and mannitol found the different diffusion coefficients may have been significant in the act of particle formation (Vehring 2008). For spray drying of single components, both compounds presented a $Pe > 1$ which suggested that shell formation during drying and a hollow particle may be possible. As surface enrichment (E) is the measure of surface concentration relative to overall particle concentration, the higher MF surface enrichment suggested that a higher concentration of MF would be present at the surface compared to mannitol. For spray drying that provided equal mixing, the higher diffusion coefficient of mannitol suggested that mannitol may diffuse through the droplet towards the surface faster than MF. However, the higher concentration and surface enrichment level of MF present, would allow a significant mass at the surface. For co-spray drying using the three-fluid nozzle, as seen in Figure 6.1, the different layering of the feeds was expected to influence particle formation. The influence of nozzle configuration has been previously reported for co-spray drying for microencapsulation of omeprazole sodium with Eudragit L100 in order to protect the drug compound from acidic degradation (Sunderland et al. 2015).

For configuration 1, mannitol was present in the outer feed and as it exhibited a fast diffusion coefficient, an excess of mannitol at the surface was expected. The inner MF feed would require MF to travel further to the surface than mannitol but due to the higher concentration,

MF was still expected at the surface. For configuration 2, MF was present in the outer feed and as such was expected at the particle surface. The mannitol present in the inner feed was able to travel quicker to the surface than MF of configuration 1, and therefore was expected at the surface. These expectations of particle formations are presented in Figure 6.2.

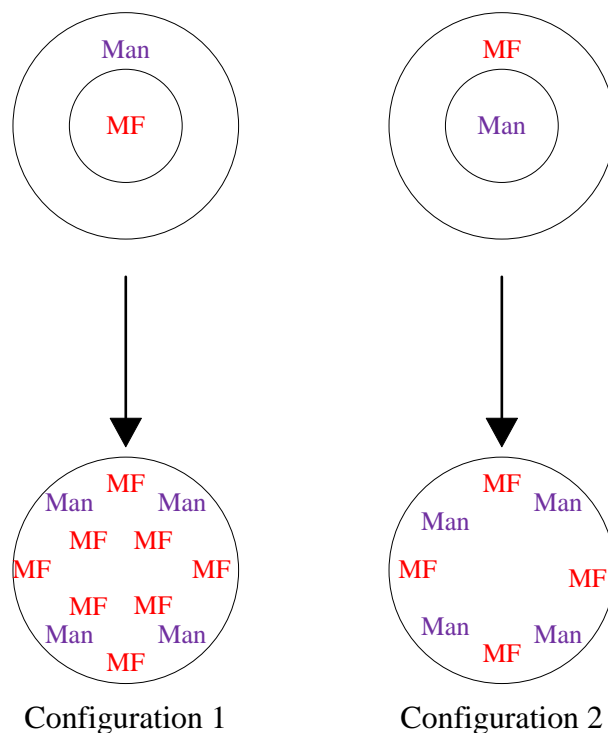


Figure 6.2. Expected particle structures for configurations 1 (where mannitol dominates the surface and MF present but in lower concentration) and 2 (equal quantities of MF and mannitol) based on theoretical drying calculations.

The different particles produced using the selected configurations were then analysed using different characterisations techniques.

XRPD Analysis

Configuration 1 and 2 produced polycrystalline composite samples consisting of three different phases; MF form A, β -mannitol and α -mannitol. Samples were identified by

comparison of XRPD patterns to starting material reference patterns (Figure 6.3). These data consisted of sharp diffraction peaks that showed peak similarity to the starting material patterns. There was no evidence of an elevated background scattering that would result from any significant amorphous content. In order to identify the different phases present in the polycrystalline samples, analysis using a multi-phase Pawley type fit using Topas (Bruker AXS 1999-2014) was conducted (Figure 6.4 and Figure 6.5) using the lattice parameters for the reported crystal forms of each component (see CSD refcodes of all known forms of MF and mannitol Table 6.5). Two or more lattice parameters for different combinations of polymorphs of each component were included in the fit to account for all of the observed peaks. The fit with the lowest residual and where visual inspection confirmed that all peaks in the observed data from the co-spray dried particles were accounted for was used to identify which crystalline phases were present in the samples.

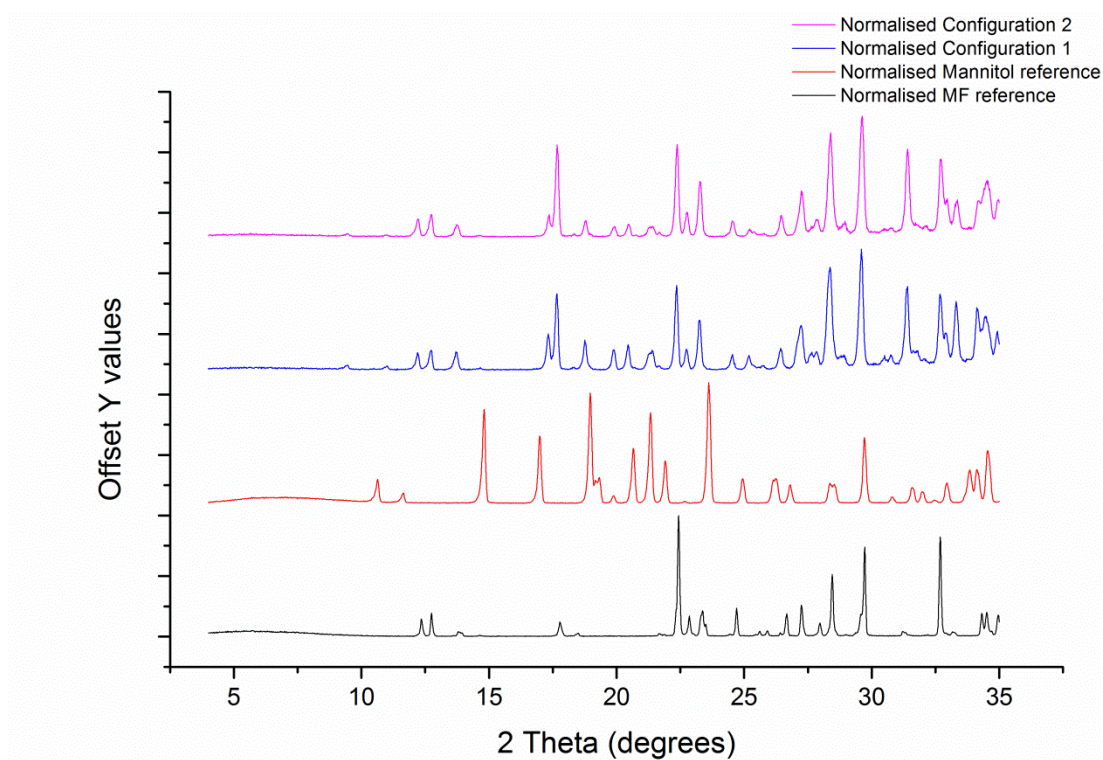


Figure 6.3. Starting material reference XRPD patterns for MF and mannitol compared with the XRPD patterns from spray dried composite particles of configurations 1 and 2.

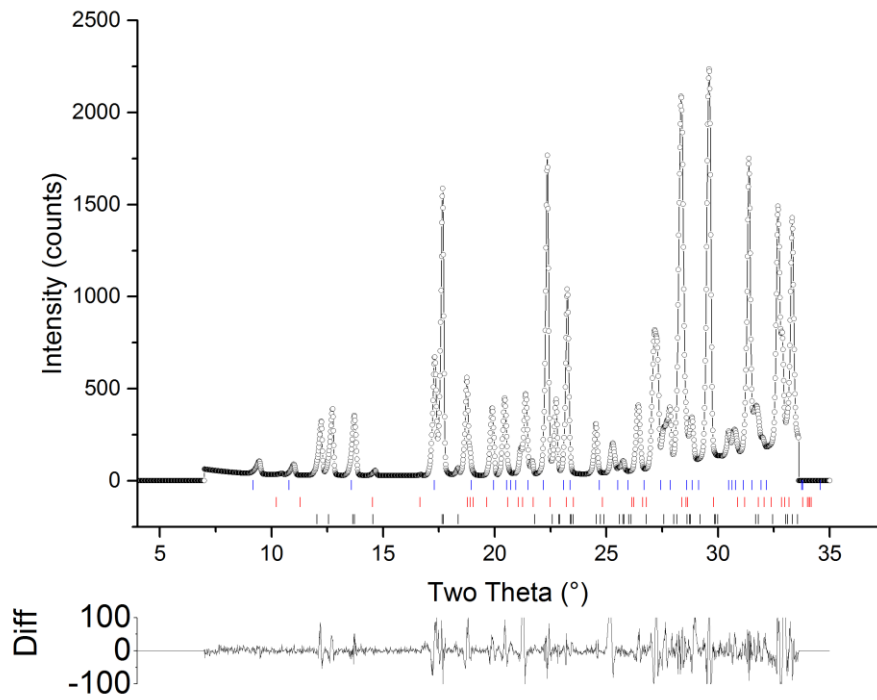


Figure 6.4. Multi-phase Pawley fit of the data for co-spray dried configuration 1. Calculated profile (o) (MF I, β -mannitol I and α -mannitol I), and difference plot (Yobs - Ycal).

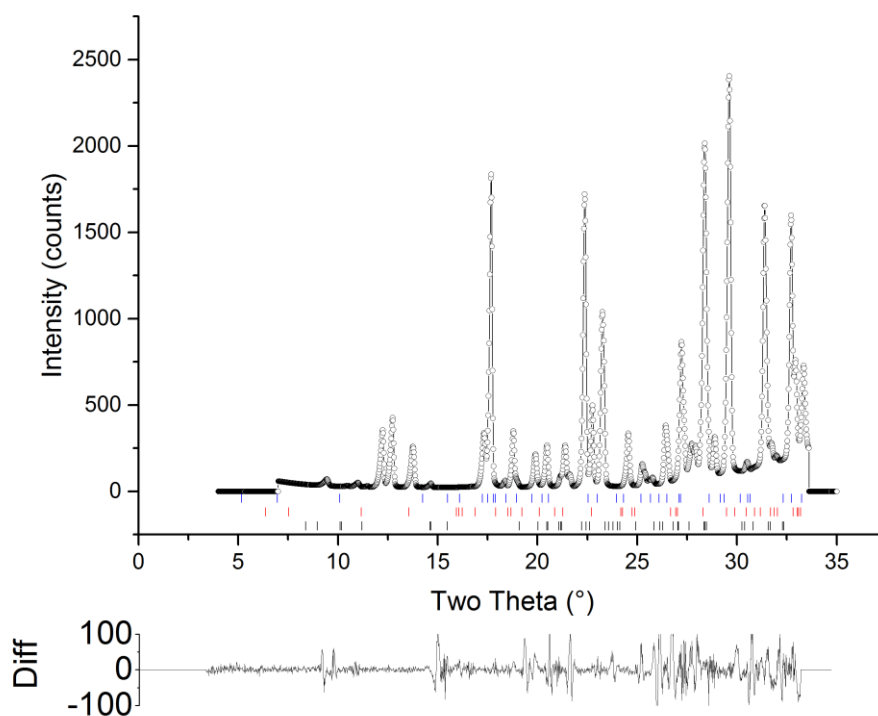


Figure 6.5. Multi-phase Pawley fit of the data for co-spray dried configuration 2. Calculated profile (o) (MF I, β -mannitol I and α -mannitol I), and difference plot (Yobs - Ycal).

Table 6.5. Phase identifications of configurations 1 and 2 by CSD refcodes showing the refined lattice parameters obtained from each of the fits.

Sample	Form	CSD Refcode	Space Group	a (Å)	b (Å)	c (Å)	α (°)	β (°)	γ (°)	Volume
Mannitol reference	β	DMANTL11	P212121	8.6790(1)	16.8962(2)	5.54972(7)	90	90	90	813.823
MF reference	A	JAMIRIY0	P21/c	7.9231(12)	13.894(2)	7.9231(12)	90	114.48	90	793.797
Configuration 1	β		P212121	8.657	16.939	5.610	90	90	90	822.798
	α		P212121	8.932	18.746	4.874	90	90	90	816.141
	A		P21/c	8.003	13.937	7.962	90	114.995	90	804.979
Configuration 2	β		P212121	8.678	16.879	5.618	90	90	90	823.128
	α		P212121	8.917	18.721	4.860	90	90	90	811.559
	A		P21/c	7.994	13.913	7.954	90	114.93	90	802.274

The multi-phase Pawley type fit confirmed the presence of MF form A, β -mannitol and α -mannitol through fitting of the lattice parameters detailed in Table 6.5, to these data with no evidence of peaks that did not correspond to these phases. Spray drying of pure β -mannitol with the two-fluid nozzle previously reported the production of β and α -mannitol (Vanhoorne et al. 2016). Spray drying with the three-fluid nozzle therefore showed no novel effect on the crystalline forms of MF and mannitol but provided composite polycrystalline particles as a physical mixture.

DSC Analysis

Phase identifications of MF form A, β -mannitol and α -mannitol present in configuration 1 and 2 were supported by characterisation of thermal behaviour using DSC. DSC analysis of configurations 1 and 2 were compared to the reference profiles of pure MF and β -mannitol (Figure 6.6).

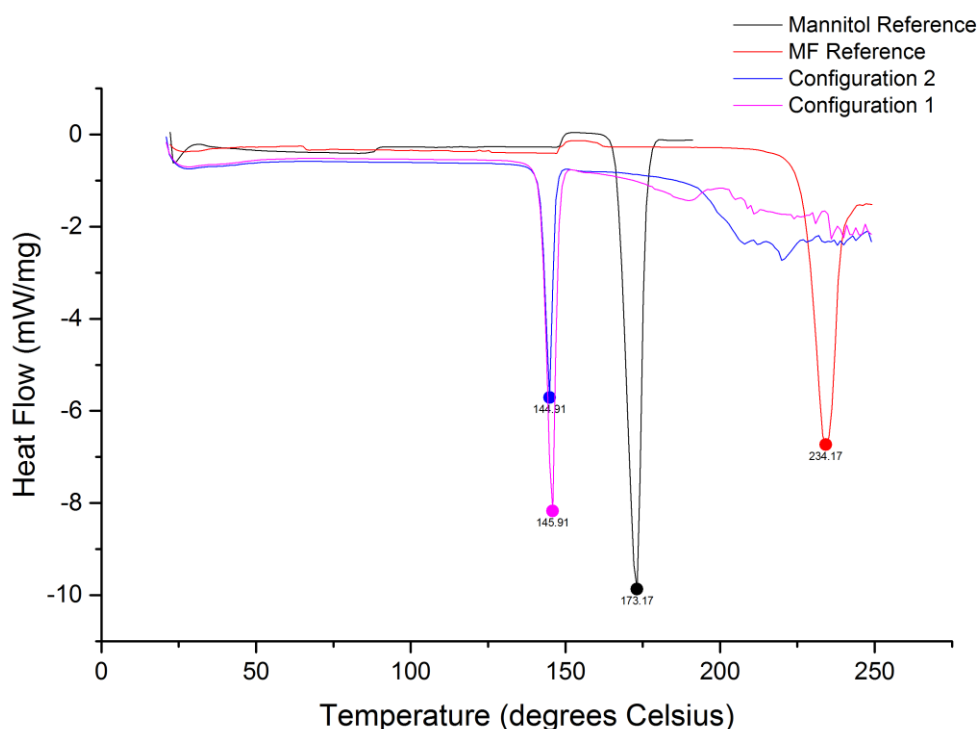


Figure 6.6. DSC profiles of MF and mannitol references and configurations 1 and 2.

The profiles for configuration 1 and 2 showed significantly different melting behaviours compared to the references of MF and β -mannitol. The melting temperatures for β and α -mannitol have been reported as the same temperature of 166 °C (Burger et al. 2000, Vanhoorne et al. 2016) and the melting temperature for MF at 232 °C (Barot et al. 2012). Configurations 1 and 2 presented melting temperatures of 146 and 145 °C respectively whilst mannitol and MF reference melting temperatures were measured at 173 and 234 °C.

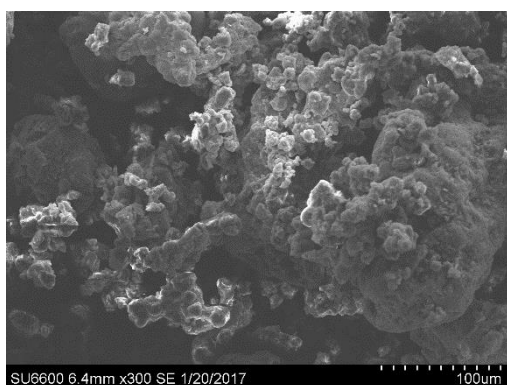
The DSC profiles for the two configurations showed only a single melting endotherm, with no high melting point evident that would be consistent with the melt of a polymorph and its recrystallisation and subsequent melting of a higher temperature form. This suggested that on heating the sample, the crystalline MF and mannitol present at room temperature (as confirmed by the XRPD results) form a possible eutectic melt on heating to ca. 145 °C (Cherukuvada and Guru Row 2014). A eutectic melt has previously been reported for a mixture of β and α mannitol with NaCl at 150 °C (Telang et al. 2003). A full phase diagram looking at the melting behaviours over a range of compositions would be required to determine if a eutectic composition has been found.

As the different nozzle configurations were proposed to have a direct effect on the internal microstructure of the composite particle, configurations 1 and 2 were analysed using SEM coupled with EDX and Raman Mapping. The goal was to map the distribution of MF and mannitol on the particle surfaces.

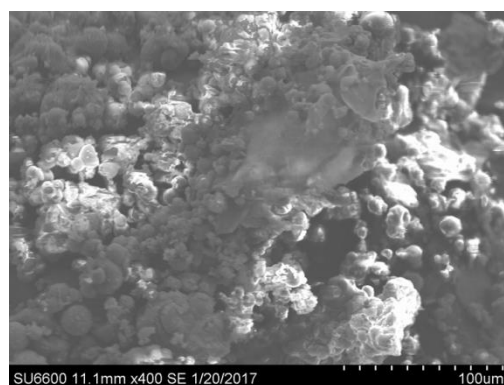
SEM Imaging

SEM images for configuration 1 (Figure 6.7a) showed composite particles that were highly agglomerated. The primary particles within the agglomerates had an approximate diameter between 5-10 μm , whilst individual agglomerates varied between 10-50 μm . The

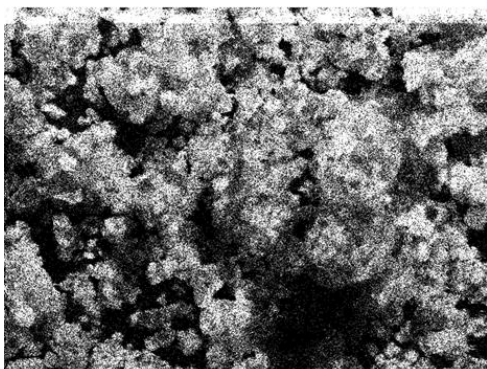
agglomerates were at the upper size range expected for the two fluid with the Büchi mini dryer (Büchi Labortechnik AG). The primary particles within the agglomerates showed evidence of both spherical and multi-faceted particles which may be expected for amorphous and crystalline systems (Mullin 2001). The SEM image for configuration 2 (Figure 6.7b) showed composite particles of a highly agglomerated nature with a particle sizes of 5-10 for primary particles and of 10 – 50 μm for the agglomerates.



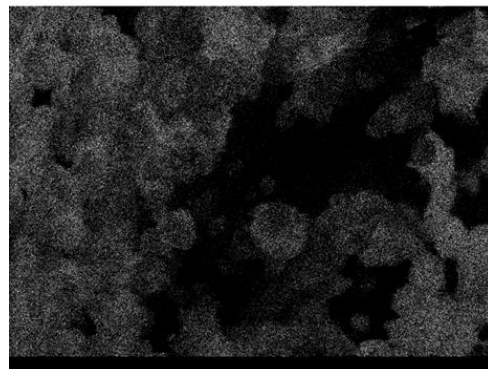
(a)



(b)



(c)



(d)

Figure 6.7. SEM images: (a) SEM of configuration 1, (b) SEM of configuration 2, (c) X-ray map of chlorine distribution of configuration 1 and (d) X-ray map of chlorine distribution of configuration 2 gained from EDX analysis.

Further analysis for particle structure utilised SEM coupled with EDX to identify elemental occurrences on the particle surface. Chlorine was selected as an indicator for MF surface presence by assessing the relative intensity of the EDX signal for this element. Both samples were analysed under similar conditions (Figure 6.7c and d).

The SEM EDX analysis enabled the identification of MF at the surface of both composite particles and suggested a higher concentration of MF present at the surface of configuration 1 than 2. As this was a qualitative assessment of the surface composition the concentration difference of MF can only be assumed from the higher intensity image of configuration 1 to 2. However, this result contradicted the expected concentration that may be expected from the consideration of physical parameters relating to drying, which indicated configuration 1 would be in excess of mannitol at the surface (Figure 6.2).

Raman Mapping

To identify the distribution of MF and mannitol on the surface of configuration 1 and 2 samples, Raman mapping was conducted. Raman spectroscopy was expected to be able to differentiate the different compounds and different crystalline forms of both components. Using Raman imaging, the location of different components and phases on the surface of the particles was visualised. Reference Raman spectra for the two raw material forms (Figure 6.8) were collected using a Raman microscope (Section 3.2.2.2) and the resultant spectra of the composite samples were used to create a map, coloured according to the Raman intensity measured at each point.

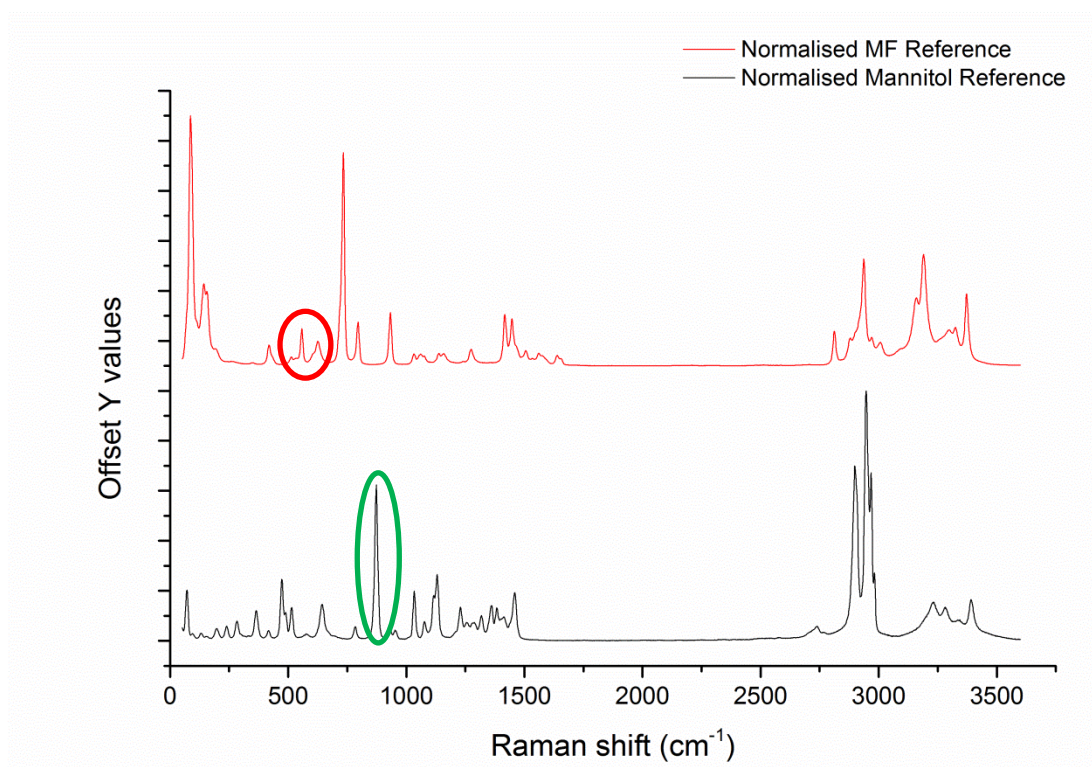


Figure 6.8. Reference Raman spectra for MF and mannitol highlighting differential peak regions; 500 – 600 cm⁻¹ for MF (red) and 800 – 900 cm⁻¹ for mannitol (green).

MF was identified from a peak found between 700 – 800 cm⁻¹ and mannitol identified from a peak between 500 – 600 cm⁻¹. The reported Raman spectra for β and α -mannitol showed similar peak positions (Vanhoorne et al. 2016). These peaks were colour coded green and red respectively. Raman maps from a single particle, with every attempt to select representative particles of comparable size are shown in Figure 6.9 and Figure 6.10.

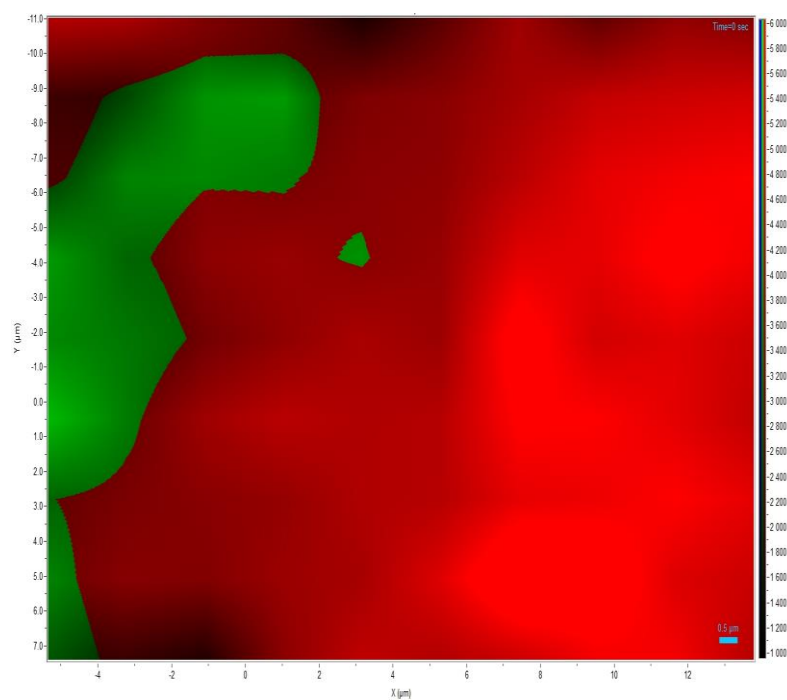


Figure 6.9. Surface composition identification by Raman mapping of a particle produced using configuration 1 showing MF in red and mannitol in green. The peak regions at 700 – 800 and 800 – 900 cm^{-1} were used to indicate the presence of MF and mannitol, respectively.

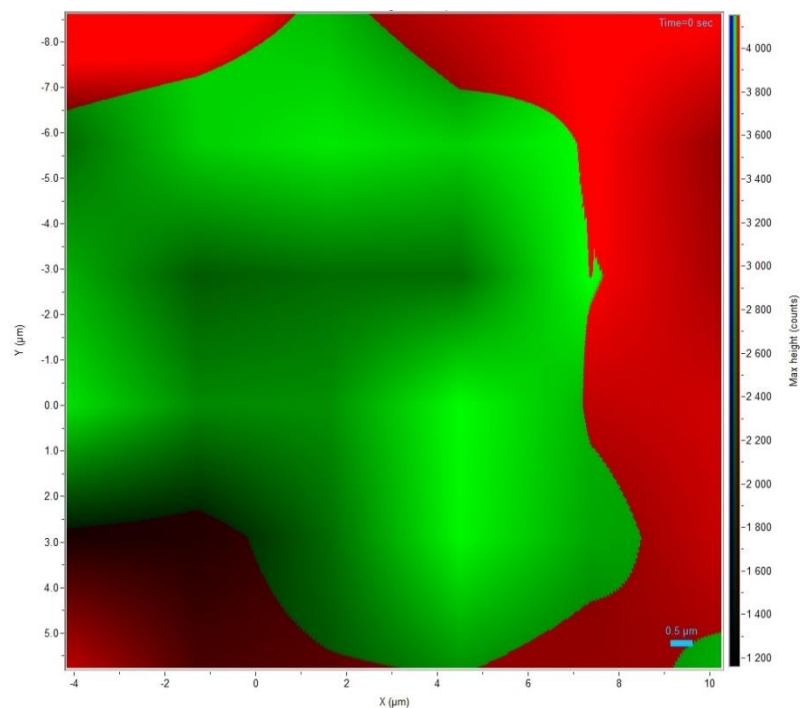


Figure 6.10. Surface composition identification by Raman mapping of a particle produced using configuration 2 showing MF in red and mannitol in green. The peak regions at 700 – 800 and 800 – 900 cm^{-1} were used to indicate the presence of MF and mannitol, respectively.

The Raman maps indicated that for configuration 1, a higher proportion of MF was present on the particle surface than configuration 2 which showed a predominance of mannitol. These results provided further contradictions to the assumed particles outcome. However, as the maps measured the surface composition of a specific region of a particle surface and not the entire surface, they may not represent the surface composition of the overall particle surface.

Particle Sizing

Particle size and size distribution of samples from configurations 1 and 2 were measured using the Malvern Morphologi G3 to determine the CE diameter of each configuration against the volume distribution (Figure 6.11). The CE diameter illustrated a mono-modal trend though broad particle size distribution for both configurations. Configuration 1

returned a $D_{v,50}$ of $52.29\mu\text{m}$ and a span of $1.539\mu\text{m}$ whilst configuration 2 had a $D_{v,50}$ of $34.21\mu\text{m}$ and a span of $1.799\mu\text{m}$.

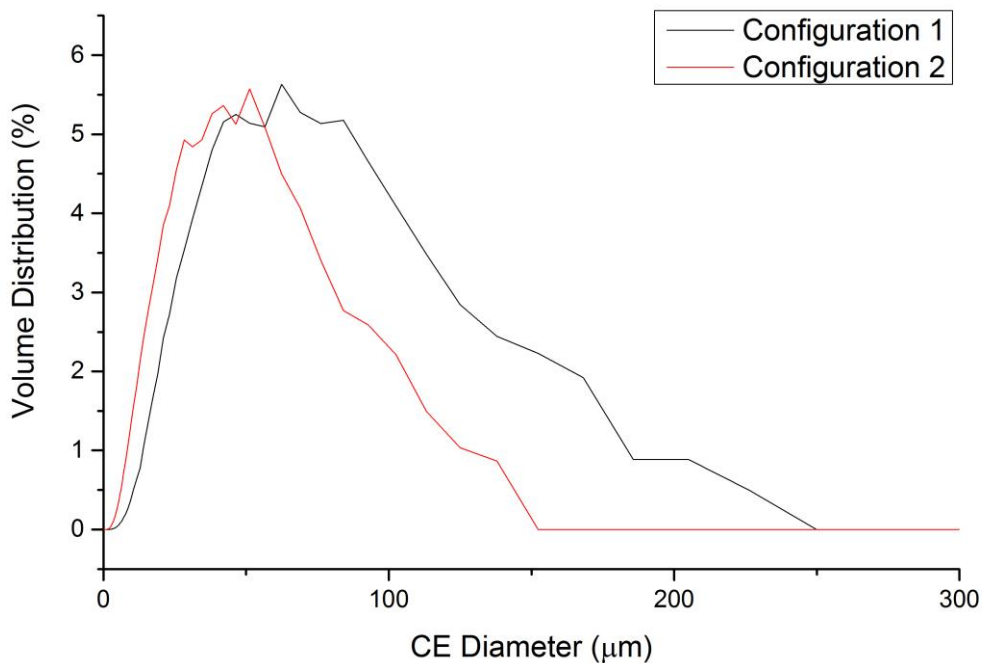


Figure 6.11. Particle size and size distribution measurements for configurations 1 and 2.

6.3.1.2. MF – Lactose Composites

MF and lactose were successfully co-spray dried using the three-fluid nozzle creating two different composite particles based on nozzle configuration. The setup for the MF and lactose co-process was the same as used for MF-mannitol. The two composite particle samples produced consisted of the two different configurations; configuration 3, where MF was the inner feed and lactose was the outer feed and configuration 4, where MF was the outer feed and lactose was the inner feed (Table 6.3).

Selected physical parameters describing for MF and lactose (based on the conditions seen in Table 6.2) are provided in Table 6.6. Specifically the diffusion coefficient and evaporation rate, Peclet number and calculated surface enrichment are listed in Table 6.6.

Table 6.6. Theoretical drying kinetics for MF and lactose calculated from equations 1.2, 1.3, 1.4 and 1.14 (Vehring 2008).

Drying Kinetics	MF	Lactose
Diffusion Coefficient, D (m ² /s)	7.711×10^{-10}	8.02×10^{-10}
Evaporation Rate, κ (m ² /s)	1.808×10^{-08}	1.808×10^{-08}
Peclet Number, P_e	2.93	2.82
Surface Enrichment, E	1.666	1.637

The theoretical drying kinetics for MF and lactose found relatively similar drying rates and structure assessments that were expected to produce similar particles structures for single component and equally mixed drying of MF and lactose. A hollow particle with a preference for surface enrichment may be expected for MF and lactose due to the $Pe > 1$. The similar surface enrichment for MF and lactose suggested a similar concentration of component on the surface. For co-spray drying with the three-fluid nozzle, the different configuration was expected to produce particles with an overall surface composition dominance of the outer feed Figure 6.12.

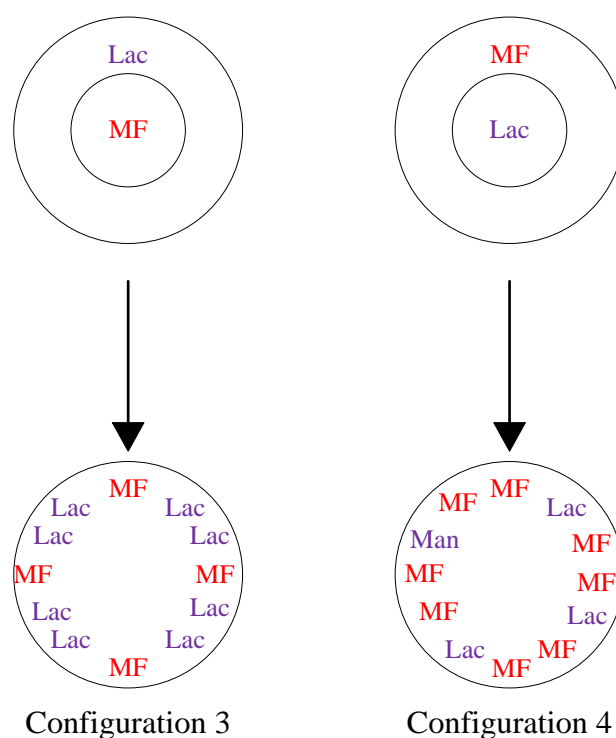


Figure 6.12. Expected particle structures for configuration 3 (lactose dominates surface) and 4 (MF dominates surface) based on theoretical drying calculations.

XRPD Analysis

Configuration 3 and 4 produced polycrystalline composite samples consisting of three different phases; MF form A, α -lactose monohydrate and anhydrous lactose. Samples were first analysed for crystal form by XRPD (Figure 6.13). XRPD data showed peak similarity to starting material patterns with sharp diffraction peaks with no evidence of an elevated background scattering indicative of significant amorphous content. The polycrystalline samples were identified for phases present similar to the MF-mannitol composites using multi-phase Pawley type fit analysis within Topas (Figure 6.14 and Figure 6.15) with the unit cells for each of the known crystal forms (CSD refcodes and lattice parameters are shown in Table 6.7). The same approach as described in (section 6.3.1.1) to identify the crystalline forms present was applied.

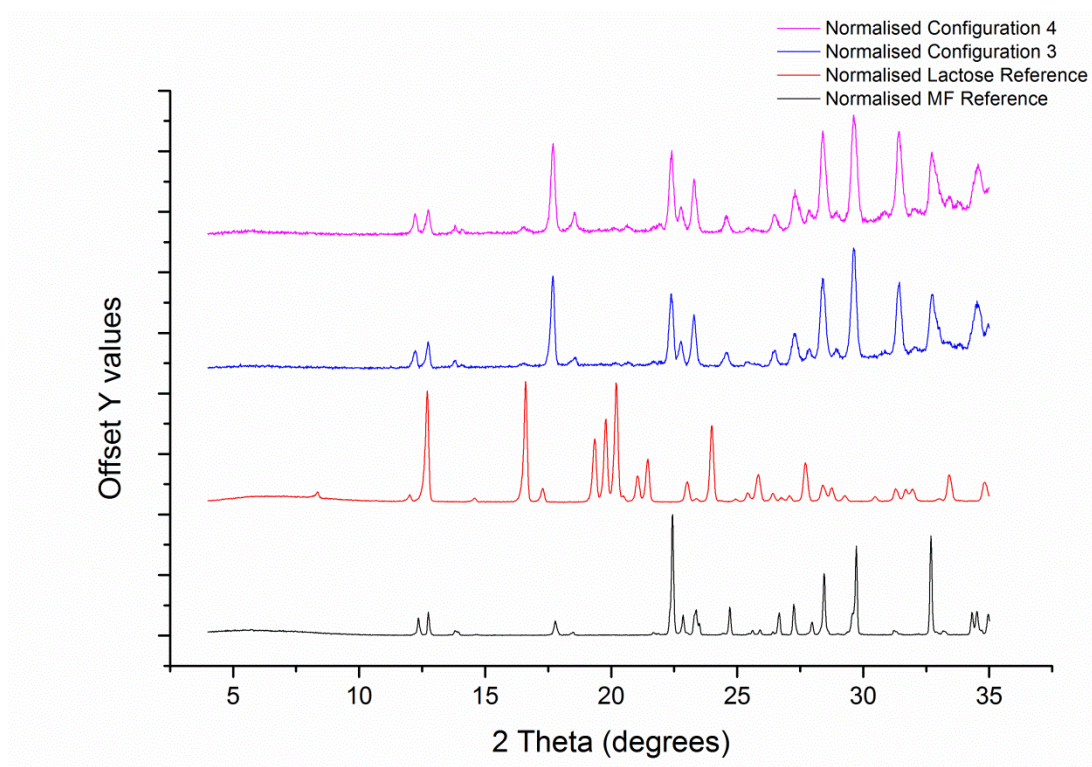


Figure 6.13. Starting material reference XRPD patterns for MF and lactose compared with the XRPD patterns from spray dried composite particles of configurations 3 and 4.

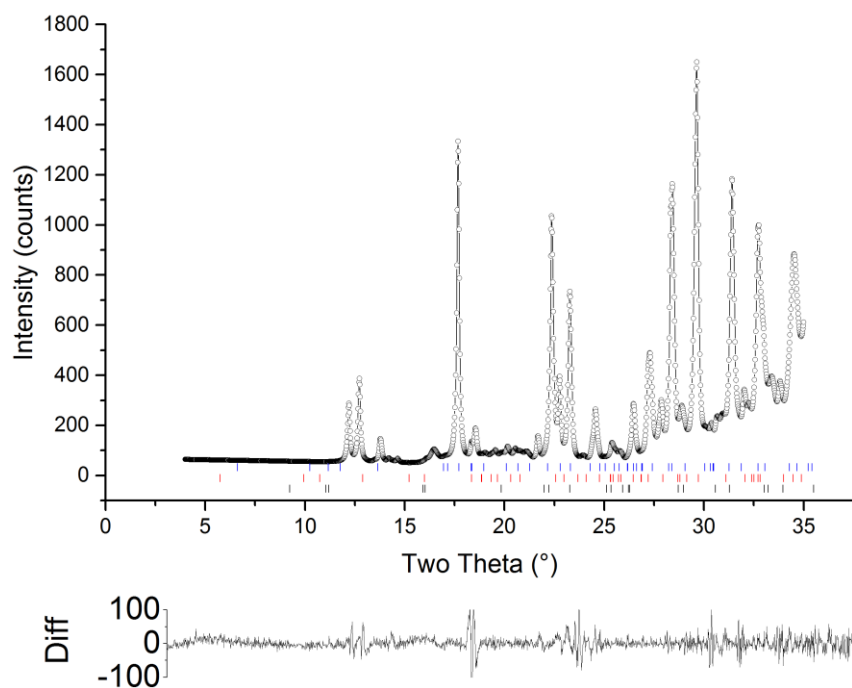


Figure 6.14. Multi-phase Pawley fit of the data of co-spray dried configuration 3. Calculated profile (o) (MF I, α -monohydrate I and anhydrous I) and difference plot (Yobs - Ycal).

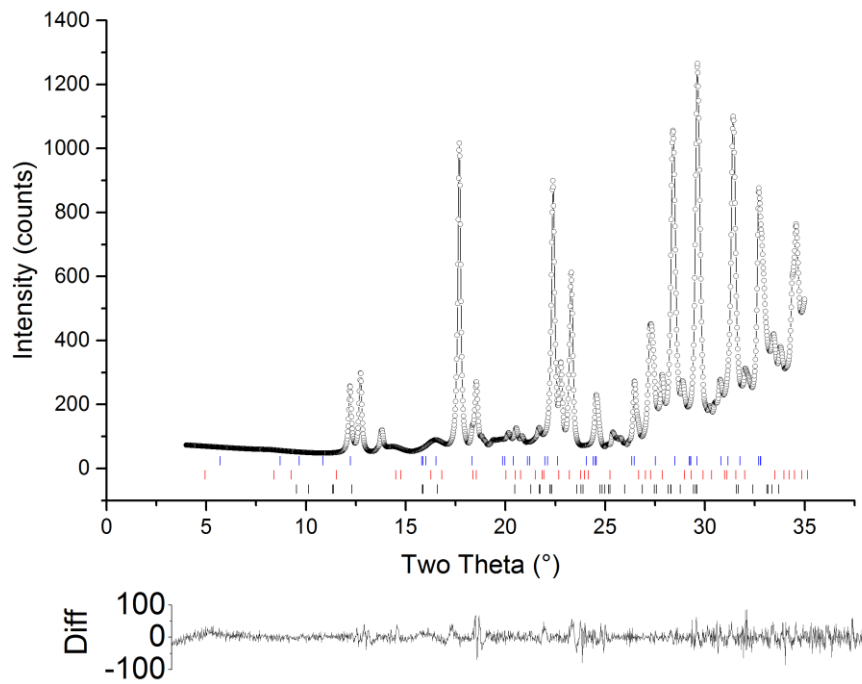


Figure 6.15. Multi-phase Pawley fit of the data of co-spray dried configuration 4. Calculated profile (o) (MF I, α -monohydrate I and anhydrous I) and difference plot (Yobs - Ycal).

Table 6.7. Phase identifications of configurations 3 and 4 by CSD refcodes showing the refined lattice parameters obtained from each of the fits.

Molecule	Form	CSD Refcode	Space Group	a (Å)	b (Å)	c (Å)	α (°)	β (°)	γ (°)	Volume
MF reference	A	JAMRIY01	P21/c	7.9231(12)	13.894(2)	7.9231(12)	90	114.48	90	793.797
Lactose reference	α -monohydrate	LACTOS02	P21	7.98(2)	21.68(6)	4.836(10)	90	109.78(25)	90	787.295
Configuration 3	MF A		P21/c	7.987	13.912	7.945	90	114.884	90	800.944
	Anhydrous		P1	7.680	19.719	5.020	91.399	107.074	96.591	719.268
	α -monohydrate		P21	8.005	21.525	4.847	90	109.648	90	786.711
Configuration 4	MF A		P21/c	8.000	13.902	7.962	90	115.038	90	802.423
	Anhydrous		P1	7.605	19.802	5.008	91.271	106.907	96.571	715.766
	α -monohydrate		P21	7.937	21.494	4.686	90	108.906	90	756.458

The multi-phase Pawley type fit confirmed the presence of MF form A, α -lactose monohydrate and anhydrous lactose by fitting of the lattice parameters presented in Table 6.7 to the XRPD sample data, with no evidence of unconfirmed new peaks. Spray drying of lactose has been extensively reported to produce the amorphous solid-state form, with varying crystallinity degrees observed under different experimental conditions (Buckton et al. 2002, Islam and Langrish 2010). However, co-spray drying with the polymer PEG produced crystalline lactose mixtures of α -monohydrate, anhydrous and β -lactose (Chidavaenzi et al. 2001a). Therefore, the use of the three-fluid nozzle for spray drying of MF showed some similarities to previous studies albeit as a polycrystalline physical mixture.

DSC Analysis

The confirmation of MF form A, α -monohydrate and anhydrous lactose phase presence in configurations 3 and 4 were further supported by DSC; sample profiles were compared to pure references of MF and α -lactose monohydrate (Figure 6.16).

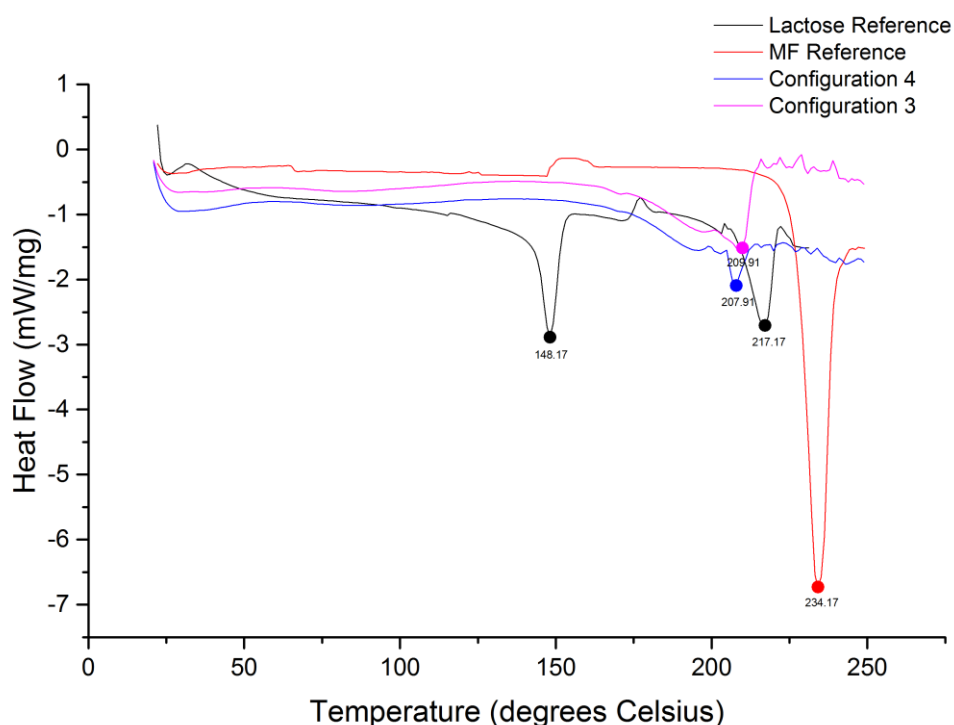


Figure 6.16. DSC profiles of MF and lactose references and configurations 3 and 4.

The profiles for configurations 3 and 4 showed different thermal behaviours compared to the reference thermograms for MF and lactose. Reference MF melting temperature were measured at 234 °C whereas lactose showed a conversion of forms through two melting endotherms at temperatures of 148 °C for α -lactose monohydrate to 216 °C for anhydrous lactose. Configurations 3 and 4 displayed relatively small melting endotherms at 209 and 208 °C respectively. As XRPD has confirmed the presence of α -lactose monohydrate and anhydrous lactose, these peaks may be a result of a eutectic melt of MF and the phases of lactose but a full phase diagram consisting of different compositions would be required to confirm if a eutectic melt has occurred.

SEM Imaging

As before, in order to map the surface distribution of MF and lactose, SEM was used to image the surface composition and coupled with EDX to probe chemical composition. The SEM image for configuration 3 (Figure 6.17a), showed highly agglomerated composite particles. The SEM images showed large agglomerated particles with an approximate diameter of 50-100 μm with primary particle of diameters approximately 5-10 μm . The primary particles were largely spherical in shape with some evidence of crystal facets. The SEM image for configuration 4 (Figure 6.16b) showed a distinct difference in particle morphology from configuration 3. Particles appeared highly agglomerated with evidence of primary particle of spherical morphology and approximated diameters of 10-20 μm .

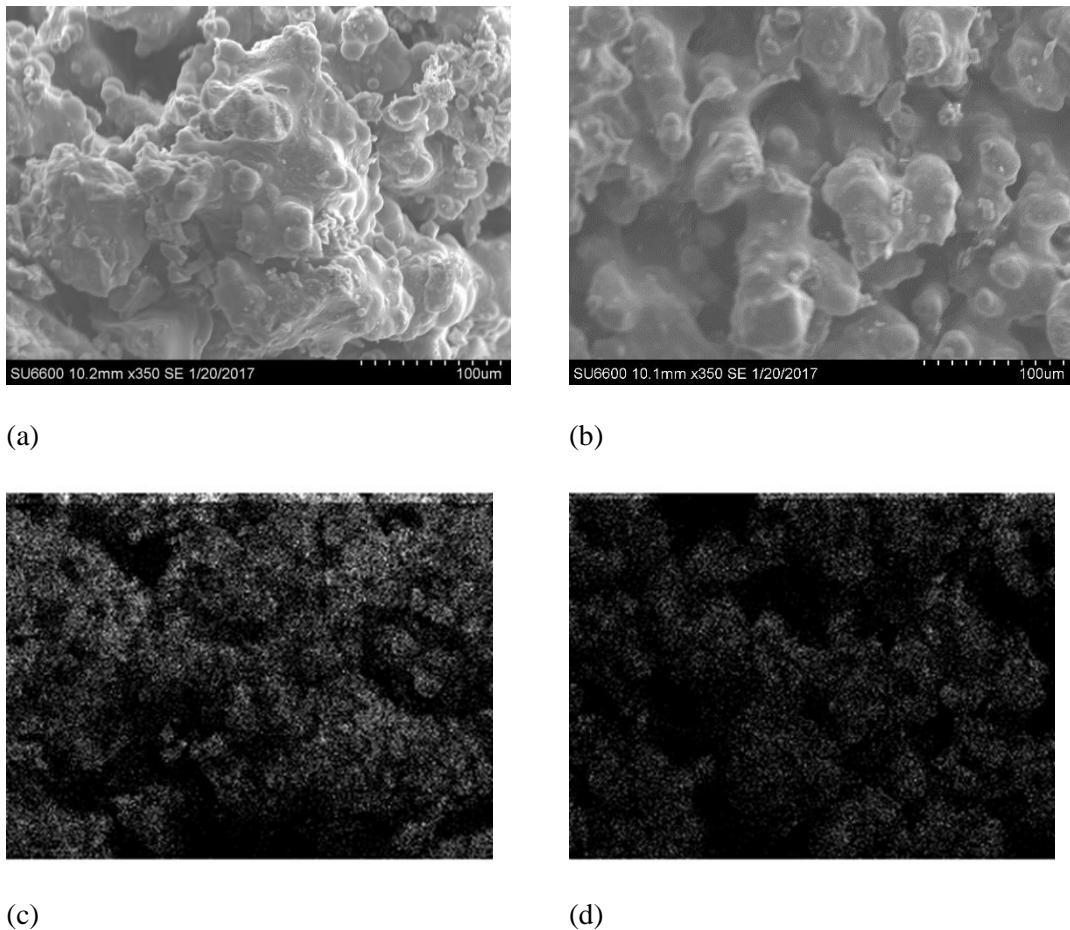


Figure 6.17. SEM images: (a) SEM of configuration 3, (b) SEM of configuration 4, (c) X-ray map of chlorine distribution of configuration 3 and (d) X-ray map of chlorine distribution of configuration 4 gained from EDX analysis.

As with the MF-mannitol composites, further analysis for phase identifications at the particle surface was made using SEM with EDX (Figure 6.17c and d). The analysis found that MF could be identified at the surface of both configurations with a slightly higher concentration assumed for configuration 3. However, these results contradicted the assumption that the outer feed of the three-fluid nozzle would dominate the surface concentration. Based on the similar theoretical drying kinetics, these results indicated equal mixing of the feeds before surface formation which may explain the relatively similar surface concentration of MF.

Raman Mapping

Raman mapping was again used to identify the distribution of MF and lactose at the surface of configuration 3 and 4 samples. Raman spectra of the raw materials forms (Figure 6.18) and composites sample spectra was used to create a colour coded map for configuration 3 (Figure 6.19) and 4 (Figure 6.20).

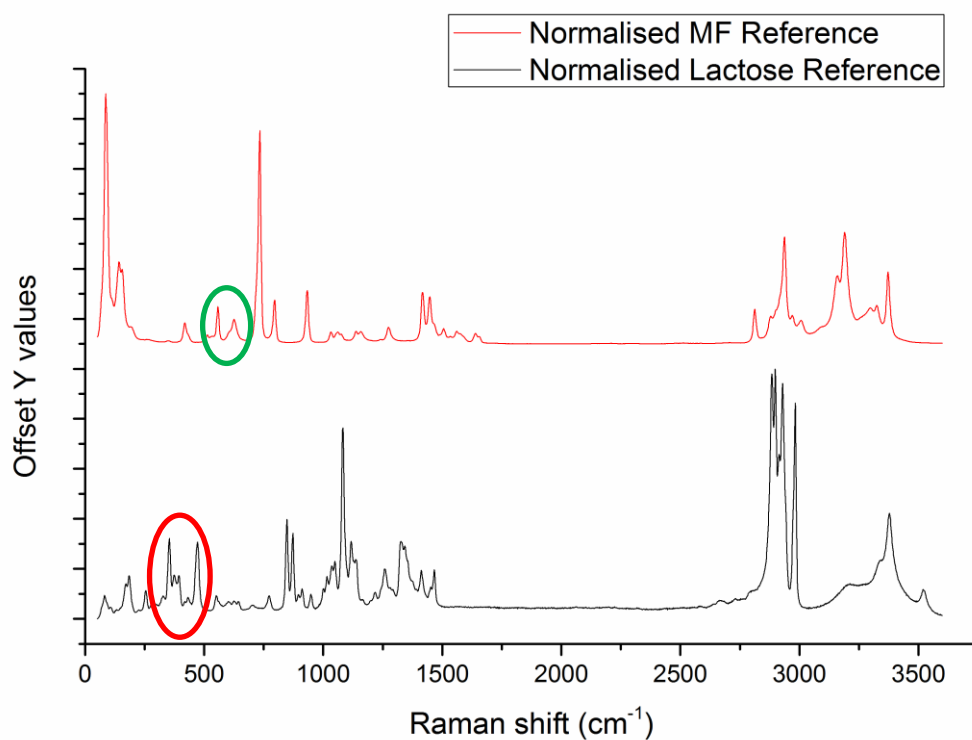


Figure 6.18. Reference Raman spectra for MF and lactose highlighting differential peak regions; 500 – 600 cm⁻¹ for MF (green), 250 – 500 cm⁻¹ (red) for lactose.

MF was identified from peaks found between 500 – 600 cm⁻¹ and lactose identified from peak positioned at 250 – 500 cm⁻¹. Reported Raman spectra for α -monohydrate and anhydrous lactose have shown difference in peaks between 400 – 500 cm⁻¹ (Kirk et al. 2007) which has been selected for marking for Raman mapping. MF peaks have been coloured green with lactose peaks shown in red. The Raman maps for configuration 3 and 4 are presented in Figure 6.19 and Figure 6.20.

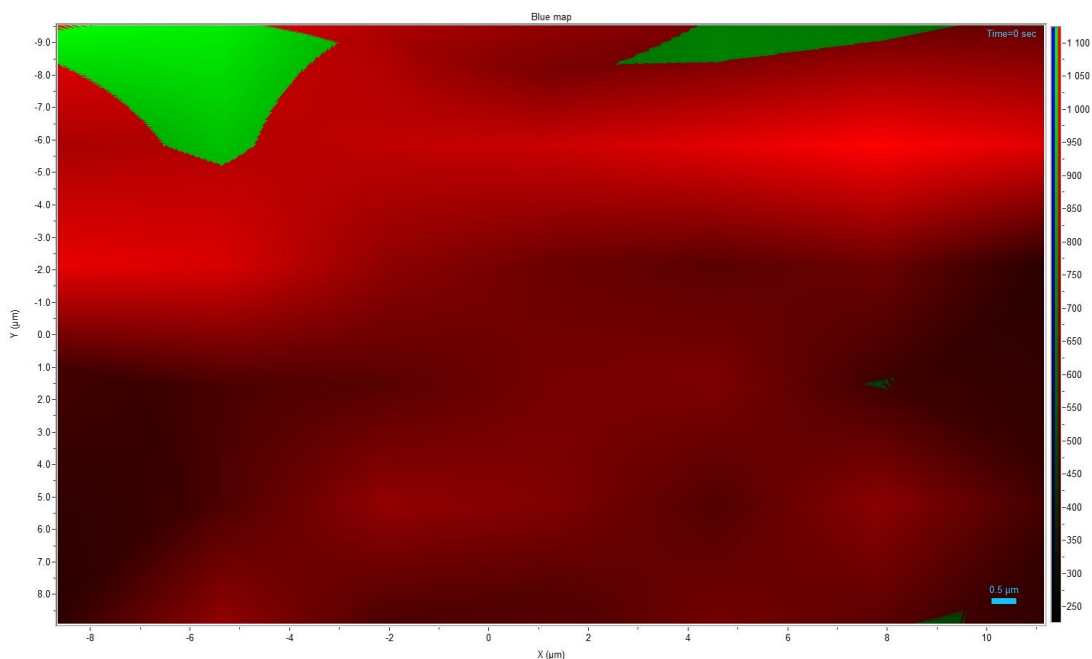


Figure 6.19. Surface composition identification by Raman mapping of a particle produced using configuration 3 showing MF in green and lactose in red. The peak regions at 500 – 600 and 250 – 500 cm^{-1} were used to indicate the presence of MF and lactose, respectively.

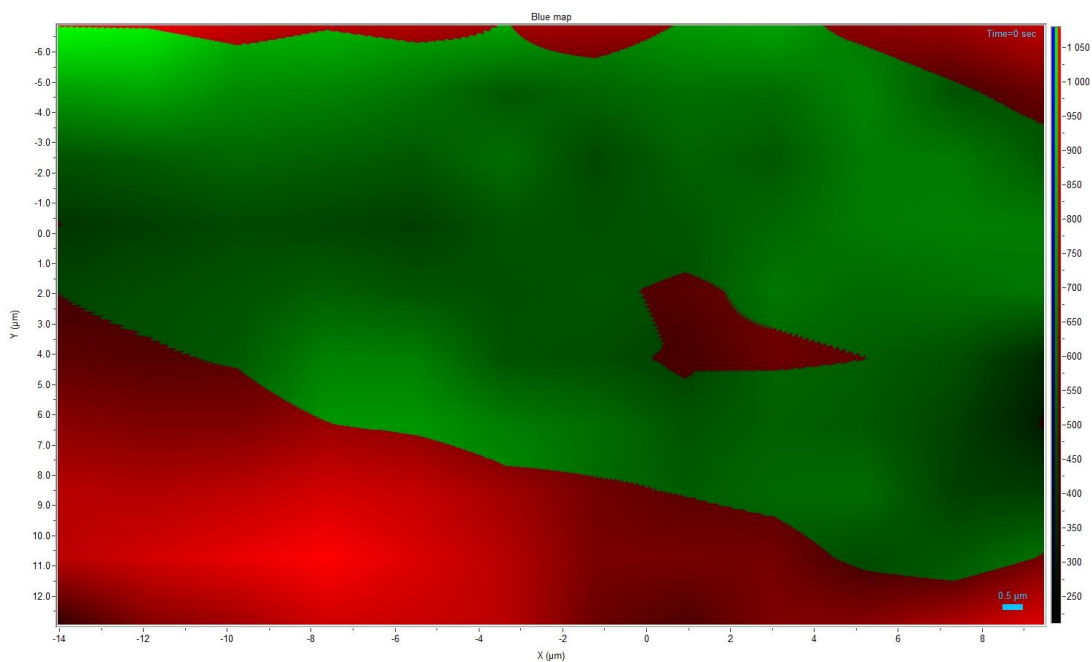


Figure 6.20. Surface composition identification by Raman mapping of a particle produced using configuration 4 showing MF in green and lactose in red. The peak regions at 500 – 600 and 250 – 500 cm^{-1} were used to indicate the presence of MF and lactose, respectively.

The Raman maps show that for configuration 3, a predominance of lactose was present on the surface and for configuration 4, roughly equal amounts of MF, lactose were present on the particle surface. Although the maps cannot be representative of the particle structures as a whole, the map for configuration 3 supported the theoretical drying kinetic expectations for particle structures with a dominance of the outer feed. Configuration 4 would suggest an equal distribution of phases present on the surface but as they show a higher proportion of MF than configuration 3, this may be attributed to the presence of MF in the outer feed.

Particle Sizing

Particle size and size distribution of configurations 3 and 4 were analysed using the Malvern Morphologi G3 to determine the CE diameter for each configuration against volume distribution (Figure 6.21). The CE diameter distribution for both configurations showed a broad mono-modal particle size distribution. Configuration 3 had a D_{v50} of 81.58 μm and a span of 1.221 μm . Configuration 4 had a D_{v50} of 51.12 μm and a span of 1.523 μm .

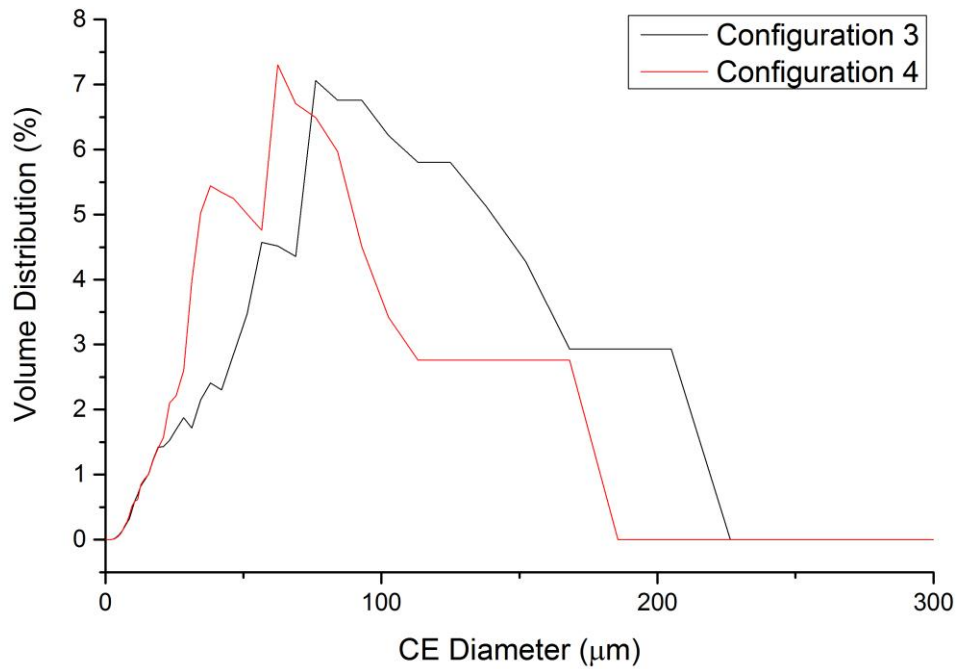


Figure 6.21. Particle size and size distribution measurements for configurations 3 and 4

Of the four different configurations tested using the three-fluid nozzle to co-spray dry multicomponent composite particles, the overall driving force for particle formation has been the drying kinetics. The expected particle outcomes from the three fluid nozzle alone, has not been evident in the composite particles. The drying kinetics for each component has shown that the composite surface will comprise of both components in different concentrations. In particular, the MF-lactose composites with similar drying kinetics have shown this clearly from the Raman mapping. However, the drying kinetics were unable to completely define the composite particle structures which may be a result of the kinetic data based on single component kinetics and does not take into account the presence of the second component.

6.4. Summary

The aim of this work was to investigate the capability of co-spray drying with the three-fluid nozzle as an approach to produce multicomponent or composite crystalline particles. The different feed fluid configurations were analysed for the formation of MF-mannitol and MF-lactose composites. Co-spray drying produced polycrystalline composite particles with different polymorphic forms produced from mannitol and lactose, although there was no evidence that these are affected by the nozzle configuration or presence of MF. Theoretical drying parameters were calculated with expected particle structure based on these calculations and the influence of the configuration set-up (Figure 6.2 and Figure 6.12). For the MF-mannitol composites, mixtures of three phases were found. Upon heating in DSC, a possible eutectic mixture was produced and was the first report of this for this system. SEM with EDX and Raman mapping showed a distribution of all component on the surface contradicting the expected particle outcome from the nozzle configuration. For the MF-lactose composites, mixtures of three phases were also found with a possible eutectic mixture made upon heating. SEM with EDX and Raman mapping showed a relatively equal distribution of all components on the surface which was consistent with expectations based on the drying parameters. The drying parameters were therefore found to have the greatest influence on the resultant particle composition compared with the nozzle configuration. This suggested that equal mixing may occur during atomisation irrespective of feed separation by the three-fluid nozzle for miscible feeds. For components that show relatively similar drying parameters, such as Pe and E , the equal mixing in the droplet would be expected to gain an equal composition of the components in the particles. For components that show different drying parameters, equal droplet mixing may enable the behaviour of the components in the droplet, such as the diffusion coefficient, to determine particle outcomes. Therefore, the drying parameters can offer an approach to design particle outcomes for multicomponent co-processing.

Chapter 7. Conclusion and Future Work

Spray drying is a powerful and extensively used technique for a wide range of industries with the potential to improve manufacture of pharmaceuticals. The opportunity to utilise as a continuous process offers a robust route that can integrate crystallisation, drying and isolation mechanisms with opportunities to engineer particle properties for an improvement of final product performance. The capability for crystallisability prediction is of particular interest as this application can incorporate spray drying into process modelling and workflow design that will further support the adoption of continuous manufacture through efficient and rapid process development methods.

Firstly, spray drying has been used as a method for the production of the metastable CBZ IV polymorph that has been reported previously as highly difficult to reproduce from traditional solution crystallisation (Lang et al. 2002, Grzesiak et al. 2003, Florence et al. 2006, Getsoian et al. 2008). Whilst CBZ IV has previously been reported from spray drying (Kipouros et al. 2005, Kipouros et al. 2006), no insight to the mechanism was provided. In this thesis, the unique conditions accessible within the spray dryer that promote the production and isolation of this form have been identified. The combination of high supersaturation caused by atomisation of droplets, rapid evaporation of solvent driven by elevated temperatures and rapid isolation of the polymorph enables the recovery of the previously elusive CBZ IV. In particular, the combination of these three factors will inhibit solution-mediated transformation of CBZ IV to a more stable form that is proposed to occur in traditional crystallisation methodologies preventing its successful recovery. This work therefore clearly demonstrates the capability of spray drying as a technique for polymorph and solid-state screening that can achieve the isolation of metastable forms.

The progression of this work would be to expand the range and scale of the original spray drying conditions to determine if any other polymorphs of CBZ can be produced by this method. This would enable the specific experimental conditions for each polymorph to be

calculated and if these conditions can be tracked through a change in drying kinetics. Furthermore, spray drying can be explored as a technique for metastable polymorph production by screening with further compounds. This would enable fundamental knowledge of different polymorphic systems to be expanded (Stahly 2007). However, whilst rapid drying has been shown to promote the formation of a metastable polymorph in this instance, the rapid nucleation and growth accompanying this may, for some compounds, lead to the formation of amorphous forms. Further work is also merited to explore methods to overcome this, for example, through ultrasound (Renuka Devi et al. 2015) or photochemical laser induced nucleation (Renuka Devi et al. 2015) or the use of heterogeneous surfaces or templates (Srirambhatla et al. 2016).

Secondly, it has been shown that the crystallisability of molecules from a spray drying process can potentially be predicted based on a consideration of molecular properties. This offers many advantages for rapid process selection and development workflows to decide on whether the use of spray drying may yield the desired outcome before carrying out any expensive and time consuming experimentation. The crystallisability of organic molecules has been modelled for crystal prediction using the machine learning method of random forest (RF). Initially, modelling was conducted on published crystallisability data from Van Eerdenbrugh and co-workers (Van Eerdenbrugh et al. 2010). The resulting models found a crystallisability prediction accuracy of 79 – 82 % highlighting the potential applicability of predictive modelling. RF was then employed for crystallisability prediction based on data collected from spray drying for the first time and achieved a predictive accuracy of 71.55 %. However, the lack of compound diversity within the relatively small training set size restricted the overall validity of the models. The supplementation of known amorphous form compounds to the spray dryer model improved the predictive accuracy to 79 %. The increase in compound diversity demonstrates the capability of RF modelling for crystallisability prediction. Furthermore, a test case for the crystallisability prediction model was carried out

with BCS compounds, to determine if the molecular properties that relate to nucleation kinetics and favour crystalline or amorphous outcomes, may also relate to BCS performance. This work provides a strong indication of the practicality of crystallisability predictive modelling for spray drying that can be highly useful moving towards continuous manufacturing.

Given the initial success of the spray dryer crystallisability predictive models, development of this work would involve the expansion of the training and test set number and diversity to provide a more accurate predictive capability. This would include experimental screening of more complex compounds existing within different regions of the PCA plot to provide a higher validity for predictive screening of pharmaceutically relevant compounds. Furthermore, as the spray dryer model predicts crystallisability of aqueous based compounds, further models could be created predicting the crystallisability of compounds in different organic solvents and different spray dryer conditions. These models would highlight the scope of the technique for crystallisability prediction and illustrate the value of RF modelling for crystallisation and manufacture.

Finally, co-spray drying using the three-fluid nozzle was successfully implemented to produce multicomponent composite particles consisting of different phases of MF, mannitol and lactose. The three-fluid nozzle operated with two separate feed streams and one gaseous stream that allowed different configurations of MF – mannitol and MF – lactose to be investigated. It was proposed that the outer streams of the nozzle would show overall dominance on the particle surfaces with this explained through the calculation of theoretical drying parameters. Four different configurations were tested, with physical mixtures confirmed through XRPD and Pawley fit analysis consisting of multiple polymorphs of mannitol and lactose. Particle surface composition was analysed by SEM coupled with EDX and Raman mapping, and found a mixed distribution of phases present. This suggests that

particle formation of the multicomponent composites appears to be most influenced by the drying kinetics of each compound as opposed to the nozzle configurations. This work has demonstrated the capability of co-spray drying with the three-fluid nozzle for crystalline phases.

Further work regarding the co-spray drying of MF-mannitol and MF-lactose would involve the investigation into internal structure using further analytical techniques such as the NANO-CT. The internal structures would provide further information on the mechanisms of multicomponent droplet drying. Better understanding of this would provide a more rational basis to design particle structures from co-spray drying by interpretation of specific kinetic parameters and their manipulation by solvent choice or temperature selection. Further work to investigate the influence of the three-fluid nozzle on particle formation would focus on the co-spray drying of different feed systems, such as solutions and emulsions. Different feed properties such as viscosity may enable the layering of the outer and inner feeds to gain a higher degree of control over the particle outcomes and produce coated crystalline phase particles. Introduction of suspensions may also allow the formation of layered crystalline particles with modified compaction, flow or dissolution properties. Further work would also be merited in understanding the droplet formation process as a function of different flows at the nozzle. Computational fluid dynamics (CFD) could provide information on the droplet formation and local mixing within droplets. Also droplet size analysis would better inform the assumptions on the drying process, indicating the initial droplet size population. Such data, combined with levitating droplet systems could then provide more detail on the drying kinetics and how different evaporation rates may specifically influence the resultant particle morphology and specific phases of multicomponent particles. Greater control over drying residence time and temperature control than is available in the Büchi Mini Dryer may then afford a greater degree of particle engineering ability.

Finally, the approach to drying kinetics here has been based largely around solidification processes, with no explicit consideration of nucleation kinetics within droplets. The potentially complex interactions between mixing, drying, supersaturation, droplet-gas interfaces and nucleation mean this it remains challenging to model all aspects of the particle formation required to describe the size, composition and form of multicomponent crystalline particles. However, the various kinetics contributions could be decoupled through detailed measurement from single droplet experiments perhaps to inform an improved overall kinetic model for spray drying of crystalline systems.

References

Alfagih, I., et al. (2015). "Pulmonary Delivery of Proteins Using Nanocomposite Microcarriers." J Pharm Sci.

Alhalaweh, A. and S. P. Velaga (2010). "Formation of Cocrystals from Stoichiometric Solutions of Incongruently Saturating Systems by Spray Drying." Crystal Growth & Design **10**(8): 3302-3305.

Allan, P., et al. (2013). "In situ monitoring of powder blending by non-invasive Raman spectrometry with wide area illumination." Journal of Pharmaceutical and Biomedical Analysis **76**: 28-35.

Anandharamakrishnan, C. and S. P. Ishwarya (2015a). Introduction to spray drying. Spray Drying Techniques for Food Ingredient Encapsulation, John Wiley & Sons, Ltd.

Anandharamakrishnan, C. and S. P. Ishwarya (2015b). Spray Drying Techniques for Food Ingredient Encapsulation, Wiley.

Anish, C., et al. (2014). "Influences of process and formulation parameters on powder flow properties and immunogenicity of spray dried polymer particles entrapping recombinant pneumococcal surface protein A." Int J Pharm **466**(1-2): 198-210.

Arlin, J.-B., et al. (2011). "A strategy for producing predicted polymorphs: catemeric carbamazepine form V." Chem Commun (Camb) **47**: 7074-7076.

Baaklini, G., et al. (2014). "Inhibition of the spontaneous polymorphic transition of pyrazinamide gamma form at room temperature by co-spray drying with 1,3-dimethylurea." Int J Pharm **479**(1): 163-170.

Babu, N. J. and A. Nangia (2011). "Solubility Advantage of Amorphous Drugs and Pharmaceutical Cocrystals." Crystal Growth & Design **11**(7): 2662-2679.

Badman, C. and B. L. Trout (2015). "Achieving continuous manufacturing. May 20-21, 2014 Continuous Manufacturing Symposium." J Pharm Sci **104**(3): 779-780.

Baird, J. A., et al. (2010). "A classification system to assess the crystallization tendency of organic molecules from undercooled melts." J Pharm Sci **99**(9): 3787-3806.

Barot, B. S., et al. (2010). "Development of directly compressible metformin hydrochloride by the spray-drying technique." Acta Pharm **60**(2): 165-175.

Barot, B. S., et al. (2012). "Compactibility improvement of metformin hydrochloride by crystallization technique." Advanced Powder Technology **23**(6): 814-823.

Bauer, J., et al. (2001). "Ritonavir: An extraordinary example of conformational polymorphism." Pharm Res **18**(6): 859-866.

Baxendale, I. R., et al. (2015). "Achieving continuous manufacturing: technologies and approaches for synthesis, workup, and isolation of drug substance. May 20-21, 2014 Continuous Manufacturing Symposium." J Pharm Sci **104**(3): 781-791.

Benmessaoud, I., et al. (2016). "Solvent screening and crystal habit of metformin hydrochloride." Journal of Crystal Growth **451**: 42-51.

Bhardwaj, R. M., et al. (2015). "A random forest model for predicting the crystallisability of organic molecules." CrystEngComm **17**(23): 4272-4275.

Bianco, S., et al. (2012). "Modification of the solid-state nature of sulfathiazole and sulfathiazole sodium by spray drying." AAPS PharmSciTech **13**(2): 647-660.

Billinge, S. J. L., et al. (2010). "Characterisation of amorphous and nanocrystalline molecular materials by total scattering." CrystEngComm **12**(5): 1366-1368.

BIOVIA. "BIOVIA Pipeline Pilot Overview." Retrieved October 2016, from <http://accelrys.com/products/collaborative-science/biovia-pipeline-pilot/>.

Blagden, N., et al. (2014). "Pharmaceutical co-crystals – are we there yet?" CrystEngComm **16**(26): 5753.

Bogelein, J. and G. Lee (2010). "Cyclone selection influences protein damage during drying in a mini spray-dryer." Int J Pharm **401**(1-2): 68-71.

Boraey, M. A., et al. (2013). "Improvement of the dispersibility of spray-dried budesonide powders using leucine in an ethanol–water cosolvent system." Powder Technology **236**: 171-178.

Breiman, L. (2001). "Random forests." Machine Learning **45**(1): 5-32.

Briggs, N. E. B. (2015). Polymorph control of pharmaceuticals within a continuous oscillatory baffled crystalliser, University of Strathclyde.

Brittain, H. G. (1999). Polymorphism in Pharmaceutical Solids, Taylor & Francis.

Brittain, H. G. (2009). Polymorphism in Pharmaceutical Solids, Second Edition, Taylor & Francis.

Bruker AXS (1999-2014). TOPAS, Bruker AXS, www.bruker-axs.com, info@bruker-axs.de

Büchi Labortechnik (2007). The Laboratory Assistant Flawil, Switzerland, Büchi Labortechnik, AG.

Büchi Labortechnik AG, S. Mini Spray Dryer B-290 Product Brochure.

Büchi Labortechnik AG, S. "Mini Spray Dryer B-290 Technical data sheet."

Büchi Labortechnik AG, S. (1997 - 2002). Training Papers Spray Drying.

Buckton, G., et al. (2002). "The Effect of Spray-Drying Feed Temperature and Subsequent Crystallization Conditions on the Physical Form of Lactose." AAPS PharmSciTech **3**(4).

Burger, A., et al. (2000). "Energy/Temperature Diagram and Compression Behavior of the Polymorphs of d-Mannitol." J Pharm Sci **89**(4): 457-468.

Byrn, S., et al. (2015). "Achieving continuous manufacturing for final dosage formation: challenges and how to meet them. May 20-21, 2014 Continuous Manufacturing Symposium." J Pharm Sci **104**(3): 792-802.

Cal, K. and K. Sollohub (2010a). "Spray Drying Technique. I: Hardware and Process Parameters." Journal of Pharmaceutical Sciences.

Cal, K. and K. Sollohub (2010b). "Spray drying technique. I: Hardware and process parameters." Journal of Pharmaceutical Sciences **99**(2): 575-586.

Chang, J. S., et al. (2008). "Effect of Pore Size and Particle Size Distribution on Granular Bed Filtration and Microfiltration." Separation Science and Technology **43**(7): 1771-1784.

Chavda, H. V., et al. (2010). "Biopharmaceutics classification system." Systematic Reviews in Pharmacy **1**(1): 62.

Chemical Computing Group Inc. (2017). Molecular Operating Environment (MOE), 2013.08. 1010 Sherbooke St. West, Suite #910, Montreal, QC, Canada, H3A 2R7.

Chen, J., et al. (2011). "Pharmaceutical Crystallization." Crystal Growth & Design **11**(4): 887-895.

Chen, X. D. and A. S. Mujumdar (2009). Drying Technologies in Food Processing, Wiley.

Cheng, C. L., et al. (2004). "Biowaiver extension potential to BCS Class III high solubility-low permeability drugs: bridging evidence for metformin immediate-release tablet." Eur J Pharm Sci **22**(4): 297-304.

Cherukuvada, S. and T. N. Guru Row (2014). "Comprehending the Formation of Eutectics and Cocrystals in Terms of Design and Their Structural Interrelationships." Crystal Growth & Design **14**(8): 4187-4198.

Chidavaenzi, O. C., et al. (2001a). "The effect of co-spray drying with polyethylene glycol 4000 on the crystallinity and physical form of lactose." Int J Pharm **216**: 43-49.

Chidavaenzi, O. C., et al. (2001b). "The effect of co-spray drying with polyethylene glycol 4000 on the crystallinity and physical form of lactose." Int J Pharm: 43-49.

Childs, S. L., et al. (2004). "A metastable polymorph of metformin hydrochloride: Isolation and characterization using capillary crystallization and thermal microscopy techniques." Crystal Growth & Design **4**(3): 441-449.

Childs, S. L., et al. (2009). "Analysis of 50 Crystal Structures Containing Carbamazepine Using the *Materials* Module of *Mercury CSD*." Crystal Growth & Design **9**(4): 1869-1888.

Chiou, D. and T. A. G. Langrish (2008). "A comparison of crystallisation approaches in spray drying." Journal of Food Engineering **88**(2): 177-185.

Chow, A. H., et al. (2007). "Particle engineering for pulmonary drug delivery." Pharm Res **24**(3): 411-437.

Chow, K., et al. (2008). "Engineering of pharmaceutical materials: an industrial perspective." J Pharm Sci **97**(8): 2855-2877.

Coucke, D., et al. (2009a). "Effect on the nasal bioavailability of co-processing drug and bioadhesive carrier via spray-drying." Int J Pharm **379**(1): 67-71.

Coucke, D., et al. (2009b). "Effect on the nasal bioavailability of co-processing drug and bioadhesive carrier via spray-drying." Int J Pharm: 67-71.

Coulson, J. M. and J. F. Richardson (1996). Fluid Flow, Heat Transfer and Mass Transfer, Butterworth-Heinemann.

Coulson, J. M., et al. (1999). Coulson & Richardson's Chemical Engineering, Butterworth-Heinemann.

- Davey, R. and J. Garside (2000). From Molecules to Crystallizers, Oxford University Press.
- Dengale, S. J., et al. (2016). "Recent advances in co-amorphous drug formulations." Adv Drug Deliv Rev **100**: 116-125.
- Duddu, S. P., et al. (2002). "Improved Lung Delivery from a Passize Dry Powder Inhaler Using an Engineered PulmoSphere Powder® Powder." Pharmaceutical Research **19**.
- Elversson, J. and A. Millqvist-Fureby (2005). "Particle size and density in spray drying-effects of carbohydrate properties." J Pharm Sci **94**(9): 2049-2060.
- Elversson, J., et al. (2003). "Droplet and particle size relationship and shell thickness of inhalable lactose particles during spray drying." J Pharm Sci **92**(4): 900-910.
- Erdemir, D., et al. (2009). "Nucleation of Crystals from Solution: Classical and Two-Step Models." Accounts of Chemical Research: 621-629.
- European Medicines Agency (2011). ICH guideline Q11 Development and manufacture of drug substances (chemical entities and biotechnological/biological entities).
- Fleischman, S. G., et al. (2003). "Crystal Engineering of the Composition of Pharmaceutical Phases: Multiple-component Crystalline Solids Involving Carbamazepine." Crystal Growth & Design **3**(6): 909-919.
- Florence, A. (2009). Approaches to High-Throughput Physical Form Screening and Discovery. Polymorphism in Pharmaceutical Solids, Second Edition, CRC Press: 139-184.
- Florence, A. J., et al. (2003). "Indexing powder patterns in physical form screening: Instrumentation and data quality." J Pharm Sci **92**(9): 1930-1938.
- Florence, A. J., et al. (2006). "An automated parallel crystallisation search for predicted crystal structures and packing motifs of carbamazepine." J Pharm Sci **95**(9): 1918-1930.
- Getsoian, A., et al. (2008). "One-solvent polymorph screen of carbamazepine." Int J Pharm **348**(1-2): 3-9.
- Gharsallaoui, A., et al. (2007). "Applications of spray-drying in microencapsulation of food ingredients: An overview." Food Research International **40**(9): 1107-1121.
- Gohel, M. C. and P. D. Jogani (2005). "A review of co-processed directly compressible excipients." Journal of Pharmacy and Pharmaceutical Sciences **8**(1): 76-93.

Gonnissen, Y., et al. (2008a). "Process design applied to optimise a directly compressible powder produced via a continuous manufacturing process." European Journal of Pharmaceutics and Biopharmaceutics: 760-770.

Gonnissen, Y., et al. (2007). "Development of directly compressible powders via co-spray drying." European Journal of Pharmaceutics and Biopharmaceutics: 220-226.

Gonnissen, Y., et al. (2008b). "Coproducting via spray drying as a formulation platform to improve the compactability of various drugs." European Journal of Pharmaceutics and Biopharmaceutics: 320-334.

Gonnissen, Y., et al. (2008c). "Coproducting via spray drying as a formulation platform to improve the compactability of various drugs." Eur J Pharm Biopharm **69**(1): 320-334.

Granberg, R. A. and Å. C. Rasmuson (1999). "Solubility of paracetamol in pure solvents." Journal of Chemical & Engineering Data **44**(6): 1391-1395.

Gray, J. M. N. T. and V. A. Chugunov (2006). "Particle-size segregation and diffusive remixing in shallow granular avalanches." Journal of Fluid Mechanics **569**: 365.

Grzesiak, A. L., et al. (2003). "Comparison of the Four Anhydrous Polymorphs of Carbamazepine and the Crystal Structure of Form I." J Pharm Sci **92**(11): 2260-2271.

Gu, C.-H., et al. (2001). "Polymorph screening: Influence of solvents on the rate of solvent-mediated polymorphic transformation." J Pharm Sci **90**(11): 1878-1890.

Guimarães, T. F., et al. (2015). "A multivariate approach applied to quality on particle engineering of spray-dried mannitol." Advanced Powder Technology.

Hancock, B. C., et al. (2002). "Comparison of the mechanical properties of the crystalline and amorphous forms of a drug substance." Int J Pharm **241**: 73-85.

Hanover, L. M. and J. S. White (1993). "Manufacturing, composition, and applications of fructose." American Journal of Clinical Nutrition **58**(5): 724-732.

Harris, R. K., et al. (2005). "Structural Studies of the Polymorphs of Carbamazepine, Its Dihydrate, and Two Solvates." Organic Process Research & Development **9**: 902-910.

Hay, W. T., et al. (2017). "Effect of spray drying on the properties of amylose-hexadecylammonium chloride inclusion complexes." Carbohydr Polym **157**: 1050-1056.

He, Y. and C. Ho (2015). "Amorphous Solid Dispersions: Utilization and Challenges in Drug Discovery and Development." J Pharm Sci.

Healy, A. M., et al. (2014). "Dry powders for oral inhalation free of lactose carrier particles." Adv Drug Deliv Rev **75**: 32-52.

Hilfiker, R. (2006). Polymorphism in the Pharmaceutical Industry, Wiley-VCH Verlag GmbH & Co. KGaA.

Hilfiker, R., et al. (2003). "Polymorphism - Integrated Approach From High-throughput Screening To Crystallization Optimization." Journal of Thermal Analysis and Calorimetry **73**: 429-440.

Huang, D. (2011). Modeling Of Particle Formation During Spray Drying. European Drying Conference - EuroDrying, Palma, Balearic Island, Spain.

Hulse, W. L., et al. (2009). "Influence of protein on mannitol polymorphic form produced during co-spray drying." Int J Pharm **382**(1-2): 67-72.

Islam, M. I. U. and T. A. G. Langrish (2010). "An investigation into lactose crystallization under high temperature conditions during spray drying." Food Research International **43**(1): 46-56.

Jiang, H., et al. (2013). "Microencapsulation of α -Amylase by Carrying Out Complex Coacervation and Drying in a Single Step Using a Novel Three-Fluid Nozzle Spray Drying." Drying Technology **31**(16): 1901-1910.

Jin, Y. and X. D. Chen (2009). "Numerical Study of the Drying Process of Different Sized Particles in an Industrial-Scale Spray Dryer." Drying Technology **27**(3): 371-381.

Johnston, A., et al. (2008). "Targeted crystallisation of novel carbamazepine solvates based on a retrospective Random Forest classification." CrystEngComm **10**(1): 23-25.

Jørgensen, K. and T. U. o. D. D. o. C. Engineering (2005). Drying Rate and Morphology of Slurry Droplets: PhD Thesis, Department of Chemical Engineering, Technical University of Denmark.

Kadam, S. S., et al. (2011). "Combination of a Single Primary Nucleation Event and Secondary Nucleation in Crystallization Processes." Crystal Growth & Design **11**(4): 1271-1277.

Kadota, K., et al. (2015). "Preparation of composite particles of hydrophilic or hydrophobic drugs with highly branched cyclic dextrin via spray drying for dry powder inhalers." Powder Technology **283**: 16-23.

Karanje, R. V., et al. (2013). "Formulation and development of extended-release micro particulate drug delivery system of solubilized rifaximin." AAPS PharmSciTech **14**(2): 639-648.

Kašpar, O., et al. (2013). "Effect of cross-linking method on the activity of spray-dried chitosan microparticles with immobilized laccase." Food and Bioproducts Processing **91**(4): 525-533.

Kemp, I. C., et al. (2015). "Production of fine lactose particles from organic solvent in laboratory and commercial-scale spray dryers." Drying Technology **34**(7): 830-842.

Khoshkhoo, S. and J. Anwar (1993). "Crystallization of polymorphs: the effect of solvent." Journal of Physics D: Applied Physics **26**(8B): B90-B93.

Kim, T. U. and U. o. C. a. Boulder (2006). Transport of Organic Micropollutants Through Nanofiltration (NF) and Reverse Osmosis (RO) Membranes: Mechanisms, Modeling, and Applications, University of Colorado at Boulder.

Kipouros, K., et al. (2005). "Quantitative analysis of less soluble form IV in commercial carbamazepine (form III) by diffuse reflectance fourier transform spectroscopy (DRIFTS) and lazy learning algorithm." Analytica Chimica Acta **550**(1-2): 191-198.

Kipouros, K., et al. (2006). "Simultaneous quantification of carbamazepine crystal forms in ternary mixtures (I, III, and IV) by diffuse reflectance FTIR spectroscopy (DRIFTS) and multivariate calibration." J Pharm Sci **95**(11): 2419-2431.

Kirk, J. H., et al. (2007). "Lactose: a definitive guide to polymorph determination." Int J Pharm **334**(1-2): 103-114.

Koester, L. S., et al. (2004). "Bioavailability of carbamazepine:beta-cyclodextrin complex in beagle dogs from hydroxypropylmethylcellulose matrix tablets." European Journal of Pharmaceutical Sciences **22**(2-3): 201-207.

Kondo, K., et al. (2014). "Preparation of sustained-release coated particles by novel microencapsulation method using three-fluid nozzle spray drying technique." Eur J Pharm Sci **51**: 11-19.

Labiris, N. R. and M. B. Dolovich (2003). "Pulmonary drug delivery. Part II: The role of inhalant delivery devices and drug formulations in therapeutic effectiveness of aerosolized medications." British Journal of Clinical Pharmacology **56**(6): 600-612.

- Lang, M., et al. (2002). "Form IV of Carbamazepine." J Pharm Sci **91**(4): 1186-1190.
- LeClair, D. A., et al. (2016). "Evaluation of Excipients for Enhanced Thermal Stabilization of a Human Type 5 Adenoviral Vector through Spray Drying." Int J Pharm.
- Lee, Y. Y., et al. (2011). "Particle size dependence of polymorphism in spray-dried mannitol." Eur J Pharm Sci **44**(1-2): 41-48.
- Legako, J. and N. T. Dunford (2010). "Effect of spray nozzle design on fish oil-whey protein microcapsule properties." J Food Sci **75**(6): E394-400.
- Lenka, M. and D. Sarkar (2016). "Solubility of l-asparagine monohydrate in water and water-isopropanol mixed solvents: Measurements and thermodynamic modelling." Fluid Phase Equilibria **412**: 168-176.
- Li, Z., et al. (2017). "Composite particles based on particle engineering for direct compaction." Int J Pharm.
- Litster, J. (2016). Design and Processing of Particulate Products. Cambridge, Cambridge University Press.
- Littringer, E. M., et al. (2013). "The morphology of spray dried mannitol particles — The vital importance of droplet size." Powder Technology **239**: 162-174.
- Maas, S. G., et al. (2011). "The impact of spray drying outlet temperature on the particle morphology of mannitol." Powder Technology **213**(1-3): 27-35.
- Malvern Instruments Ltd. (2015). Morphologi G3 User Manual Malvern Instruments Ltd. . **MAN0410-07-EN-00**.
- Marshall, L. J., et al. (2016). "Investigation of the enhanced antimicrobial activity of combination dry powder inhaler formulations of lactoferrin." Int J Pharm **514**(2): 399-406.
- Martins, R. M., et al. (2012a). "Engineering Active Pharmaceutical Ingredients by Spray Drying: Effects on Physical Properties and In Vitro Dissolution." Drying Technology **30**(9): 905-913.
- Martins, R. M., et al. (2012b). "Microstructured ternary solid dispersions to improve carbamazepine solubility." Powder Technology **215-216**: 156-165.

- Maury, M., et al. (2005). "Effects of process variables on the powder yield of spray-dried trehalose on a laboratory spray-dryer." Eur J Pharm Biopharm **59**(3): 565-573.
- McCabe, J. F. (2010). "Application of design of experiment (DOE) to polymorph screening and subsequent data analysis." CrystEngComm **12**(4): 1110-1119.
- Mezhericher, M., et al. (2010). "Spray drying modelling based on advanced droplet drying kinetics." Chemical Engineering and Processing: Process Intensification **49**(11): 1205-1213.
- Mishelevich, A. and A. Apelblat (2008). "Solubilities of magnesium-l-ascorbate, calcium-l-ascorbate, magnesium-l-glutamate, magnesium-d-gluconate, calcium-d-gluconate, calcium-d-heptagluconate, l-aspartic acid, and 3-nitrobenzoic acid in water." The Journal of Chemical Thermodynamics **40**(5): 897-900.
- Mo, Y., et al. (2011). "Solubility of α -form and β -form of l-glutamic acid in different aqueous solvent mixtures." Fluid Phase Equilibria **300**(1-2): 105-109.
- Mokale, V., et al. (2016). "Formulation of metformin hydrochloride nanoparticles by using spray drying technique and in vitro evaluation of sustained release with 32-level factorial design approach." Drying Technology **34**(12): 1455-1461.
- Mullin, J. W. (2001). Crystallization. Oxford, Elsevier Butterworth-Heinemann.
- Murdande, S. B., et al. (2010). "Solubility advantage of amorphous pharmaceuticals: I. A thermodynamic analysis." J Pharm Sci **99**(3): 1254-1264.
- Myerson, A. S. and R. Ginde (2002). 2 - Crystals, crystal growth, and nucleation. Handbook of Industrial Crystallization (Second Edition). Woburn, Butterworth-Heinemann: 33-65.
- Myerson, A. S., et al. (2015). "Control systems engineering in continuous pharmaceutical manufacturing. May 20-21, 2014 Continuous Manufacturing Symposium." J Pharm Sci **104**(3): 832-839.
- Naikwade, S. R., et al. (2009). "Development of budesonide microparticles using spray-drying technology for pulmonary administration: design, characterization, in vitro evaluation, and in vivo efficacy study." AAPS PharmSciTech **10**(3): 993-1012.
- Nandiyanto, A. B. D. and K. Okuyama (2011a). "Progress in developing spray-drying methods for the production of controlled morphology particles: From the nanometer to submicrometer size ranges." Advanced Powder Technology **22**(1): 1-19.

Nandiyanto, A. B. D. and K. Okuyama (2011b). "Progress in developing spray-drying methods for the production of controlled morphology particles: From the nanometer to submicrometer size ranges." Advanced Powder Technology: 1-19.

Ni Ogain, O., et al. (2012). "Spray drying from organic solvents to prepare nanoporous/nanoparticulate microparticles of protein: excipient composites designed for oral inhalation." J Pharm Pharmacol **64**(9): 1275-1290.

Nijdam, J. J. and T. A. G. Langrish (2005). "An Investigation of Milk Powders Produced by a Laboratory-Scale Spray Dryer." Drying Technology **23**(5): 1043-1056.

Nolan, L. M., et al. (2009). "Excipient-free nanoporous microparticles of budesonide for pulmonary delivery." Eur J Pharm Sci **37**(5): 593-602.

Nowak, J., et al. (2009). "Adsorption behaviour of sugars versus their activity in single and multicomponent liquid solutions." J Chromatogr A **1216**(50): 8697-8704.

O'Mahony, M. A., et al. (2013). "Measuring the Solubility of a Quickly Transforming Metastable Polymorph of Carbamazepine." Organic Process Research & Development **17**(3): 512-518.

O'Mahony, M. A., et al. (2012). "Examining Solution and Solid State Composition for the Solution-Mediated Polymorphic Transformation of Carbamazepine and Piracetam." Crystal Growth & Design **12**(4): 1925-1932.

Ono, T., et al. (2004). "Process Modeling of the Polymorphic Transformation of L-Glutamic Acid." Crystal Growth & Design **4**(6): 1161-1167.

Palmer, D. S., et al. (2007). "Random forest models to predict aqueous solubility." Journal of Chemical Information and Modeling **47**(1): 150-180.

Patil, S. P., et al. (2014). "Generation of 1:1 Carbamazepine:Nicotinamide cocrystals by spray drying." European Journal of Pharmaceutical Sciences **62**: 251-257.

Patterson, A., et al. (2014). "Modelling drug degradation in a spray dried polymer dispersion using a modified Arrhenius equation." Int J Pharm **478**(1): 348-360.

Patterson, J. E., et al. (2008). "Melt extrusion and spray drying of carbamazepine and dipyridamole with polyvinylpyrrolidone/vinyl acetate copolymers." Drug Dev Ind Pharm **34**(1): 95-106.

Paudel, A., et al. (2013). "Manufacturing of solid dispersions of poorly water soluble drugs by spray drying: formulation and process considerations." Int J Pharm **453**(1): 253-284.

- Pawley, G. S. (1981). "Unit-Cell Refinement From Powder Diffraction Scans." Journal of Applied Crystallography **14**(DEC): 357-361.
- Perlovich, G., et al. (2004). "Solvation and Hydration Characteristics of Ibuprofen and Acetylsalicylic Acid." AAPA PHARMSCI **6**(1).
- Perry, R. and D. Green (2008). Perry's Chemical Engineers' Handbook, Eighth Edition, McGraw-Hill Education.
- Pilcer, G., et al. (2013). "New co-spray-dried tobramycin nanoparticles-clarithromycin inhaled powder systems for lung infection therapy in cystic fibrosis patients." J Pharm Sci **102**(6): 1836-1846.
- Písecký, J. (2005). "Spray drying in the cheese industry." International Dairy Journal **15**(6-9): 531-536.
- Poornachary, S. K., et al. (2008). "Influence of Solution Speciation of Impurities on Polymorphic Nucleation in Glycine." Crystal Growth & Design **8**(1): 179-185.
- Porowska, A., et al. (2016). "Predicting the surface composition of a spray-dried particle by modelling component reorganization in a drying droplet." Chemical Engineering Research and Design **110**: 131-140.
- Price, C. J. (1997). "Take some solid steps to improve crystallization." Chemical Engineering Progress: 34-43.
- Price, S. L. (2014). "Predicting crystal structures of organic compounds." Chemical Society Reviews **43**(7): 2098-2111.
- Prinn, K. B., et al. (2002). "Statistical Modeling of protein spray drying at the lab scale." 1-8.
- Ramasami, P. (2002). "Solubilities of Amino Acids in Water and Aqueous Sodium Sulfate and Related Apparent Transfer Properties." Journal of Chemical & Engineering Data **47**: 1164-1166.
- Rathore, A. S. (2009). "Roadmap for implementation of quality by design (QbD) for biotechnology products." Trends Biotechnol **27**(9): 546-553.
- Renuka Devi, K., et al. (2015). "Ultrasound assisted nucleation and growth characteristics of glycine polymorphs--a combined experimental and analytical approach." Ultrason Sonochem **24**: 107-113.

- Rodriguez-Spong, B., et al. (2004). "General principles of pharmaceutical solid polymorphism: a supramolecular perspective." Adv Drug Deliv Rev **56**(3): 241-274.
- Rohrs, B. R., et al. (2006). "Particle size limits to meet USP content uniformity criteria for tablets and capsules." J Pharm Sci **95**(5): 1049-1059.
- Rowe, R. C., et al. (2012). Mannitol Handbook of Pharmaceutical Excipients. R. C. Rowe, P. J. Sheskey, W. G. Cook and M. E. Fenton, Pharmaceutical Press.
- Rustichelli, C., et al. (2000). "Solid-state study of polymorphic drugs: carbamazepine." Journal of Pharmaceutical and Biomedical Analysis **23**: 41-54.
- Santhalakshmy, S., et al. (2015). "Effect of inlet temperature on physicochemical properties of spray-dried jamun fruit juice powder." Powder Technology **274**: 37-43.
- Sarma, B., et al. (2011). "Solid forms of pharmaceuticals: Polymorphs, salts and cocrystals." Korean Journal of Chemical Engineering: 315-322.
- Sarrate, R., et al. (2015). "Modification of the morphology and particle size of pharmaceutical excipients by spray drying technique." Powder Technology: 244-255.
- Schwartz, A. M. and A. S. Myerson (2002). 1 - Solutions and solution properties. Handbook of Industrial Crystallization (Second Edition). Woburn, Butterworth-Heinemann: 1-31.
- Setter, S. M., et al. (2003). "Metformin hydrochloride in the treatment of type 2 diabetes mellitus: A clinical review with a focus on dual therapy." Clinical Therapeutics **25**(12): 2991-3026.
- Shekunov, B. Y. and P. York (2000). "Crystallization processes in pharmaceutical technology and drug delivery design." Journal of Crystal Growth **211**(1-4): 122-136.
- Shen, S. C., et al. (2011). "Physical state and dissolution of ibuprofen formulated by co-spray drying with mesoporous silica: effect of pore and particle size." Int J Pharm **410**(1-2): 188-195.
- Shur, J., et al. (2008). "Cospray-dried unfractionated heparin with L-leucine as a dry powder inhaler mucolytic for cystic fibrosis therapy." J Pharm Sci **97**(11): 4857-4868.
- Siddique, H., et al. (2015). "Establishment of a Continuous Sonocrystallization Process for Lactose in an Oscillatory Baffled Crystallizer." Organic Process Research & Development **19**(12): 1871-1881.

Sigma-Aldrich (2014a). "Safety Data Sheet - D(-)-Fructose." Retrieved October 2016, from <http://www.sigmaaldrich.com/MSDS/MSDS/DisplayMSDSPage.do?country=GB&language=en&productNumber=F0127&brand=SIGMA&PageToGoToURL=http%3A%2F%2Fwww.sigmaaldrich.com%2Fcatalog%2Fproduct%2Fsigma%2Ff0127%3Flang%3Den>.

Sigma-Aldrich (2014b). "Safety Data Sheet - D-(+)-Galactose." Retrieved October 2017, from <http://www.sigmaaldrich.com/MSDS/MSDS/DisplayMSDSPage.do?country=GB&language=en&productNumber=G0750&brand=SIAL&PageToGoToURL=http%3A%2F%2Fwww.sigmaaldrich.com%2Fcatalog%2Fproduct%2Fsial%2Fg0750%3Flang%3Den>.

Sigma-Aldrich (2014c). "Safety Data Sheet - L-Ascorbic acid." Retrieved October 2016, from <http://www.sigmaaldrich.com/MSDS/MSDS/DisplayMSDSPage.do?country=GB&language=en&productNumber=A92902&brand=SIAL&PageToGoToURL=http%3A%2F%2Fwww.sigmaaldrich.com%2Fcatalog%2Fproduct%2Fsial%2Fa92902%3Flang%3Den>.

Sigma. "D-(+)-Glucose Product Information Sheet." Retrieved September 2016, from https://www.sigmaaldrich.com/content/dam/sigmaaldrich/docs/Sigma/Product_Information_Sheet/2/g5400pis.pdf.

Sigma. "Product Information - Urea." Retrieved October 2016, from https://www.sigmaaldrich.com/content/dam/sigmaaldrich/docs/Sigma/Product_Information_Sheet/1/u5378pis.pdf.

Singh, A. and G. Van den Mooter (2016). "Spray drying formulation of amorphous solid dispersions." *Adv Drug Deliv Rev* **100**: 27-50.

Sloth, J., et al. (2009). "Spray Drying of Suspensions for Pharma and Bio Products, Drying Kinetics and Morphology." *Industrial & Engineering Chemistry Research*: 3657-3664.

Soulaïrol, I., et al. (2015). "Spray-dried solid dispersions of nifedipine and vinylcaprolactam/vinylacetate/PEG6000 for compacted oral formulations." *Int J Pharm* **481**(1-2): 140-147.

Srirambhatla, V. K., et al. (2016). "Isomorphous template induced crystallisation: a robust method for the targeted crystallisation of computationally predicted metastable polymorphs." *Chem Commun (Camb)* **52**(46): 7384-7386.

Ståhl, K., et al. (2002). "The effect of process variables on the degradation and physical properties of spray dried insulin intended for inhalation." *Int J Pharm* **223**(1-2): 227-237.

Stahly, G. P. (2007). "Diversity in single- and multiple-component crystals. The search for and prevalence of polymorphs and cocrystals." *Crystal Growth & Design* **7**(6): 1007-1026.

Sunderland, T., et al. (2015). "Application of a novel 3-fluid nozzle spray drying process for the microencapsulation of therapeutic agents using incompatible drug-polymer solutions." Arch Pharm Res **38**(4): 566-573.

Sypek, K., et al. (2012). "In Situ Monitoring of Stirring Effects on Polymorphic Transformations during Cooling Crystallization of Carbamazepine." Crystal Growth & Design **12**(10): 4821-4828.

Tajber, L., et al. (2009). "Spray drying of budesonide, formoterol fumarate and their composites-II. Statistical factorial design and in vitro deposition properties." Int J Pharm **367**(1-2): 86-96.

Takeuchi, H., et al. (2005). "Solid dispersion particles of amorphous indomethacin with fine porous silica particles by using spray-drying method." Int J Pharm **293**(1-2): 155-164.

Telang, C., et al. (2003). "Crystallization of D-mannitol in binary mixtures with NaCl: Phase diagram and polymorphism." Pharm Res **20**(12): 1939-1945.

ter Horst, J. H., et al. (2015). "Fundamentals of Industrial Crystallization." 1317-1349.

The Metabolics Innovation Centre, T. "DrugBank." Retrieved October 2016, from <https://www.drugbank.ca/>.

The R Foundation. "The R Project for Statistical Computing." Retrieved October 2016, from <https://www.r-project.org/>.

Tung, H.-H. (2013). "Industrial Perspectives of Pharmaceutical Crystallization." Organic Process Research & Development **17**(3): 445-454.

U.S. Food & Drug Administration, F. "The Biopharmaceutics Classification System (BCS) Guidance." Retrieved November 2016, from <https://www.fda.gov/AboutFDA/CentersOffices/OfficeofMedicalProductsandTobacco/CDE/ucm128219.htm>.

U.S. Food and Drug Administration (2009). Guidance for Industry: Q8 (2) Pharmaceutical Development.

Van Eerdenbrugh, B., et al. (2010). "Crystallization tendency of active pharmaceutical ingredients following rapid solvent evaporation--classification and comparison with crystallization tendency from undercooled melts." J Pharm Sci **99**(9): 3826-3838.

- Vanhoorne, V., et al. (2014). "Crystal coating via spray drying to improve powder tableability." Eur J Pharm Biopharm **88**(3): 939-944.
- Vanhoorne, V., et al. (2016). "Continuous manufacturing of delta mannitol by cospray drying with PVP." Int J Pharm **501**(1-2): 139-147.
- Vehring, R. (2008). "Pharmaceutical particle engineering via spray drying." Pharm Res **25**(5): 999-1022.
- Vehring, R., et al. (2007). "Particle formation in spray drying." Journal of Aerosol Science: 728 - 746.
- Walters, R. H., et al. (2014). "Next-Generation Drying Technologies for Pharmaceutical Applications." J Pharm Sci.
- Walzel, P. (2011). "Influence of the Spray Method on Product Quality and Morphology in Spray Drying." Chemical Engineering & Technology **34**(7): 1039-1048.
- Wang, M., et al. (2012). "Production and characterization of carbamazepine nanocrystals by electrospraying for continuous pharmaceutical manufacturing." J Pharm Sci **101**(3): 1178-1188.
- Wicker, J. G. P. and R. I. Cooper (2015). "Will it crystallise? Predicting crystallinity of molecular materials." CrystEngComm **17**(9): 1927-1934.
- Wilke, C. R. and P. Chang (1955). "Correlation Of Diffusion Coefficients In Dilute Solutions." AIChE **1**(2): 264-270.
- Woo, M. W. and B. Bhandari (2013a). 2 - Spray drying for food powder production. Handbook of Food Powders, Woodhead Publishing: 29-56.
- Woo, M. W. and B. Bhandari (2013b). Spray drying for food powder production. Handbook of Food Powders processes and properties. Cambridge, UK, Woodhead Publishing: 29-56.
- Yaws, C. L. Yaws' Handbook of Thermodynamic and Physical Properties of Chemical Compounds, Knovel.
- Yi, T., et al. (2008). "A new solid self-microemulsifying formulation prepared by spray-drying to improve the oral bioavailability of poorly water soluble drugs." Eur J Pharm Biopharm **70**(2): 439-444.

Yu, L. (2001). "Amorphous pharmaceutical solids: preparation, characterization and stabilization." Advanced Drug Delivery Reviews **48**: 27-42.

Yu, L. X. (2008). "Pharmaceutical quality by design: product and process development, understanding, and control." Pharm Res **25**(4): 781-791.

Yu, L. X., et al. (2014). "Understanding pharmaceutical quality by design." AAPS J **16**(4): 771-783.